Groundwater Recharge Modelling

A case study in the Central Veluwe, The Netherlands

Hiwot Ghiday Gebreyohannes

February, 2008

Groundwater Recharge Modelling
A case study in the Central Veluwe, The Netherlands

by

Hiwot Ghiday Gebreyohannes

Thesis submitted to the International Institute for Geo-information Science and Earth Observation in partial fulfilment of the requirements for the degree of Master of Science in Geo-information Science and Earth Observation, Specialisation: Groundwater Assessment and Modelling.

Thesis Assessment Board

Chairman	Dr.Ir. M.W. Lubczynski	WRS, ITC, Enschede
External Examiner	Dr.Ir.P.Droogers	Future Water, Wageningen
First Supervisor	Dr.A.S.M.Gieske	WRS, ITC, Enschede
Second Supervisor	Dr.Ing.T.H.M.Rientjes	WRS, ITC, Enschede

INTERNATIONAL INSTITUTE FOR GEO-INFORMATION SCIENCE AND EARTH OBSERVATION
ENSCHEDE, THE NETHERLANDS

Disclaimer

This document describes work undertaken as part of a programme of study at the International Institute for Geo-information Science and Earth Observation. All views and opinions expressed therein remain the sole responsibility of the author, and do not necessarily represent those of the institute.

Dedicated to
My Dearest mother with Love and Gratitude
‘Who encouraged me to knowledge’

Abstract

Quantitative understanding of the process of groundwater recharge is fundamental to the sustainable management of groundwater resources since the recharge magnitude directly affects the amount of water that can be extracted from aquifers. The objective of this study was to assess the effect of meteorological forcing on groundwater recharge and water table fluctuations in the Central Veluwe (The Netherlands) which is characterized by deep phreatic groundwater and dense vegetation.
Two models were used to simulate soil moisture flow in the unsaturated zone, namely: the **S**oil-**W**ater-**A**tmosphere-**P**lant system (SWAP) and the **E**xtended model for **A**quifer **R**echarge and soil moisture **T**ransport through the unsaturated **H**ardrock (EARTH). Both models make use of daily precipitation and potential evapotranspiration data to simulate soil water content, actual evapotranspiration, percolation, recharge and groundwater level fluctuations. The precipitation data was obtained by spatial interpolation of daily precipitation records from four stations within the study area and the potential evapotranspiration was calculated using Makkink and Penman-Monteith equations. Land cover classification for this study was done by considering LANDSAT ETM images, topographic maps and ground truth data as collected during field trips, while vegetation height was determined with LIDAR derived AHN data.

Soil moisture, actual evapotranspiration, percolation, recharge and groundwater level fluctuations were simulated for a period of twenty years (1973-1992) and the simulated groundwater levels were compared with the observed levels. Both models appear to simulate the slow groundwater level fluctuations of the study area with high accuracy in the first 15 years of the simulation period. However, systematic deviations occurred in the last 5 years of the simulations probably as a result of increased groundwater abstractions in the area. In this research the effects of the abstractions cannot be quantified further since these are not considered in the design of the model structures.

In this study, the SWAP and EARTH approaches have nearly identical results. The long-term mean annual total evapotranspiration that also includes evaporation from tree interception is found to be 515 mm while the groundwater recharge amounts to 345 mm. Groundwater recharge is only 39% of the mean annual precipitation and implies that 61% of precipitation is lost by evapotranspiration. This study also reveals that the highest recharge fluxes are from the area covered by mixed forest, light coniferous forest, heath and Molinia grass.

The annual actual evapotranspiration is nearly constant throughout the modelling period. In contrast, the recharge rate shows a high temporal variability and follows a pattern similar to precipitation. The overall conclusion of this study is that groundwater level fluctuations in the Central Veluwe are affected by natural climatic variations and anthropogenic influences.

Key words: Soil water flow modelling, groundwater recharge and groundwater level fluctuations

Acknowledgements

First and foremost I would like to acknowledge the enabling environment created by the World Bank (International Bank for reconstruction and development) through the Joint Japan/World Bank Graduate Scholarship program (JJ/WBGSP).

I am grateful to my organization for granting my leave of absence to pursue further studies and for all the help they have rendered this far.

Special thanks go to my first supervisor Dr. A.S.M. Gieske for his guidance, un-reserving support, encouragement and suggestions from the commencement of this work. Not forgetting his ability of instilling hope when things appeared going in the negative direction.

I greatly thank to my second supervisor Dr.ing.T.H.M.Rientjes for his support, encouragement, invaluable suggestions and comments to improve my research work.

I thank the Veluwe water board province of Gelderland for providing me with groundwater abstraction data for the research work. I would like to acknowledge the Dinoshop subsurface data archive of The Netherlands for letting me to use the groundwater level data.

I wish to express my appreciation to all the staff and support members of the Water Resources and Environmental Management (WREM) division for their willingness to help when ever called upon at any time and not failing to mention their love and concern to my entire being at ITC.

I can not end without acknowledging the support received from my fellow classmates. I really enjoy being with you. I will remember you for making my life more pleasant in The Netherlands.

My sincerest thanks to my family for always being there for me.

Last but not least to all ITC Ethiopian community for providing home feeling environment.

Table of contents

List of figures

List of tables

1. Introduction

1.1. Rationale

Groundwater recharge is an important component of the water balance and evaluation of groundwater resources largely depends on it (Freeze and Cherry, 1979). Thus quantification of the rate of natural groundwater recharge is a basic prerequisite for efficient groundwater resources management, i.e. for developing an effective watershed management strategy that will ensure the protection of groundwater resources not only from climate change, but also from other stresses (Lerner et al., 1990). However, accurate spatial and temporal characterization of groundwater recharge can be difficult due to its dependence on a multitude of hydro-metrological elements such as rainfall, evapotranspiration and hydrogeological heterogeneity (Lerner et al., 1990).

Water movement in top soils determines the rate of recharge to the groundwater, rate of plant transpiration, soil evaporation and runoff. Therefore an accurate description of unsaturated zone water movement and accurate methods for determination of parameters and input data are essential to derive proper estimation of groundwater recharge.

Different methods are available to estimate groundwater recharge. Among these hydrological models are advanced tools to estimate recharge and related hydrological processes at a regional scale. The advantage of hydrological models is that the impact of transferring water between competing sectors can be simulated. However, the framework applied for modelling groundwater recharge involves several practical problems that affect the results of these models. The main problems are the low accuracy of the model input data. The performance of these models could be improved by a refined input time series which include more process - based knowledge about evapotranspiration and accurate conceptualization and parameterization of the modelled system.

The main objective of the research presented in this thesis therefore is to study the effect of meteorological forcing on the groundwater recharge distribution and groundwater level fluctuations in the central part of Veluwe using two vadose zone models (SWAP & EARTH).

1.2. Problem statement

Due to its relatively high position and highly porous sandy soils, the Veluwe is a large-scale infiltration area of enormous significance for the flow pattern and abstraction of groundwater in The Netherlands. Groundwater resource is a fundamental importance to meet the rapidly increasing agricultural, industrial and domestic water supply requirements in the central part of the Veluwe area. This resource is almost the only key to economic development in the area and hence the quantification of groundwater recharge is a necessity for the efficient and sustainable groundwater resource management. Gehrels (1999) concluded that the method of estimating actual evapotranspiration and changes in soil water storage determines the accuracy of the water balance. However, due to the lack of basic understanding of the spatial and temporal variability of hydrological processes, water management is becoming a major challenge.

The groundwater recharge distribution and causes of groundwater level fluctuations in the study area are not well understood due to limited knowledge of the soil water flow through the thick unsaturated

zone and of the actual evapotranspiration from the densely populated and spatially variable forest covers. It is commonly accepted that forests pose a difficult problem with regard to the determination of actual evapotranspiration. This is because climatic conditions below the canopy are different from those above while crop factors needed to estimate evapotranspiration are sparsely known for natural and semi-natural vegetation covers. Evapotranspiration depends not only on atmospheric but also on vegetation type and a substantial amount of precipitation is intercepted by the forest before it reaches the ground. So the present study aims at increasing our understanding of the groundwater recharge and groundwater level fluctuations of the area by introducing a refined top system to the unsaturated zone models (SWAP and EARTH) i.e. by using Penman-Monteith and Makkink methods for the evapotranspiration calculation.

1.3. Objectives, research questions and research hypothesis

1.3.1. General objective

The general objective of the study is to assess groundwater recharge through unsaturated zone water flow modelling using EARTH & SWAP models in the central Veluwe.

1.3.2. Specific objectives

- Estimation of daily potential evapotranspiration using Makkink and Penman-Monteith Equations
- System conceptualization to identify the processes, driving forces and parameters that have to be considered during the soil water flow modelling in the unsaturated zone.
- Modelling and model calibration
- Assessment of the effect of meteorological forcing on groundwater recharge and groundwater level fluctuations
- Estimation of mean annual recharge of the study area

1.3.3. Research Questions

To address the aforementioned objectives the following research question are posed:

- Is there a significance difference in the calculated water balance components by using the Makkink and Penman-Monteith derived evapotranspiration
- Which processes, driving forces and parameters have to be considered during modelling?
- Are the simulated results obtained from the two models (SWAP, EARTH) comparable? If not what could be the justification? And which model is relatively best suited for this?
- What are the possible driving forces for the seasonal and long-term groundwater level fluctuation in the study area?
- Which vegetation types have a dominant effect on the groundwater recharge of the area?

1.3.4. Research Hypotheses

- It is possible to obtain a good estimate of groundwater recharge by the application of unsaturated zone hydrological models (such as SWAP & EARTH).
- It is possible to describe and increase our understanding of the processes leading to groundwater level fluctuations in the area.
- Estimation of the influence of forest on groundwater recharge of the area is feasible.

1.4. General methodology

Two one-dimensional hydrological models were used to assess the groundwater recharge and to study the groundwater level fluctuations in the central Veluwe. The methodology followed in this study was based on the objective of the study, and all the activities performed to meet the objective were categorized into three different stages namely: pre-field work, field work and post-field work activities.

In the initial stage a literature survey was carried out to a) understand the process of soil water flow in the unsaturated zone, b) to assess methods available for forest evapotranspiration calculation and to understand how the SWAP and EARTH models work for simulating soil water flow in the unsaturated zone. Besides, primary data such as time series meteorological and hydrological data and cloud free satellite images were collected at this stage.

In the second stage a field survey was conducted to collect ground truth data and to have a general understanding of the study area. GPS tracks and way points of different land covers were collected using hand held GPS to assist the georeferencing of the images and land cover mapping of the study area.

In the third and final stage collected data were analysed. Image processing and calculation of evapotranspiration, modelling, model calibration and modelling result analysis were also carried out under this stage. Finally conclusions and recommendations for further study were made based on the results obtained.

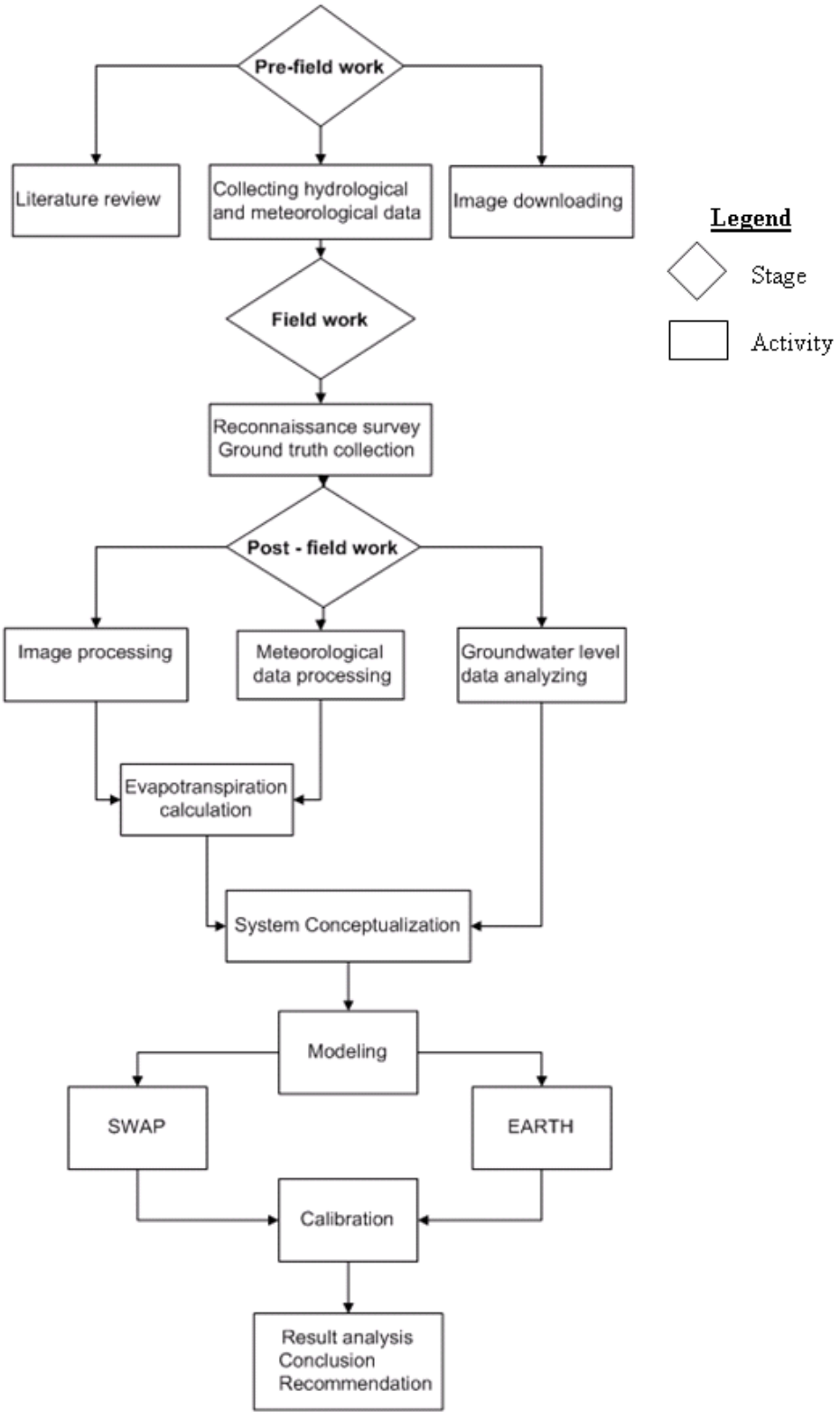

Figure 1.1 Major steps of the study

1.5. Thesis outline

The content of this thesis is briefly outlined as follows.
Chapter 1 deals with the general introduction, problem statement and objective of the study, research questions and proposed hypotheses.
Chapter 2 reviews literature studies on the physical background of groundwater recharge and various methods of recharge estimation, and principles of soil water flow in the unsaturated zone.
In chapter 3 a short description of the study area in terms of location, topography, geomorphology, geology and hydrogeology, climate and land cover is presented.
Chapter 4 describes the type, duration and source of available data. It also deals with description of data collected from the field.
Chapter 5 is dedicated to modelling soil water flow in the unsaturated zone. In this chapter a description is given on the selected sites, a short overview of the EARTH and SWAP models and the relevant soil water flow mathematical equations, the required model input data and parameters.
In Chapter 6 the model calibration, the calibration evaluation, the sensitivity analysis and the conclusion of the model calibration are presented.
In chapter 7 the general thesis research is discussed and summarized.
Finally conclusions and recommendations for further research are presented in chapter 8.

2. Literature Review

2.1. Concepts of Groundwater Recharge

Groundwater recharge can be defined as the amount of water added to the groundwater reservoir in excess of soil moisture deficits and evapotranspiration by direct percolation through the vadose zone. It is the resultant of variable weather conditions, root water uptake, processes of soil water flow, and vadose zone properties (Gehrels, 1999).

There are various sources of recharge to a groundwater system. Direct (precipitation) recharge in which water is added to the groundwater reservoir in excess to soil moisture deficits and evapotranspiration. Indirect recharge is that type where water percolates to the water table through the beds of surface watercourses. The current study deals with direct recharge.

Quantitative understanding of the process of groundwater recharge is fundamental to the sustainable management of groundwater resources in such a way that:

1. The amount of recharge dictates the amount of water that can be extracted sustainably from the aquifers.
2. Recharge has a great importance to assess the impact of climate changes on groundwater resources and aquifer vulnerability to contaminants.

2.2. Factors that affect groundwater recharge

Groundwater recharge is affected by many parameters and complex processes which themselves are influenced by many factors. Precipitation is affected by climatic factors such as wind and temperature, resulting in complex and dynamic distributions while the intensity and spatial distribution of precipitation influences the amount of recharge.

Large scale vegetation determines the amount of net rainfall, infiltration rate, deep drainage and the available storage capacity of the groundwater system. Any change in vegetation, say from forest to grassland can have a large effect on recharge. The nature of land cover has a big influence on recharge and hence groundwater recharge modelling should not assume that vegetation is a constant factor. For example, the removal of the indigenous vegetation in large parts of south eastern Australia more than 100 years ago caused a significant increase in ground water recharge.

Vegetation influences recharge through interception and transpiration. The amount of stored water that can be removed by vegetation depends mainly on the rooting depth. Shallow rooted grasses will remove less water than deeper rooted shrubs and trees (Jyrkama and Sykes, 2007).

It is well known that the degree of water saturation of the root zone determines the distribution of hydraulic conductivity and as a result the percolation to the groundwater table. It also influences the water uptake by roots and thus the actual evapotranspiration (Berendrecht, 2004). Thus the process of groundwater recharge is not only influenced by the spatial and temporal variability in the major climate variables, but is also dependent on the spatial distribution of land-surface properties and the depth and hydraulic properties of the underlying soils.

2.3. Groundwater recharge estimation techniques

Estimating the rate of aquifer replenishment is the most difficult of all measures in the evaluation of ground water resources. Estimation of groundwater recharge requires modelling of the interaction between all of the important processes in the hydrological cycle such as infiltration, surface runoff, evapotranspiration and groundwater level variations (Jyrkama and Sykes, 2007).
The most important methods available for estimating groundwater recharge can be categorized as follows. Direct measurements, Water balance methods, Hydrological models and Tracer methods (Simmers, 1997).

2.3.1. Direct measurement - Lysimeter

A lysimeter is a device consisting of an in situ weighable column or volume of soil for which the inflow and outflow water can be measured and changes in storage can be monitored by weighing. This technique is used to determine evaporation in a natural environment by measuring the other water balance components, but as is mentioned above measuring recharge using this technique at reasonable spatial scale is difficult.

2.3.2. Water balance methods/soil moisture balance

The basis of the soil moisture balance method of estimating recharge is that the soil becomes free draining when the moisture content of the soil reaches a limiting value called the field capacity. To determine when the soil reaches this critical condition, it is necessary to simulate soil moisture conditions throughout the year. This involves the representation of the relevant properties of the soil and the capacity of crops to collect moisture from the soil and to transpire water to the atmosphere. If no crops are growing or if there is only partial crop cover, bare soil evaporation must be considered. Bare soil evaporation is important both in semi-arid locations to represent soil moisture conditions at the end of the dry season and in temperate climates where recharge occurs in winter when evaporation is usually the major loss from the soil. Transpiration and evaporation often occur at less than their potential rate due to crop stress arising from limited soil moisture availability. The input to the soil moisture balance is infiltration which equals the daily precipitation minus interception or runoff. The soil moisture balance is often written as:

$$R = P - D - ET - \Delta W \quad \textbf{(2.1)}$$

where R is recharge [L], P is precipitation [L], D is net runoff [L], ET is actual evapotranspiration [L] and ΔW is the change in soil moisture storage [L].

2.3.3. Hydrological models

Different types of models are available for determining recharge: one-dimensional semi-distributed numerical models such as SWAP, one-dimensional lumped parametric models such as EARTH and three-dimensional fully distributed numerical groundwater flow models such as MODFLOW. The advantage of the hydrological models is that the impact of transferring water between competing sectors can be simulated and the effects of man-induced scenarios on regional hydrology can be studied. The disadvantage though is that considerable expertise in model use and extensive field data are required to make proper model simulations at regional scale feasible.
The unsaturated zone physically based numerical models such as SWAP solve the unsaturated zone water flow equation i.e. the Richards equation for porous media. In contrast to the lumped parametric water balance models, numerical models allow detailed evaluation of the effects on groundwater recharge of vadoze zone hydraulic properties and their spatial variabilities. These methods are based

on soil profile partitioning with a number of homogeneous layers with their own characteristic hydraulic properties. They simulate the transformation of precipitation into flow taking into account all the intermediate processes such as evapotranspiration, interception, infiltration, and runoff. They are therefore able to estimate recharge at many points and at many times. For simulating recharge, boundary and initial conditions must be imposed on the models together with hydraulic soil properties and vegetation properties.

Parametric models such as EARTH use a numerical or analytical relationship between precipitation and recharge. These models have been developed to deal with conceptual recharge situations that can not be encompassed by existing numerical models. Examples are recharge through hard rock formation. Gehrels (1999) used both the SWAP and EARTH models to predict groundwater fluctuations in the Veluwe area which is characterized by porous media, and both models could describe the deep groundwater level fluctuation quite well. Thus the parametric models such as Earth can be used both in porous and hard rock formations.

Another common method is to use a fully distributed three-dimensional numerical groundwater flow model (such as MODFLOW) to estimate recharge by adjusting the recharge input value in the model until groundwater levels calculated by the model match the aquifers measured water levels. One problem with this approach is that any change in aquifer parameters such as hydraulic conductivity and aquifer storage also affects the calculated water levels. Often the uncertainty associated with transmissivity is larger than the uncertainty associated with recharge, thus the accuracy of the estimated recharge may be low.

2.3.4. Tracer methods

There are three kinds of tracers. However, the most commonly used in this field are the environmental tracers. These are dissolved substances introduced into the large scale water cycle either by nature or by man over long periods. They are able to trace water movement over long periods in contrast to artificially applied tracers which show water movement over small spatial and temporal scales. The most important tracer is chloride.

2.4. Water Dynamics in the Unsaturated Zone

Transport of soil water affects heat and solute transport in soils, defines rates of biological processes in soil and water supply to plants, governs transpiration and ground water replenishment, controls runoff, and has many other important functions in the environment. Therefore, simulations of water transport in soil have many applications in hydrology, meteorology, agronomy, environmental protection, and other soil-related disciplines.

The fact that water moves through the unsaturated soil was recognized by Buckingham (1907) who related the flow rate to suction gradients. In the mechanical concept only suction gradients were considered as the cause of water movement through the unsaturated soil. However, water may also move through unsaturated soils by other driving forces such as thermal, electrical, or solute concentration gradients (Feddes et al., 1988). Considering that suction gradient is the cause of water movement in the unsaturated soils, Darcy's law can be written as (Feddes et al., 1988):

$$q = -K\nabla h \qquad \textbf{(2.2)}$$

where q is the flux [L T^{-1}], K is hydraulic conductivity [L T^{-1}] and ∇h is gradient of head [-]

According to Van Dam (2000) water flow in the unsaturated zone is predominantly vertical, and can generally be simulated as one-dimensional flow. Hence for one-dimensional vertical flow Darcy's law can be written as:

$$q = -K(\theta)\frac{\partial(h(\theta)+z)}{\partial z} \quad \textbf{(2.3)}$$

where q is soil water flux [L T^{-1}], θ is volumetric soil water content [L^3/L^3], $K(\theta)$ is the unsaturated hydraulic conductivity subject to θ [L T^{-1}], $h(\theta)$ is pressure head subject to θ [L] and z is elevation head [L].

Under transient conditions, when water content changes with time, conservation of matter is formulated by the continuity equation:

$$\frac{\partial\theta}{\partial t} = \frac{\partial q}{\partial z} - R_w + R_s \quad \textbf{(2.4)}$$

where θ is volumetric water content [L3/L3], t is time [T]), q is soil water flux [L T^{-1}], R_w is the sink of soil water e.g. root water abstraction [L3/L3/T] and R_s is source term [L3/L3/T].

2.4.1. Differential equation of unsaturated flow

Richards (1931) formulated the partial differential equation for water flow in unsaturated soil. He suggested that Darcy's law originally devised for saturated flow in porous media is also applicable to unsaturated flow in porous media. Thus combination of the mass conservation and Darcy's equation leads to the partial differential equation of the unsaturated flow. Considering the one-dimensional case of vertical flow and introducing the differential soil water capacity C(h)=∂θ/∂h, the combination of the mass conservation equations and Darcy's equation provides the general unsaturated water flow equation that is commonly referred to as (Richards Equation):

$$\frac{\partial\theta}{\partial t} = C(h)\frac{\partial h}{\partial t} = \frac{\partial}{\partial z}K(h)\left[\frac{\partial h}{\partial z}+1\right] - R_w + R_s \quad \textbf{(2.5)}$$

2.4.2. Numerical solution of soil water flow equation

The equations describing water behaviour in the top soil should be solved numerically because of soil heterogeneity, non-linearity of soil physical properties as both the hydraulic conductivity and the soil water pressure head depend on the soil water content, non-uniform root water uptake, rapidly changing boundary conditions, and complex interactions. Due to the non-linearity of the soil physical properties there is no closed-form analytical solution. However, the Richards equation can be used as a basis for numerical soil water flow by specifying appropriate boundary and initial conditions, dividing the soil into thin layers, and applying the equation to each layer sequentially at small increments of time (Dingman, 2002). The partial differential flow equation can be solved numerically by a finite difference, a finite element or a boundary element technique. According to Van Dam (2000) for one-dimensional flow the finite difference method is advantageous because it needs no mass lumping to prevent oscillations. The other advantage of the finite difference method is its simplicity and efficiency in treating the time derivatives.

2.5. Soil physical properties

The most important soil physical properties for water movement in the unsaturated zone are the relationships between the soil pressure head (h), water content (θ) and hydraulic conductivity (K) for each distinct soil layer.

The accuracy of groundwater recharge estimation depends to a great extent on the exact knowledge of these soil hydraulic functions. It appears that the ability of the numerical models for simulating flow and mass transport in the unsaturated zone to fully characterize the simulated system has not kept pace with the numerical and modelling expertise. Probably the single most important factor limiting the successful application of the unsaturated flow theory to actual field problems is the lack of information regarding the parameters entering the governing transfer equation. The relationships between the water content θ, the pressure head *h* and the hydraulic conductivity *K* are generally summarized in the retention function θ(*h*) and the unsaturated hydraulic conductivity function *K*(θ) (Figure 2.1).

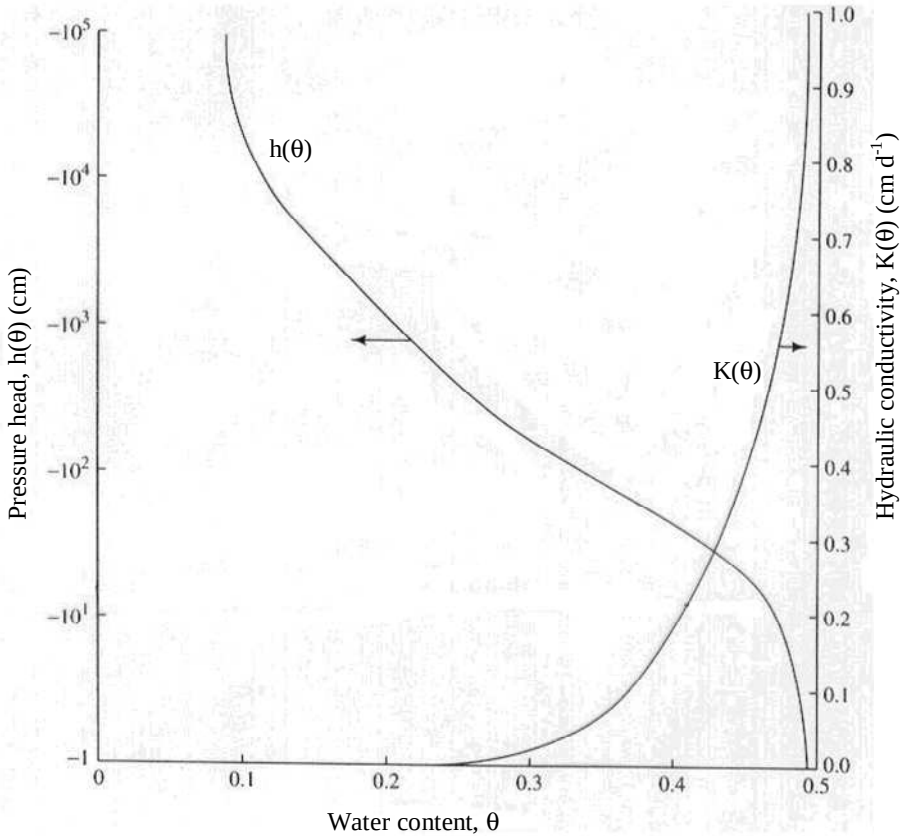

Figure 2.1 Typical form of soil hydraulic relations, h(θ) - θ and K(θ) - θ for unsaturated soils (Dingman, 2002)

These soil hydraulic functions need to be specified for each distinct soil layer. Although tabular forms of θ (*h*) and *K*(θ) have been used for many years, currently analytical expressions are generally applied for a number of reasons. Analytical expressions are more convenient as model input and a rapid comparison between horizons is possible by comparing parameter sets.

Several analytical functions have been proposed to empirically describe the relationship between the effective soil water content, S_e and the soil pressure head, h. The flexible and smooth equation by Van Genuchten (1980) is the most widely used relation:

$$S_e = \frac{1}{\left[1+(h\alpha)^n\right]^m} \qquad \textbf{(2.6)}$$

where α [L^{-1}] and n [-] are empirical constants affecting the shape of the retention curve, and m [-] is usually defined as m=1-1/n. S_e is the effective degree of saturation [-] or reduced water content ($0 \leq S_e \leq 1$), defined as:

$$S_e = \frac{(\theta - \theta_r)}{(\theta_s - \theta_r)} \quad \textbf{(2.7)}$$

where θ_r and θ_s are the residual and saturated water content respectively.
Knowing this soil-water retention curve, the unsaturated hydraulic conductivity is described according to Mualem (1976):

$$K(S_e) = K_s S_e^{\lambda} \left[1 - (1 - S_e^{1/m}\right]^2 \quad \textbf{(2.8)}$$

where $K(S_e)$ is the unsaturated hydraulic conductivity as a function of effective soil water content [L T^{-1}], K_s is the saturated hydraulic conductivity [L T^{-1}] and λ is a shape parameter [-] depending on $\partial K/\partial h$.

3. Description of the study area

3.1. Location and topography

The Veluwe is a forest-rich ridge of hills in the central part of The Netherlands and in the western part of the province Gelderland (Figure 3.1). It is part of the sand area of the central Netherlands. Apart from this the most notable feature of this area is the occurrence of hilly ranges. These ensure that the Veluwe looms above the surrounding lowlands as an imposing massif, at least by Dutch standards. Another feature of the Veluwe is its relatively elevated position. The highest 'mountains' lie 100 meters or more above NAP. The Toerenberg at Apeldoorn is the highest point of The Netherlands outside south Limburg. The study area is characterized by undulating topography ranging in elevation from 9 m at the edges to 95 m at the central part (Figure 3.2). The central Veluwe features many different landscapes including woodland, heath, and Europe's largest sand drifts. A large part of the Veluwe is assigned as a National Nature Reserve. The fringes of the Veluwe are more densely populated, with cities such as Apeldoom, Arnhem, Amersfoort, Deventer, Zwolle, Harderwijk and Zutphen.

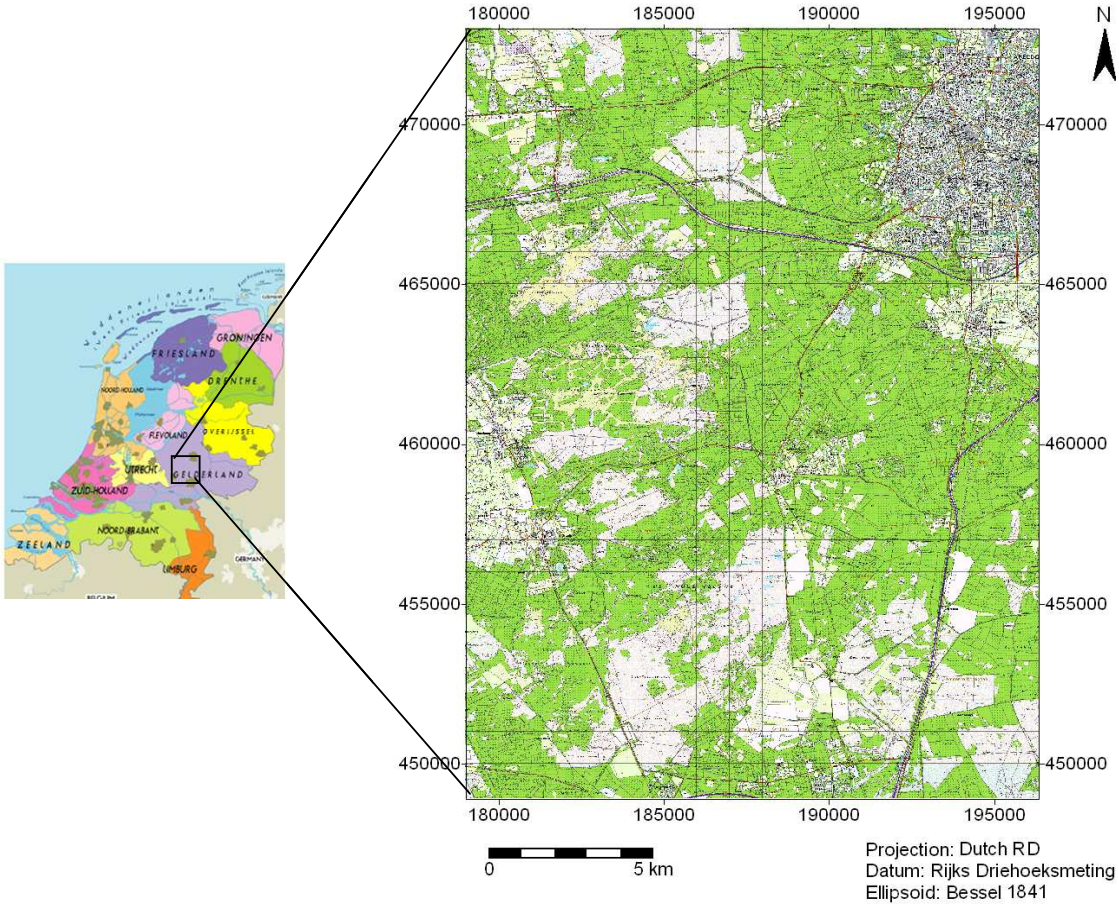

Figure 3.1 Location of the study area

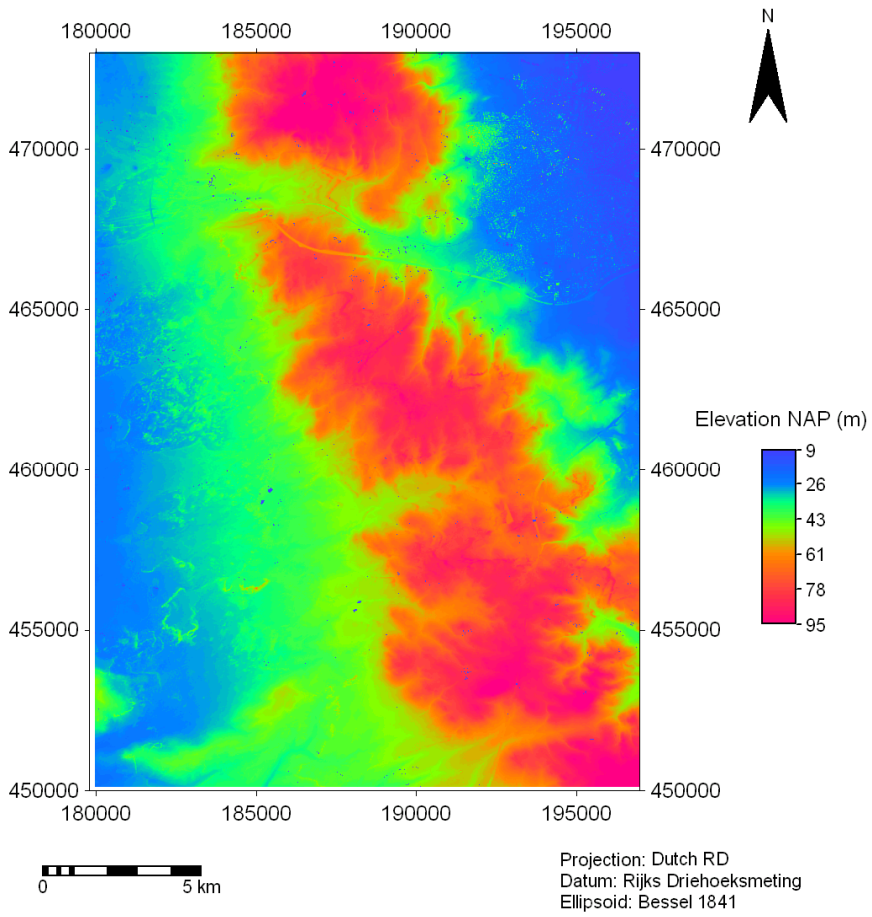

Figure 3.2 Topography of the study area (National Land Registry)

3.2. Climate and weather

The present climate of the Netherlands is classified as a semi-humid maritime climate with cool summers and mild winters. The weather is dominated by frequent appearances of depressions and prevalent westerly winds, resulting in variable weather conditions over short time spans. Westerly winds prevail during the whole year and bring humid marine air on land and occasional easterly winds bring dry air with low wind speeds from the European continent. The winds have a strong influence on the rainfall patterns in the country (De Vries, 1974).

3.2.1. Rainfall and reference evapotranspiration

The mean annual precipitation for the Netherlands is about 792 mm. Precipitation falls for about 7% of the time mostly as rain (only 3% falls as snow) (Dufour, 2000).The wettest areas are the hilly regions of the Veluwe and the very south of the country, where orographic enhancement of rainfall is of local importance.

The mean annual precipitation in the study area is found to be about 880 mm, with the driest year as low as ~584 mm in 1976 and the wettest year reaching up to 1235 mm in the year 1998 (Figure 3.3).

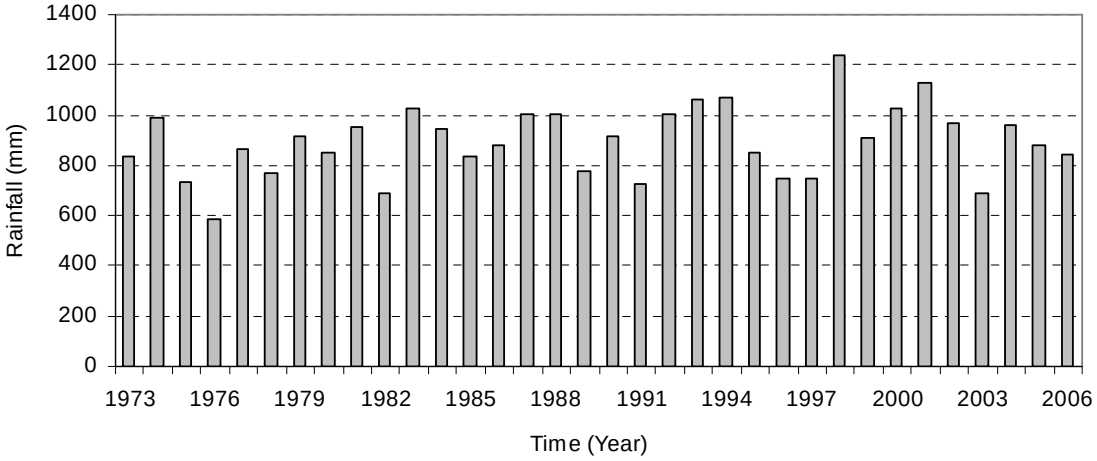

Figure 3.3 Annual rainfall of the study area (1973-2006)

The mean monthly rainfall distribution of the area shows a moderate annual cycle with the driest month in February (51 mm) and the wettest month in December (93 mm) i.e. the rainfall is fairly distributed over the year and over the area (Figure 3.4 and Figure 3.5).

The mean annual reference crop evapotranspiration according to Makkink is about 580 mm y^{-1} at the main KNMI station of De Bilt. In the present study, the mean annual reference crop evapotranspiration for the study area was calculated using the climatic data from the De Bilt meteorological station with a 34 years average using Penman and Makkink methods.

Mean annual reference evapotranspiration values of about 614 and 577 mm were obtained respectively for Penman and Makkink. The reference evapotranspiration obtained from Makkink method is nearly identical to the country's average annual reference evapotranspiration. The mean annual precipitation for the Veluwe area, 880 mm, exceeds the mean annual evapotranspiration by 303 mm. For this reason there is an annual precipitation excess in the Veluwe area of on average 303 mm.

In the annual cycle the monthly Penman reference evapotranspiration increases from 14.2 mm in December to 106 mm in July, whereas the Makkink result is about 8 mm in December and reaching up to 94 mm in July. The seasonal variation of evapotranspiration is very large due to its dependence on solar radiation, wind speed and temperature. The evapotranspiration varies with vegetation type and season. However, the mean monthly precipitation shows precipitation amounts that vary little over the year i.e. there is hardly any seasonal precipitation pattern in the central Veluwe area.

Average total precipitation exceeds average total evapotranspiration. However, during the growing season a precipitation deficit usually develops (Figure 3.5). The seasonal cycle of precipitation and evapotranspiration in the study area indicates a water surplus in the winter period (October and March) and precipitation deficit in the summer period (April to September). This shows that the groundwater recharge in the area mainly occurs during winter.

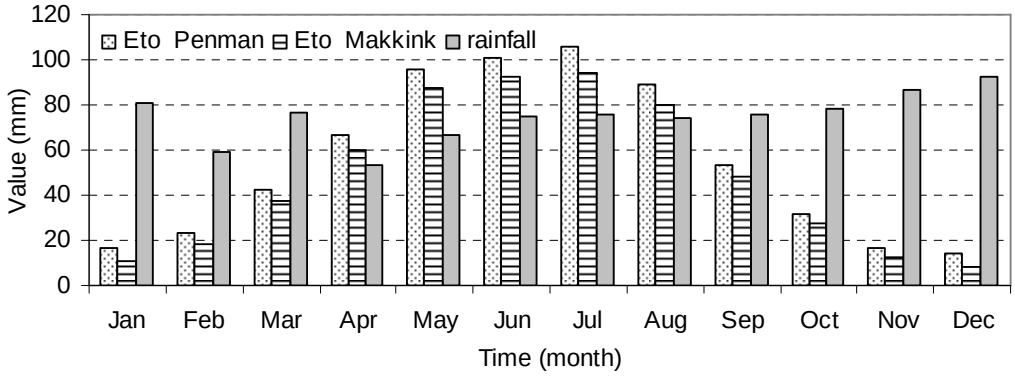

Figure 3.4 Seasonal variations in reference evapotranspiration and rainfall rate (1973-2006)

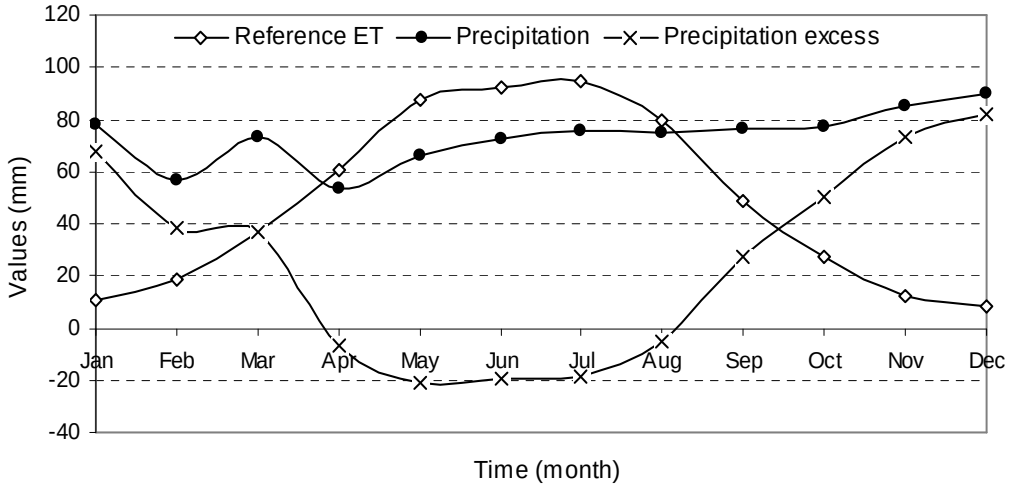

Figure 3.5 Mean monthly precipitation, evapotranspiration and precipitation excess (1973-2006)

3.2.2. Temperature, relative humidity and global radiation

The mean monthly temperature of the study area as recorded at De Bilt (1973-2006) varies between 2 ^{0}C in January and 17 ^{0}C in July (Figure 3.6). July and August are the warmest months of the year with a maximum temperature of about 21^{0}C. The months of December, January and February are the coldest months in the area with average temperature of 0.8, -0.2 and -0.3 ^{0}C respectively.

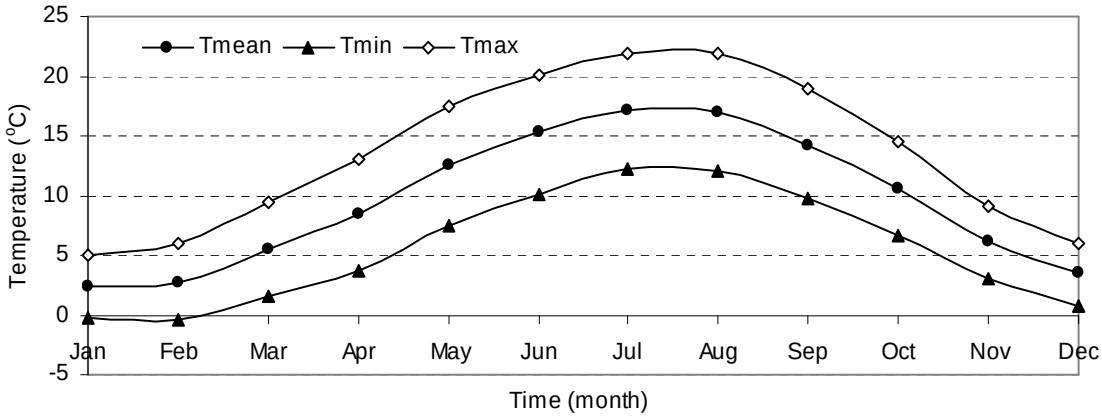

Figure 3.6 Mean monthly temperature of the study area (1973-2006)

The mean relative humidity of the Veluwe area is 87% in winter and 77% in summer. It varies between 74.5% in the month of May to 89% in the month of December (Figure 3.7).

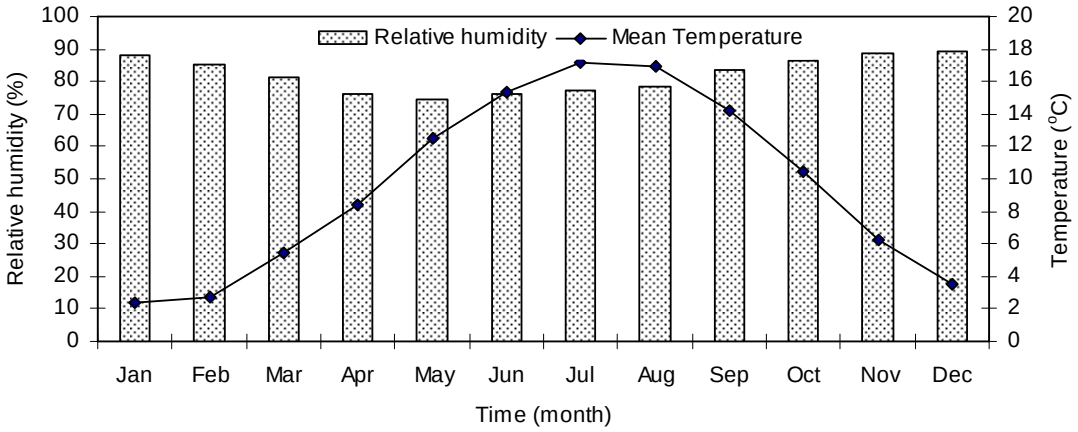

Figure 3.7 Mean monthly temperature and relative humidity of the study area (1973-2006)

The energy received at the earth's surface is provided mostly by incoming shortwave (global) radiation. The global radiation shows variations within a year due to the position of the earth's surface with respect to the sun. Figure 3.8 shows the mean monthly variation of solar radiation in the Veluwe area. The study area receives high energy from solar radiation in the summer season but lower energy in the winter season.

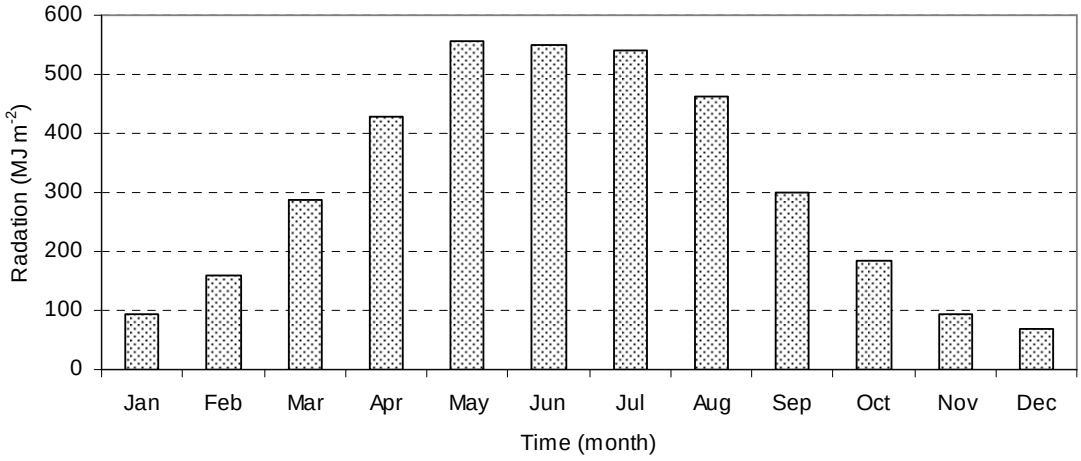

Figure 3.8 Mean monthly solar radiation of the study area (1973-2006)

3.3. Geomorphology and Geology

The Veluwe area is a gently undulating area ranging in elevation from 20 to 100 m above mean sea level. The geomorphology of the present landscape of the area is the result of glacial, fluvio-glacial and eolian processes.

The geological formation of the Veluwe area described by De Vries (1974) is summarized as follows. Over most of The Netherlands the uppermost several hundred meters of the subsurface geology consists of formations deposited in the Tertiary and Quaternary which together form the most recent era, the Cenozoic. The ice pushed ridges are mainly composed of highly gravelly, coarse Sandy River deposits left by the precursor of the Maas and Rhine rivers prior to the advance of the inland ice.

During the coldest periods of the Pleistocene (200,000 years ago), the arrival of inland ice from the Scandinavian area temporary put an end to the dominating effect of the rivers and their extensive deltas. The inland ice sheet flowed from the Scandinavia into the Netherlands reaching the imaginary line Haarlen-Utrecht-Nijmegen. This forced the large rivers including Rhine to change their course more to the west in front of the ice sheet. The ice tongues eroded deep glacial basins and pushed up the earlier river-formed deposits on both sides into ice-pushed ridges. In this way a series of ice pushed ridges (as high as a 100 m above mean sea level) and large basins were created in the central Netherlands. The Veluwe is one of these ice pushed ridges. During this pushing phase locally boulder clay (Drente Formation) was deposited in the glacial basins of the Veluwe particularly in the IJssel valley.
During the Weichselian age inland ice from Scandinavia expanded southward again but did not reach the Netherlands. Periglacial conditions prevailed in the Veluwe and the Netherlands as a whole and the rivers deposited massive layers of coarse sands and gravel (Kreftenheye Formation). However, the country experienced cold to extreme cold conditions and the underground was frozen also in the Veluwe. Consequently, rainfall and snow melt water could not find a way through the underground. This led to the development of superficial drainage in the Veluwe. The dry and cold periglacial climate towards the end of this period favored a strong eolian activity and during this period there was little vegetation and large areas were bare. So in the Veluwe and elsewhere in the Netherlands an extensive thin blanket of sand was deposited. This so called cover sand was spread out over the older coarse deposits as a slightly undulating cover. Unlike the sand of the ice pushed ridges the cover sand is fine and well sorted containing intercalations of peat, loam and coarser sand of fluvial and periglacial origin (Twente Formation).

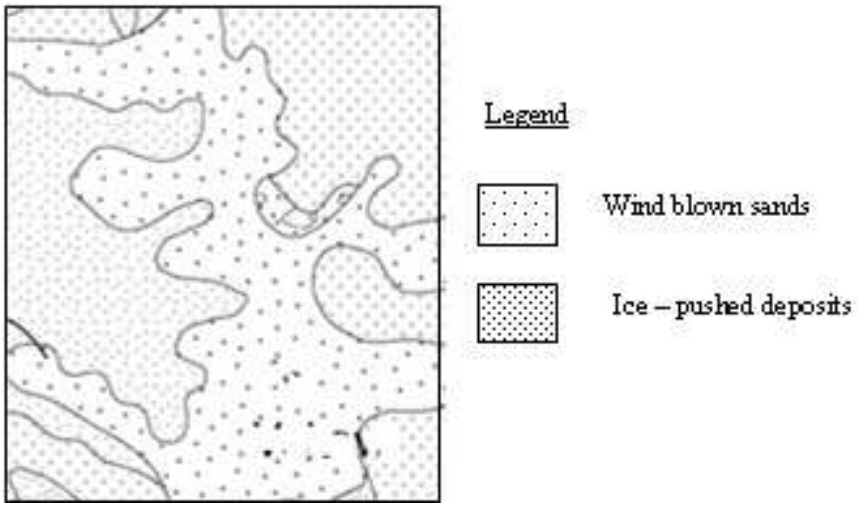

Figure 3.9 Geological map of the study area (After RGD, 1985)

The sea level rise during the Holocene through the post glacial rise in temperature led to marine sedimentation and formation of peat along the coasts but in the higher Pleistocene areas such as the Veluwe ridges sedimentation was limited due to the presence of the drift sands. The climate became milder again which is favorable for vegetation growth (forests and heath lands) and underneath these vegetation soils started to develop. Frozen underground disappeared and surplus rainfall could now drain easily into the sandy subsoil. However, in the middle ages human activity increasingly

influenced nature and caused deforestation of large areas and the soil became less protected against the wind. The Pleistocene cover sands were now reactivated into the Holocene drift sands that formed large inland dunes (Kootwijk Formation). Cover sand areas where the groundwater was deep and where there was little vegetation were extremely vulnerable to wind erosion and the flat-to-gently-undulating cover sand landscape of the last ice age was changed to blowout hollows and drift sand dunes. In general, the Veluwe was formed in several phases and due to this the internal geological structure of the ice pushed ridges of the Veluwe is rather complex.

3.4. Hydrogeology

The ice pushed ridges formed in the glacial stage are important for the hydrogeology of The Netherlands because these ridges are formed by lobes of the ices sheets, which under the pressure of the huge mass of ice behind them were able to 'bulldoze' vast amounts of older fluviatile material into ridges of porous and permeable sand. The Veluwe is the best known example of ice pushed ridges. It is an infiltration area of enormous significance for the flow pattern and abstraction of groundwater in the country. Because the hills are made of sand, rain water infiltrates rapidly and then flows at a depth of tens of meters to the edges where it reaches the surface again. There is less surface water in the high grounds of the Veluwe which means that there is more groundwater below the surface. This groundwater flows out laterally and is discharged at the edges by river drainage and diffuse seepage discharges into lower areas like Gelder and the IJssel valleys and the border zone of the Noord Veluwe. The groundwater flow in The Netherlands can be divided into one-dimensional parallel flow patterns and two-dimensional radial flow patterns. Parallel flow is generally found in the areas in which the groundwater flow is restricted upstream by Pre-Pleistocene deposits, whereas radial flow occurs in the plateau-shaped areas surrounded by oval shaped discharge areas. Due to the elliptical shape of the regional topography, the groundwater flow pattern of the Veluwe area is somewhere between radial and parallel flow patterns (De Vries, 1974). The direction of the main groundwater divide roughly follows the topography and is approximately north-south. Groundwater levels in the central Veluwe are around 40 m above sea level and the depth of the unsaturated zone varies from less than 1 m along the edges to more than 60 m in the center (Gehrels, 1999). The unconfined aquifer has a thickness of 150 to 250 m with transmissivity of 5000 to 10000 $m^2 d^{-1}$ and specific yield values ranging between 0.2-0.30 (Figure 3.10).

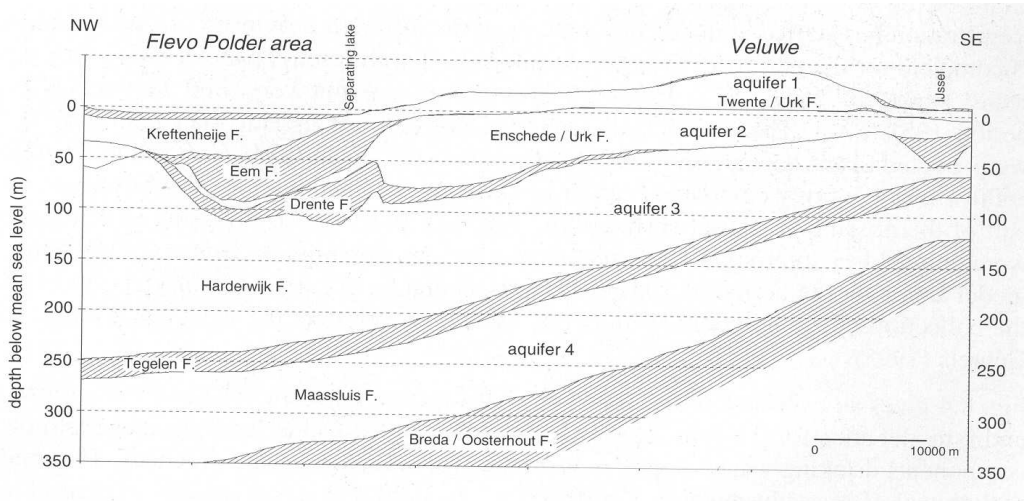

Figure 3.10 Main aquifers and aquitards of the Flevo polders and the Veluwe area (Gehrels, 1999)

The geological formations and the thickness of each aquifer are different. For full description of the aquifers the reader is referred to Gehrels (1999). In general the structure of the Veluwe groundwater resources is very complex in the sense that water levels are not smooth and continuous every where. Due to the glacial pushing, originally horizontal dense clay layers became inclined or even sub-vertical position causing major local or spatial 'jumps' or discontinuities in groundwater level.

3.4.1. Groundwater Level fluctuations

The groundwater regime in the Veluwe depends on the groundwater recharge and abstraction. The most important factor for recharge in the Veluwe area is the precipitation excess i.e. the difference between precipitation and evaporation. So to understand the annual recharge of the groundwater it should be realized that not the precipitation but primarily the precipitation excess is important (Dufour, 2000). Groundwater level fluctuations in the Veluwe area show different behavior at different locations.

In the central Veluwe where the groundwater table is very deep, the groundwater level shows low frequency and high amplitude fluctuations whereas areas with shallow groundwater table show high frequency and low amplitude fluctuations (Figure 3.11). This can be understood by realizing that groundwater level response to precipitation surplus is direct and quick along the edge (shallow groundwater) but slow for the deep groundwater in the central Veluwe. That is groundwater levels in the central Veluwe only slightly reflect the succession of dry and wet seasons but are more susceptible for long term variations in average rainfall. This slow response is due to two reasons: one is due to the thick unsaturated zone which can buffer the short-term rainfall events while the other reason is the large spatial scale of the aquifer system together with high drainage resistance and high specific yield (Gehrels, 1999).

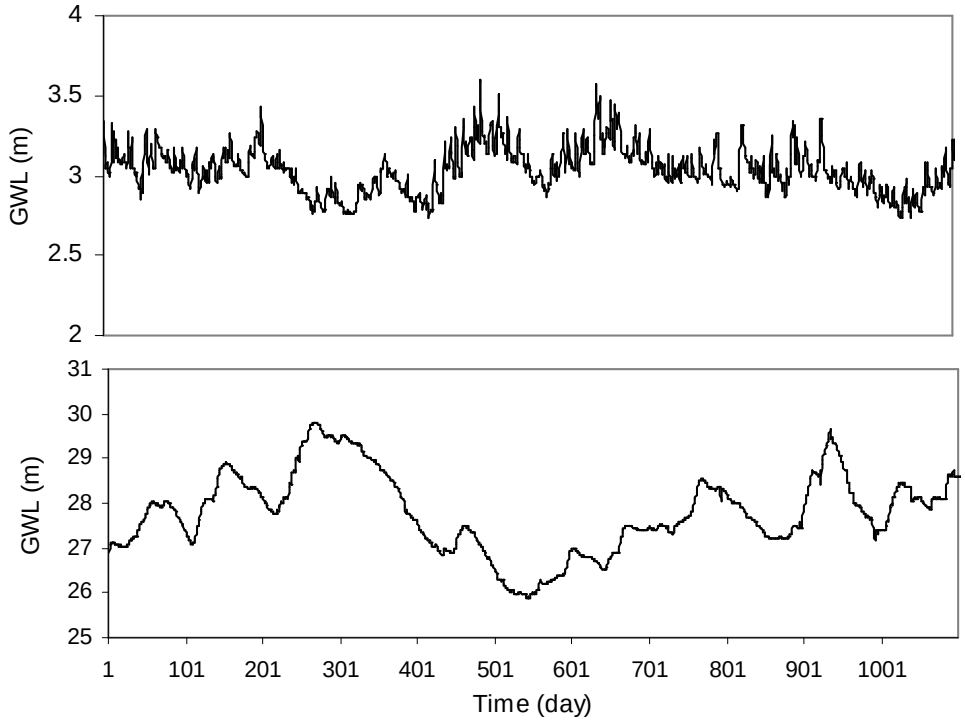

Figure 3.11 An Example of a daily time series of shallow groundwater level (26hp0039) near the NW boundary of the Veluwe area, top and a deep groundwater level (33ap0065) in the central Veluwe, bottom

3.5. Soils, Land use and Vegetation

The soil types in the study area are generally podzolic sand soil, characterized by poor mineral content. They are thus generally low in agricultural value, forests being their most common and practical coverage. The subsurface can be characterized as sub-horizontally bedded, discontinuous, thrusted sediments of coarse fluvial sands and gravel (Urk and Enschede formations), overlain by 2-4 m mainly finer, well-sorted eolian cover sand (Twente Formation). The cover sands are sometimes interspersed with thin sheets of washed-off coarser fluvio-glacial deposits. There are three soil types in the study area: sand dunes with little soil development, 'dry' podzol soils (moderately well drained), and 'wet' podzol soils (poorly drained). All the soils are poor in loamy material, and vary between textures of fine sand (in the eolian deposits) to coarse sand (in the fluvial deposits) (Gehrels, 1999).

In the past a large part of the central Veluwe area was characterized by arid drifting sands and extensive heath lands with small oak trees, while villages and pastures were concentrated in the lowlands around the Veluwe. Thus in the mid-eighteenth centuries the Hoge Veluwe consisted almost entirely of drifting sand and heath lands with only ten percent comprising forest and agricultural area. However, the intensive use of the heath lands for tending of sheep and the cutting of heath sods during the Middle Ages brought about a renewed sand drift and the vegetation locally disappeared and the former Pleistocene cover sands were easily eroded by the wind. By the end of the 19th century, the heath lands were no longer used for the tending of sheep or the cutting of heath sods. Large areas of wind-blown sands and heath lands were now forested.

Because of the less fertile sandy soils and deep groundwater, the higher part of the central Veluwe is not used for agricultural purposes, except the existence of some villages at the flanks of the study area which are making a living of agriculture and animal husbandry. At present most part of the central Veluwe is covered with forest with relatively small area of heath and grasslands.

A land cover classification map of the study area was prepared using the Landsat image of August 16, 2002 (Figure 3.12). A large part of the area is covered by forest, heath and grassland with a small share of arable land, open drift sand and build-up areas. According to the land cover classification map the heath and Molinia grass cover 22% of the total area. The forests cover a total of about 63% of the study area. The remaining 15% is covered by the other land cover units. They are mainly grouped into three types: light and dark coniferous, deciduous and mixed forests. The light coniferous forest is mainly composed of Scots pine and Larch trees, Scots pine being the dominant tree in the study area. The dark coniferous forest includes Douglas fir, Spruce and others, Douglas fir being the dominant. The deciduous forest is composed of Oak, Beech, Birch and others, Oak being the dominant tree species in the study area. The land cover map of the area indicates that 20% of the area is covered by light coniferous, 2% by dark coniferous, 3% by deciduous and 38% by mixed forest, thus the mixed forest is by far the dominant forest type in the study area.

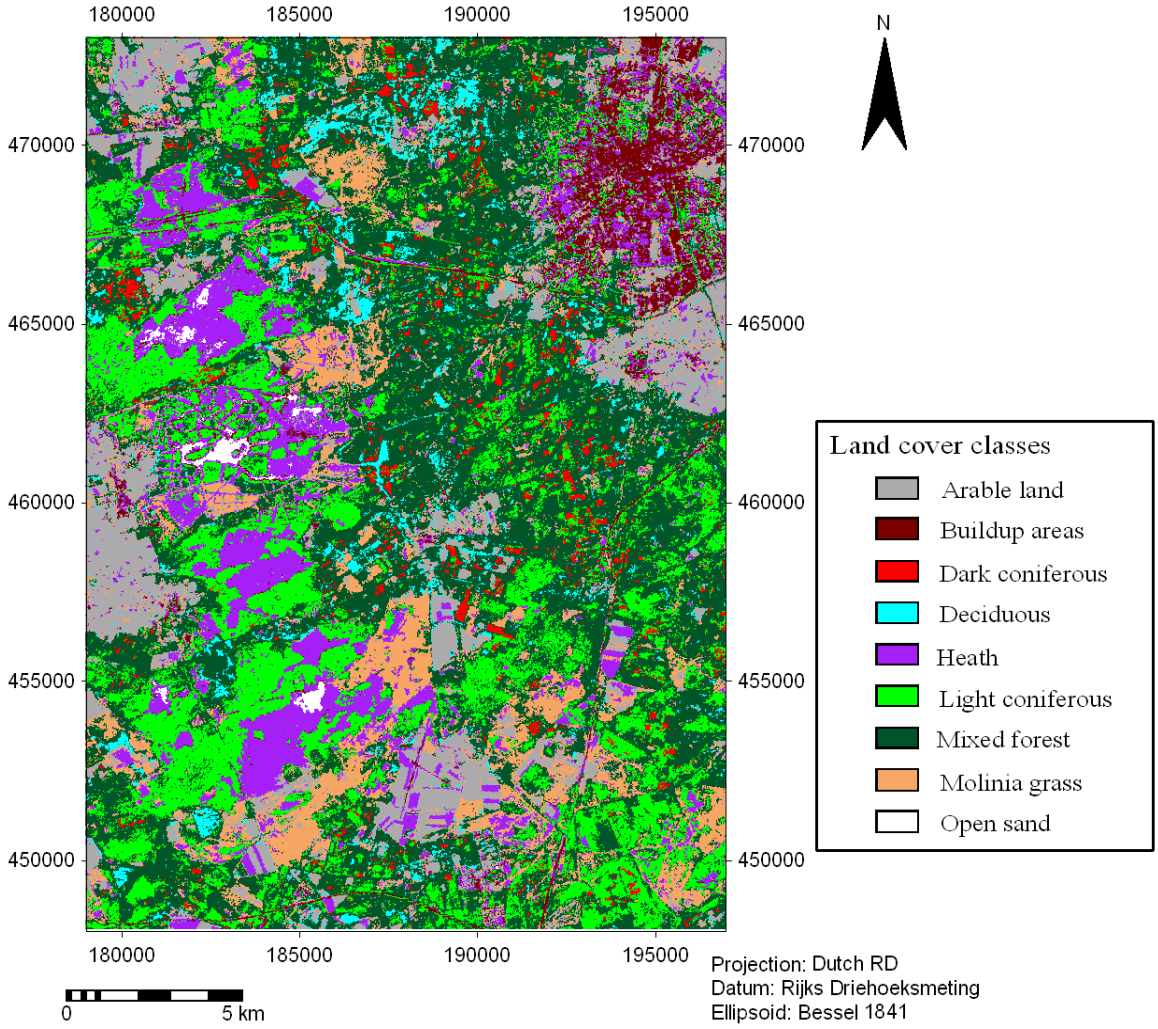

Figure 3.12 Land cover map of the study area

4. Description of available data and field observations

4.1. Available data

4.1.1. Meteorological and borehole data

Daily climatic data (1906-2006) including global radiation, precipitation, relative humidity, hours of bright sunshine, average air temperature, minimum air temperature, maximum air temperature and wind speed from the De Bilt meteorological station were accessed through the archive of Royal Netherlands Meteorological institute (KNMI) (Appendix 3). Daily rainfall data from 1971 up to September, 30, 2007 from stations of Elspeet, Harskamp, Kootwijk and Beekbergen was purchased from the KNMI (Appendix 4).

Table 4.1 Location of rainfall stations

Station name	Coordinates (Dutch RD)		Elevation above NAP (m)
	X	Y	
Elspeet	182000	478000	34
Harskamp	179000	463000	19
Kootwijk	185000	465000	39
Beekbergen	194000	464000	25

Daily groundwater level data for the interest area was accessed from Dino Loket website (http://dinolks01.nitg.tno.nl/dinolks/DINOloket.jsp). A total of about 300 borehole data for the central Veluwe was retrieved from the website, but only six boreholes were selected for modelling purposes based on the representativeness of the major natural vegetation types and availability of long term record data (Appendix 5).

Table 4.2 Selected boreholes and their location

Borehole code	Coordinates (Dutch RD)		Elevation above NAP (m)	Land cover type
	X	Y		
B33D0002	191650	458900	65	Mixed forest
B33A0065	185440	464660	46	Molinia grass
B33A0113	189780	471810	78	Deciduous
B33A0067	181030	463970	26	Light coniferous (Scots Pine)
B33A0103	183390	472340	41	Heath
B33D0217	193505	460835	60	Dark coniferous (Douglas Fir)

4.1.2. Top maps, Satellite images and AHN data

Topographic map of 1: 25000 scale and 5 m resolution was obtained from the National Land Registry (kadaster). The topographic map for the study area is constructed from 25 sheets using the image mosaic function of ERDAS software. The topographic map was then used to georeference the Landsat images and provided useful information during land cover classification.

Sixteen sheets of AHN (Average height of The Netherlands) maps with resolution 5 m of the Veluwe and surrounding area in Grid format and XYZ points representing vegetation height above NAP (New Amsterdam Level) were obtained from the National Land Registry (kadaster).
The satellite images used for the present study are the series of Landsat ETM+7 images from 2000 to 2002. The images of August 26, 2000 and August 16, 2002 were collected from databases as FST files and the image of May 25, 2001 was downloaded from the Geodata warehouse of ITC http://intranet.itc.ni/support/ archive. The geometric and radiometric correction was done using the calibration data from the metadata of the images. The study area is delineated using ILWIS software. The basic image information required for calculation of surface reflectance and leaf area index are extracted from the metadata, and are summarized in Table 4.3.

Table 4.3 List of Landsat ETM+7 images (2000-2002)

No.	Acquisition date	Julian day	Over pass time	Solar zenith angle (degree)	Sun to Earth distance (AU)
1	Aug 26, 2000	239	10:18:37	44	1.0099
2	May 25,2001	145	10:17:30	34	1.0130
3	Aug 16,2002	228	10:15:50	41	1.0123

4.2. Field observations and collected data

A field survey was conducted to collect ground truth data and to have a general understanding of the study area. GPS tracks and way points of different land covers were collected using hand held GPS to assist the georeferencing of the images and land cover mapping of the study area. In addition to this two Museums (visitor's center park Hoge Veluwe and New Land Heritage center Lelystand) were visited during the field trip. A lot of information about the geological formation and the groundwater flow pattern, the forest and soil types of the Veluwe area was acquired from visitor's center park Hoge Veluwe. General information on the land reclamation of the fluveoland and groundwater levels of the area was obtained from New Land Heritage Center.

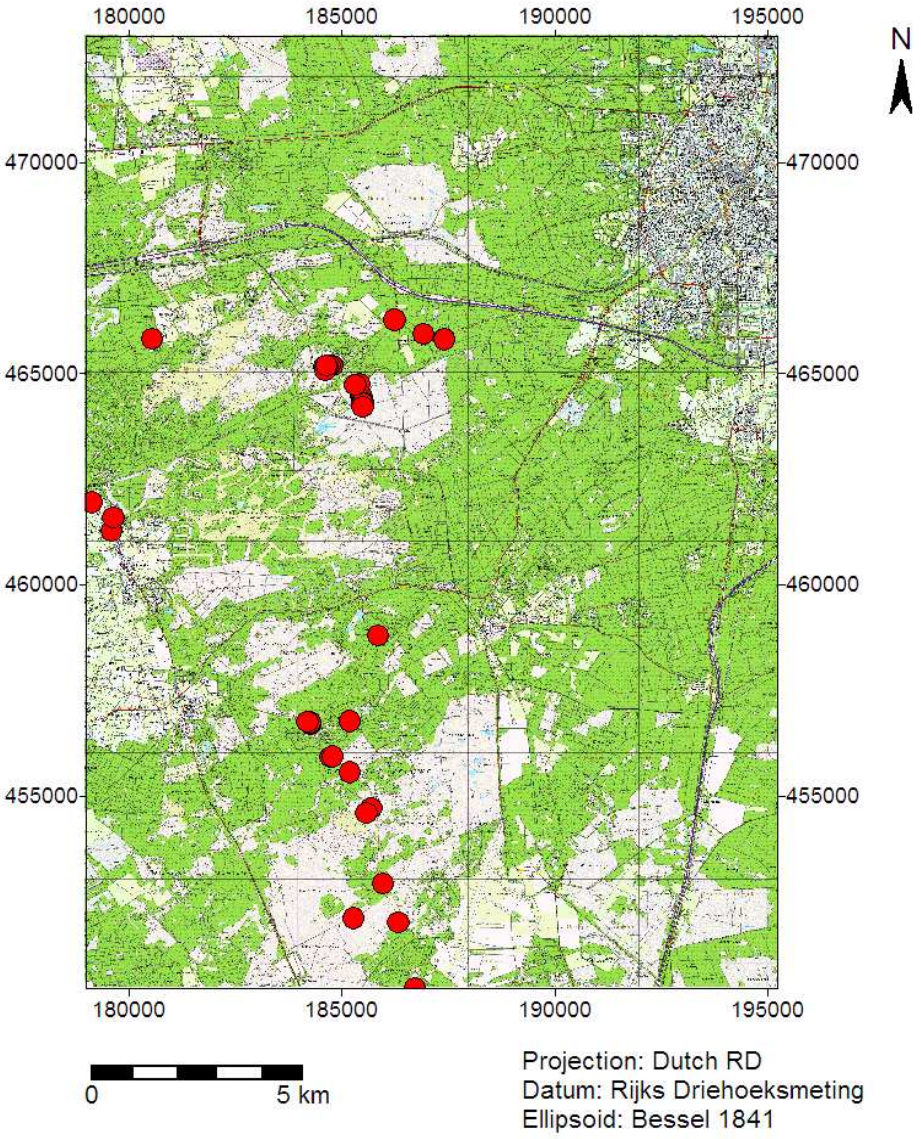

Figure 4.1 Location of collected GPS points

5. Soil water flow modelling

Water flow in the unsaturated zone is predominantly vertical, and can generally be simulated as one-dimensional flow (Romano et al., 1998). In the present study, two different methods were used to simulate the soil water flow in the unsaturated zone. The first method uses a physically based numerical model (SWAP) based on Richards equation (Van Dam, 2000), and the second method applies a conceptual reservoir-type model (EARTH) based on a simplified water balance equation (Van der Lee and Gehrels, 1997).

Six sites (boreholes) were selected to conduct the soil water flow modelling namely: B33A0065, B33A0067, B33A0103, B33A0113, B33D0002 and B33D0217 (Figure 5.1). The selection of the sites was based on the presence and representativeness of the dominant natural vegetation covers and the availability of long record groundwater level measurements. This was done with the help of the land cover map of the area. The main objective of this is to take into account the spatial variation of vegetation and by doing so to assess the influence of each vegetation type on the groundwater recharge of the area. Both the SWAP and EARTH models were applied at the five sites and the calculations with both models were carried out on a daily basis.

5.1. Description of selected borehole sites

B33A0065 – Molinia grass

This site is located near the Radio station in Kootwijk at geographical coordinates of 185440 E and 464660N and at 46 m above NAP. It is found in the central part of the study area about 8 km west of Apeldoorn. The terrain is locally flat with sandy soils. The dominant vegetation type at this location is Molinia grass with small patches of Heath. The length of the grass leaves is 50-60 cm during summer and less during winter (Gehrels, 1999). The grassland is surrounded by Scots pine forests. The average groundwater level at this location is 28 m above NAP and the thickness of the unsaturated zone is about 18 m.

B33A0103 - Heath

Borehole B33A0103 is located at 183390 E and 472340 N geographical coordinates and at 42 m above NAP and about 8 km west of Apeldoorn in the northern end of the study area. In contrast to Radio Kootwijk site the dominant vegetation species in this site is Heath. The area is characterized by sandy soils and the average groundwater level at this location is 20 m above NAP. The thickness of the unsaturated zone is 22 m.

BH33A0067 – Scots pine

Borehole BH33A0067 is found about 12 km west of Apeldoorn at 181030 E and 463970 N geographical coordinates and about 26 m above NAP. The site is located west of the study area and the vegetation is dominated by Scots pine. The area is characterized by sandy soil and shallow groundwater table. The average groundwater level at this location is 23 m above NAP and the thickness of the unsaturated zone is about 3 m.

B33A0113 – Deciduous forest

Borehole B33A0113 is found about 5 km west of Apeldoorn in the northern part of the study area at 189780 E and 471810 N geographical coordinates. Its elevation is about 78 m above NAP. The sediments in this site consist of coarse to very coarse badly sorted fluvial sands and gravel (Gehrels, 1999). The dominant vegetation type is Oak. The average groundwater level in the area is 28 m above NAP. This location is characterized by deep groundwater table in which the thickness of the unsaturated zone is about 50 m.

B33D0217 – Douglas fir forest

This site is located about 6 km south of Apeldoorn. It is in the eastern side of the study area at 193505 E and 460835 N geographical coordinates and 60 m above NAP. The dominant tree species in the area is Douglas fir. The average groundwater level in the area is 35 m above NAP, and the thickness of the unsaturated zone is about 25 m.

B33D0002 – Mixed forest

This site is found about 7km southwest of Apeldoorn at about 65 m above NAP. The vegetation types are mixed i.e. coniferous and deciduous. The average groundwater level is about 42 m above NAP, and the thickness of the unsaturated zone is 23 m.

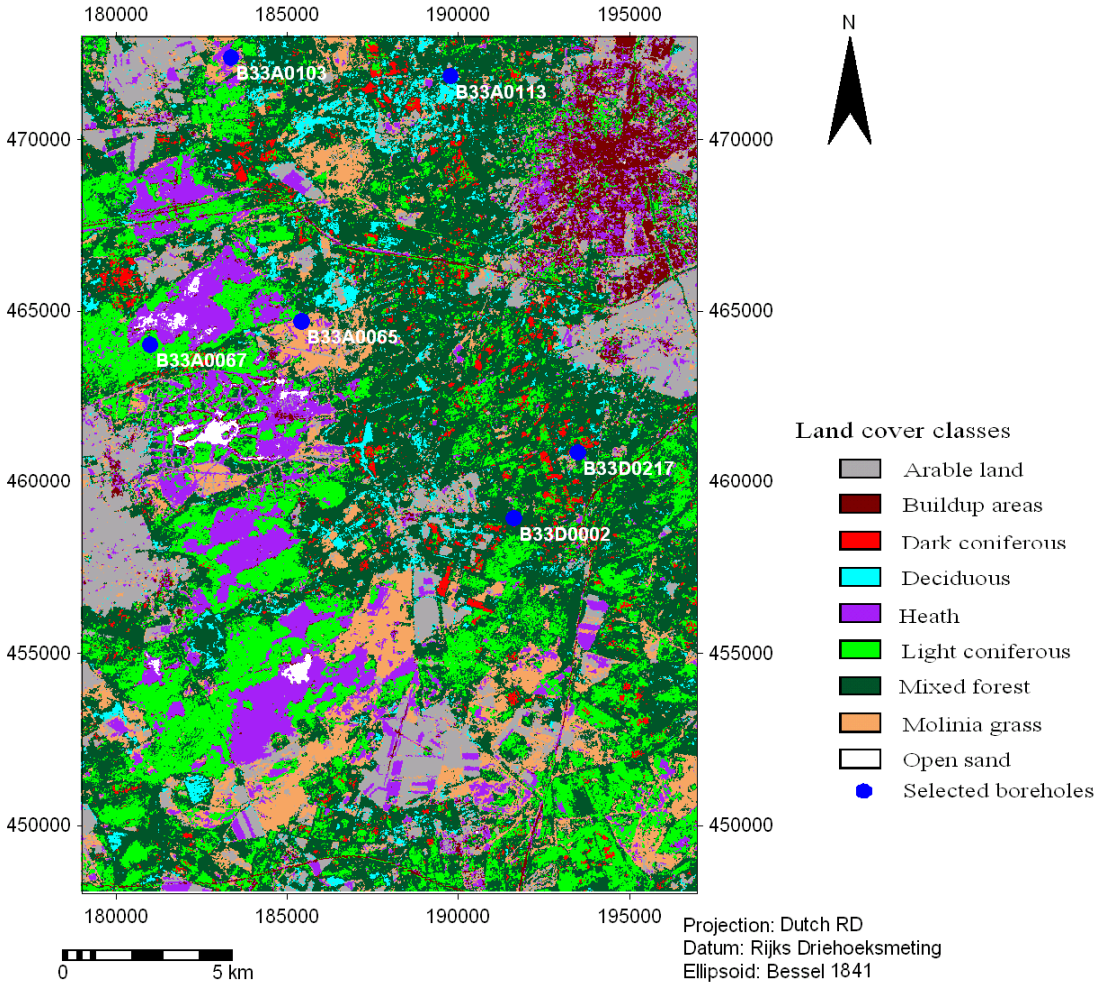

Figure 5.1 Location of selected boreholes

5.2. EARTH modelling

5.2.1. Short overview of EARTH model

The **E**xtended model for **A**quifer **R**echarge and soil moisture **T**ransport through the unsaturated **H**ardrock (EARTH) model version used in this study is EARTH 1.2. It is a lumped parametric hydrologic model used for the simulation of precipitation excess, soil water content, actual evapotranspiration, percolation (recharge) and groundwater level fluctuations. The model represents the unsaturated zone by a number of subsequent reservoirs or modules as illustrate in Figure 5.2.

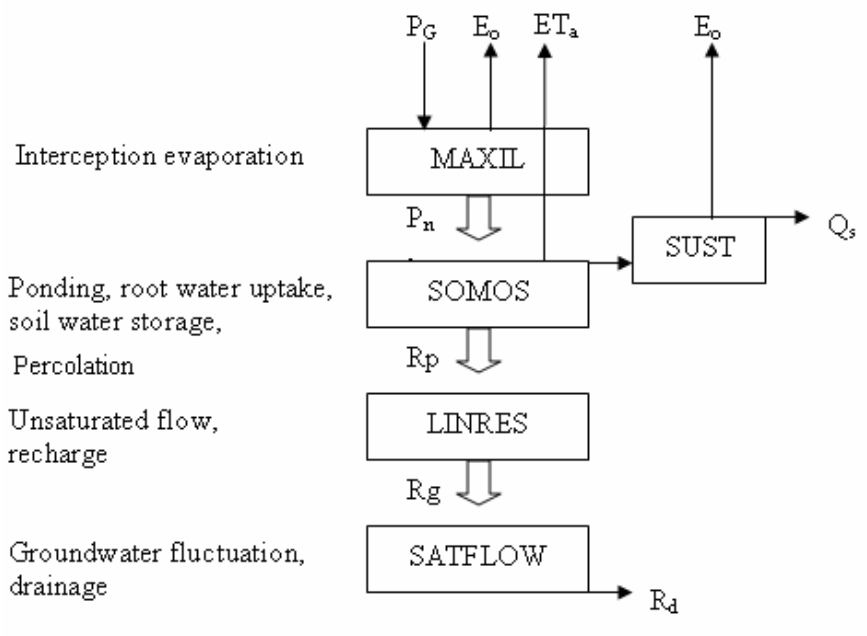

Figure 5.2 Flow chart of EARTH Model (Van der Lee and Gehrels, 1990)

The main model elements are described below.

5.2.1.1. MAXIL: Maximum Interception Loss

Gross precipitation is reduced by interception loss by vegetation canopy before it reaches the ground. The fraction of the precipitation which reaches the soil surface, precipitation excess or net precipitation (P_n) is calculated with a one parameter, the maximum interception loss (MAXIL). P_n is calculated with the formula:

$$P_n = P_G - MAXIL - E_o \quad \textbf{(5.1)}$$

where P_G is gross precipitation [L] and E_o is evaporation from open water body [L].

5.2.1.2. SOMOS: Soil Moisture Storage

The soil moisture storage, SOMOS, describes the water storage in the root zone. It represents the root zone depth including the land surface. In this reservoir infiltrating water (P_n) is subjected to four main processes: actual evapotranspiration, percolation, ponding and /or surface runoff. The remaining part is the change in soil moisture storage which can be calculated according to mass balance as:

$$\frac{dS}{dt} = P_n - ET_a - R_p - E_o(SUST) - Q_s \quad \textbf{(5.2)}$$

where, *S* is the soil water content or soil moisture [L] defined by volumetric soil moisture content (W) and an effective root zone thickness (D) such that S=WD. ET_a represents the actual evapotranspiration rate [L T^{-1}] and R_p is the flux below the root zone [L T^{-1}]. E_o *(SUST)* is the evaporated fraction of ponding water [L T^{-1}] and Q_s is surface runoff [L T^{-1}].
The actual evapotranspiration is determined by potential evapotranspiration, and the actual, maximum and residual soil water contents. The relation between actual evapotranspiration and soil moisture is often taken to be linearly:

$$ET_a = ET_p\left[\frac{S - S_r}{S_m - S_r}\right] \quad \textbf{(5.3)}$$

when the residual soil moisture content (S_r) is assumed to be zero then

$$ET_a = ET_p\left[\frac{S}{S_m}\right] \quad \textbf{(5.4)}$$

where S, S_m and S_r represent actual, maximum and residual soil moisture content respectively [L].

5.2.1.3. SUST: Surface Storage

When the amount of water in SOMOS reaches a certain threshold, defined as saturation ($S=S_m$) and the infiltration rate exceeds percolation rate, ponding or runoff may occur leading to losses i.e. ponding occurs after saturation of the top soil. In the EARTH model surface storage is represented by the reservoir SUST. This reservoir has a maximum capacity denoted by $SUST_{max}$ [L] which is the maximum amount of ponding water that can be stored at the surface. The amount of ponding water greater than $SUST_{max}$ will bring about surface runoff, Q_s [L T^{-1}] which is considered to be loss for recharge calculation cases. As the study area is characterized by highly porous coarse-grained sandy soils zero surface ponding was simulated in the present study. The sandy soils have a high infiltration capacity. As a result the net precipitation usually infiltrates completely. The water balance of the reservoir SUST is:

$$\frac{dSUST(t)}{dt} = P_n(t) - E_p(t) - R_p(t) - E_o(t) \quad \textbf{(5.5)}$$

where E_o represents (Penman) open water evaporation
After passing the root zone the downward flux of the soil moisture from the root zone to the saturated zone is described by Darcy's law:

$$R_p = K(s)\left(\frac{dh_p}{dz} + 1\right) \quad \textbf{(5.6)}$$

where R_p is percolation [L T^{-1}], *K(s)* is the unsaturated hydraulic conductivity as a function of soil water content [L T^{-1}], and dh_p/dz is the hydraulic head gradient taken positive downward. For deep unsaturated zones such as the central Veluwe (study area), the movement of soil water below the root zone is mainly governed by gravity. Capillary gradients usually play a minor role because the water content is near to the soil field capacity. Therefore it can be assumed that the pressure head remains constant with depth, so equation (5.6) can be reduced to:

$$R_p = K(s) \quad \textbf{(5.7)}$$

The unsaturated hydraulic conductivity commonly is described by:

$$K(s) = \left(\frac{S - S_r}{S_m - S_{fc}} \right)^n \quad \textbf{(5.8)}$$

where n is a soil constant, and S_{fc} is the soil water content at field capacity.

5.2.1.4. LINRES: Linear Reservoirs

These reservoirs represent the percolation zone and describe the downward flux from the root zone to the last reservoir, the saturated zone. Moisture percolating down from the soil moisture reservoir (SOMOS) can no longer be lost by evapotranspiration. However, the groundwater table may be deep and therefore there is a delay before the moisture actually reaches the water table. This delay in the percolation zone is modelled by a series of linear reservoirs. The percolation zone (LINRES) redistributes the incoming flux R_p into an outgoing flux R_g [L T^{-1}]. It needs only two parameters, the time constant (f) and number of reservoirs (n). It is useful and accurate optimization part of the model in order to fit the calculated and measured groundwater levels. The time coefficient f smoothes the input in time and the number of reservoirs determines the place in time of the weighed center.
The percolation-zone transfer function is based on the general form of a convolution integral describing the output of a dependent variable $R_g(t)$ as a result of a variable input (percolation below the root zone $R_p(t)$) through a system (the percolation zone) that is represented by a transfer function:

$$R_g(t) = \int_0^\infty R_p(t-\tau) F(\tau) d(\tau) \quad \textbf{(5.9)}$$

where F is defined as time lag τ and R_g is described in terms of R_p at time t-τ.

5.2.1.5. SATFLOW: Saturated Flow

SATFLOW is the last reservoir of the EARTH model. It calculates the groundwater level with the estimated recharge from the percolation zone. This is a simple one-dimensional parametric groundwater model, where the parameters have a semi-physical meaning. This system is described by a first order differential equation (Van der Lee and Gehrels, 1990) as:

$$\frac{dh}{dt} = \frac{R}{STO} - \frac{h}{RC} \quad \textbf{(5.10)}$$

where *STO* is storage coefficient [-], *R* is recharge [L T^{-1}], *h* is groundwater level [L] above local drainage base H and *RC* is saturated recession coefficient [-].
According to Van der Lee (1989), the recession coefficient is proportional to storage coefficient and the drainage resistance, described by the formula:

$$RC = \beta . STO . \gamma \quad \textbf{(5.11)}$$

where γ is specific drainage resistance [T], and β is coefficient of proportionality [-].
When the moisture reaches the groundwater table it will affect the water level according to the aforementioned reservoir function, equation 5.10. The water flow fluctuates around an average value where outflow is balanced by average recharge. According to De Vries (1974), the outflow (drainage flux R_d [L T^{-1}]), which is assumed to have a linear relation with the groundwater level is described by:

$$R_d = \frac{h_d}{\gamma} \quad \textbf{(5.12)}$$

where h_d is the groundwater level above some reference level [L], and γ is the specific drainage resistance [T].

For horizontal flow to a drainage system, the specific drainage resistance γ can be written as:

$$\gamma = \frac{L^2}{\beta T} \quad \textbf{(5.13)}$$

where L is flow path [L], T is aquifer transmissivity [$L^2\ T^{-1}$], and β is a shape factor [-] varying between 2 for radial flow and 4 for parallel flow.

5.2.2. Model input

The input for EARTH model includes meteorological data which are defined as upper model boundary, hydrological data and input values for model parameters. The meteorological data includes daily precipitation and potential evapotranspiration data. The hydrological data refers to daily groundwater level data which were used for model calibration. The model parameters include maximum, initial and residual soil moisture, soil moisture at field capacity, saturated hydraulic conductivity, unsaturated reservoir coefficient, saturated recession coefficient, number of reservoirs, storage coefficient, initial groundwater level and local base level.

In the present study, the upper boundary of the EARTH model is defined by daily net precipitation and potential evapotranspiration at the soil surface. (Figure 5.3) The net precipitation P_n [$L\ T^{-1}$] was obtained by subtracting the interception loss P_i [$L\ T^{-1}$] from the observed gross precipitation P_G [$L\ T^{-1}$] as:

$$P_n = P_G - P_i \quad \textbf{(5.14)}$$

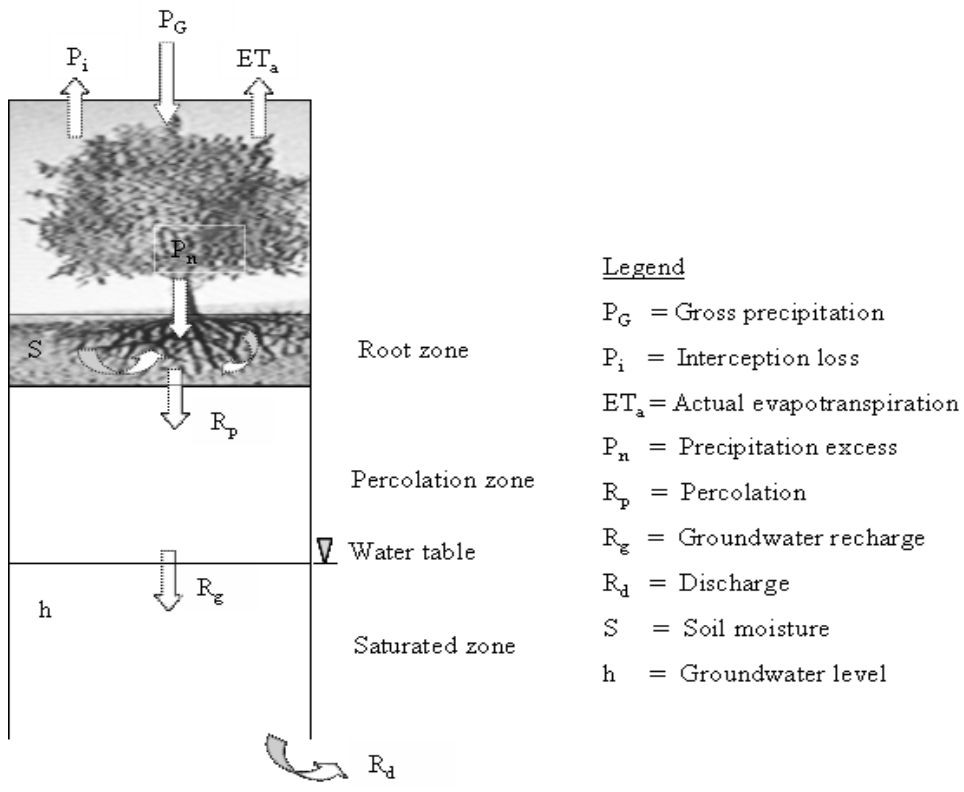

Figure 5.3 Schematization of soil water flow in the model

The procedures employed to calculate the daily precipitation, interception and potential evapotranspiration are presented below.

5.2.2.1. Precipitation (P_G)

The daily precipitation data for twenty years was obtained by spatial interpolation of daily precipitation records from the four meteorological stations of Elspeet, Harskamp, Kootwijk and Beekbergen which are located in the vicinities of the six selected sites. Van den Berg (1995) reported that the station Kootwijk shows a deviating trend in comparison to the surrounding KNMI stations (Elspeet, Kootwijk, Beekbergen and Harskamp). Hence rainfall analysis was carried out to check if the problem still exists in the current modelling period (1973-1992). Daily and monthly correlation of the Kootwijk station with the other three stations was analyzed and the result shows that the station Kootwijk is highly correlated with the other stations (Table 5.1 and Table 5.2). Besides the monthly and yearly rainfall for the four stations indicate that the trend of the Kootwijk station nicely fits with the other stations (Figure 5.4 and Figure 5.5). From this analysis the Kootwijk station does not show any deviating trend from the other stations in the current modelling period, and can therefore be used in the present study together with the other three stations.

Table 5.1 Daily rainfall correlation result

Station name	Elspeet	Kootwijk	Beekbergen	Harskamp
Elspeet	1			
Kootwijk	0.89	1		
Beekbergen	0.88	0.91	1	
Harskamp	0.88	0.92	0.9	1

Table 5.2 Monthly rainfall correlation result

Station name	Elspeet	Kootwijk	Beekbergen	Harskamp
Elspeet	1			
Kootwijk	0.98	1		
Beekbergen	0.95	0.96	1	
Harskamp	0.97	0.99	0.95	1

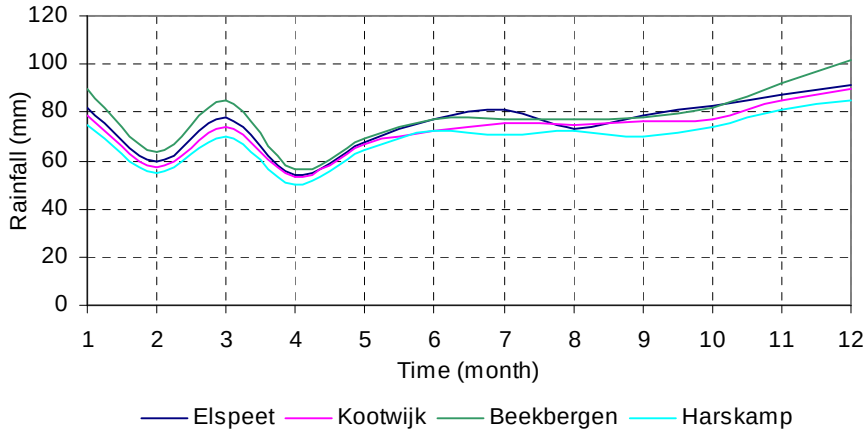

Figure 5.4 Mean monthly rainfall for the four stations (1973-2006)

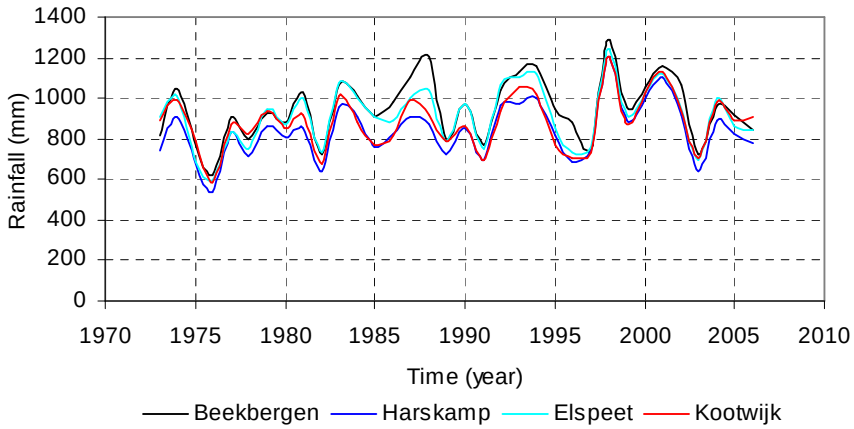

Figure 5.5 Annual rainfall for the four stations (1973-2006)

5.2.2.2. Canopy interception (P_i) and Potential evapotranspiration (PET)

Canopy interception (P_i)

Interception is a significant component of the water balance for forests, as the rainfall intercepted is not available for recharge. Due to a high leaf area index many forests are capable of intercepting significant amounts of precipitation. Studies of Rutter et al. (1971) and Cooper and Lockwood (1987) show that interception loss is high in temperate humid climates where precipitation is distributed evenly over the seasons. Thus for forests the processes of interception and transpiration should be considered separately. In the present study, the interception loss is calculated separately as a percentage of gross precipitation. Interception loss for different forest types is provided by Dolman et al. (2000). They found P_i = 26% for light coniferous (Scots pine), 38.5% for Douglas fir, 28.2% for deciduous and 27% for mixed forest. The interception loss for Molinia grass and Heath is assumed to equal and is taken to be 6%.

Potential evapotranspiration (PET)

Quantitative information on the response of forest transpiration to changing environmental factors is relevant for water management. Evapotranspiration is one of the elements that influence the recharge process and the reliability of recharge estimates. Potential evapotranspiration may be computed by any of several methods, but data availability for a particular area is a governing factor. Evapotranspiration of forest depends on external factors such as atmospheric conditions and soil water status and on internal factors such as tree physiological and biometrical conditions. Forest evapotranspiration is often modelled in terms of the single big leaf approach based on the Penman-Monteith equation (Monteith, 1965). In the present study, the daily potential evapotranspiration is calculated using two methods: Makkink reference crop evapotranspiration and the Penman-Monteith equation.

Makkink's method needs only average air temperature and incoming solar radiation. It is widely used in the Netherlands. The climatic data are obtained from De Bilt meteorological station. Hence, daily reference evapotranspiration is calculated using the reference crop evapotranspiration method according to Makkink defined by:

$$E_r = 0.65 \frac{\Delta}{\lambda_v (\Delta + \gamma)} K \downarrow \qquad \textbf{(5.15)}$$

where E_r is reference evapotranspiration [mm d^{-1}], Δ is slope of saturation vapour pressure curve [kPa $^oC^{-1}$], λ is latent heat of vaporization [MJ kg^{-1}] and K is incoming solar radiation [MJ $m^{-2}d^{-1}$].

The Makkink reference evaporation is then multiplied by a suitable crop factor to obtain an estimate of the potential evapotranspiration of an optimally growing crop as:

$$ET_p = f_M E_r \quad \textbf{(5.16)}$$

where f_M is an empirical crop factor [-] relating the rate of evapotranspiration to the type of vegetation.

Table 5.3 Makkink crop factors

Vegetation type	Crop factor
Molinia grass	0.95
Heath	0.95
Scots pine	0.64
Douglas fir	0.80
Deciduous	0.62
Mixed	0.99

The Makkink crop factors for each vegetation type under consideration are obtained from different sources. The crop factors for Molinia grass and Douglas fir is taken from Gehrels (1999) while crop factors for light coniferous (Scots pine), deciduous and mixed forest are taken from Dolman et al. (2000). According to Gehrels (1999) the water consumption of heath is almost the same as grass. Thus the crop factor for Heath is assumed to be the same as for Molinia grass. The Makkink crop factors for each vegetation types are summarized in Table 5.3.

As a second method, daily meteorological data consisting of air temperature, solar radiation, wind speed and air humidity from the De Bilt KNMI meteorological station are used to calculate daily potential evapotranspiration according to Penman-Monteith equation (Monteith, 1965):

$$\lambda ET = \frac{\Delta(R_n - G) + \rho_a C_p \dfrac{(e_s - e_a)}{r_a}}{\Delta + \gamma\left(1 + \dfrac{r_s}{r_a}\right)} \quad \textbf{(5.17)}$$

where ET is the potential transpiration rate of the canopy [mm d^{-1}], R_n is net radiation [MJ m^{-2} d^{-1}], Δ represents the slope of the saturation vapour pressure [kPa $^oC^{-1}$], G is soil heat flux [MJ m^{-2} d^{-1}], (e_s-e_a) represents the vapour pressure deficit [kPa], ρ_a is the mean air density at constant pressure [Kg m^{-3}], C_p is the specific heat of the air [MJ kg^{-1} $^oC^{-1}$], λ is latent heat of vaporization [MJ kg^{-1}], γ is psychrometric constant [kPa $^oC^{-1}$], and r_s [s m^{-1}] and r_a [s m^{-1}] are the (bulk) surface and aerodynamic resistance.

Net radiation is aggregated as net incoming short wave radiation and net outgoing long wave radiation, and G is assumed to be zero for the daily evapotranspiration calculations.

In addition to the meteorological data, plant biophysical parameters such as canopy height, displacement height, the aerodynamic terms and the canopy reflectance are also necessary to apply the aforementioned Penman-Monteith equation. The approaches used to calculate the plant biophysical parameters are described as follows.

5.2.2.3. Vegetation biophysical parameters

Surface Reflectance (R_o)

The surface reflectance of the different vegetation types under consideration are derived from Landsat satellite data. Three images of Landsat ETM+7 (August 26, 2000, May 25, 2001 and August 16, 2002) were used for the calculation of surface reflectance. The Enhanced Thematic Mapper plus (ETM+) sensor is a multi-spectral scanning radiometer that is carried on board of Landsat 7 satellite. The sensor has provided nearly continuous acquisitions sine July 1999 with a 16-day repeat cycle and 8 bands with three different resolutions over a swath width of 183 km (Table 5.4).

Image pre-processing tasks such as geometric, radiometric and atmospheric corrections were carried out to reduce the distortion in the images created by atmospheric and satellite conditions before the calculation of the parameters. The raw images have a UTM coordinate system but do not contain reference to the location where the data is acquired. In order to match the acquired data to the real world coordinate, the image is georeferenced using the top map and the local coordinate system of the study area which is created using the Dutch RD coordinate system.

Table 5.4 Spectral bands of Landsat ETM+7

Band number	Wavelength region	Spectral range (mm)	Resolution	Swath width (km)	Repeat cycle (day)
1	VIS	0.45-0.52	30	183	16
2	VIS	0.52-0.60	30	"	"
3	VIS	0.63-0.69	30	"	"
4	NIR	0.76-0.90	30	"	"
5	SWIR	1.55-1.75	30	"	"
6	TIR	10.42-12.50	60	"	"
7	SWIR	2.08-2.35	30	"	"
8	PAN	0.52-0.90	15	"	"

The surface reflectance is an important physical parameter in determining the net radiation available on the earth's surface. To calculate the reflectance, only the spectral bands in the visible, near infrared and shortwave infrared regions are important. Thus the DN values of band1, band2, band3, band4, band5 and band7 were converted to radiance using the calibration coefficients (gains and offsets) provided as metadata with the images (Appendix 1). The digital number (DN) values of the geometrically corrected ETM+ data were converted to at-satellite radiance using the following equation (Markham and Barker, 1987):

$$L_\lambda = \left(\frac{LMAX_\lambda - LMIN_\lambda}{QCALMAX - QCALMIN} \right) * (DN - QCALMIN) + LMIN_\lambda \quad \textbf{(5.18)}$$

where L_λ is at-satellite radiance [W m^{-2} sr^{-2} μm^{-1}], *QCAL*=DN, $LMAX_\lambda$ and $LMIN_\lambda$ are the spectral radiances that are scaled to *QCALMAX* and *QCALMIN* in [W m^{-2} sr^{-2} μm^{-1}], respectively, *QCALMAX*=255, and *QCALMIN*=1.

At-satellite radiances were then converted to at satellite reflectance using the following equation:

$$\rho_\lambda = \frac{L_\lambda \pi d^2}{ESUN_\lambda * \cos\theta_z} \quad \textbf{(5.19)}$$

where ρ_λ is reflectance at sensor [W m^{-2} sr^{-2} μm^{-1}], d^2 is Earth-Sun Distance [AU], $ESUN_\lambda$ is band dependent exoatmospheric irradiance [W $m^{-2}\mu m^{-1}$] and θ_z is solar zenith angle [deg].

The landsat ETM+ has narrow band in the atmospheric window. Hence the narrow band at-satellite reflectances are combined to obtain planetary broadband albedo (reflectance) according to Liang et al. (2003) as:

$$R_p = 0.356 * \alpha_1 + 0.13 * \alpha_3 + 0.373 * \alpha_4 + 0.085 * \alpha_5 + 0.072 * \alpha_7 - 0.0018 \quad \textbf{(5.20)}$$

where, R_p is planetary broadband albedo [W $m^{-2} sr^{-2} \mu m^{-1}$], α_i represent spectral reflectance

Thus the Planetary broadband albedo is converted to broad band surface reflectance through a simple atmospheric correction method formulated by Chen and Ohring (1984) as:

$$R_o = \frac{R_p - R_m}{\tau^2} \quad \textbf{(5.21)}$$

where R_o is surface reflectance, R_p is planetary broadband reflectance (albedo), R_m is the reflectance from non-reflective body, deep water body and τ is the two-way atmospheric transmittance factor. τ^2 is taken to be 0.5.

The forests show lower values of surface reflectance while grass and heath show relatively higher values. The highest values of the calculated reflectance belong to the open sand. The calculated surface reflectance for the different land cover types are presented in (Table 5.5).

There is no significant difference in the reflectance values obtained from the three images. Thus the values obtained from image, August, 16, 2002, were used for the calculation evapotranspiration.

Table 5.5 Surface reflectance of the different land cover types

Image name	Molinia grass	Heath	Scots pine	Deciduous	Douglas fir	Mixed	Open sand
Aug 26, 2000	0.17	0.16	0.14	0.20	0.15	0.11	0.40
May 25, 2001	0.21	0.17	0.13	0.23	0.17	0.17	0.58
Aug 16, 2002	0.20	0.17	0.13	0.22	0.15	0.14	0.46

To calculate the leaf area index, first Normalized Difference Vegetation Index (NDVI) and Fractional vegetation cover (f_c) were calculated.

Normalized Difference Vegetation Index (NDVI)

NDVI captures the contrast between the visible-red and near-infrared reflectance of vegetation canopies, and is defined as:

$$NDVI = \frac{\rho_n - \rho_r}{\rho_n + \rho_r} \quad \textbf{(5.22)}$$

where, ρ_n and ρ_r are reflectance in the near infrared and red bands respectively.

NDVI provides an estimate of vegetation health and a means of monitoring changes in vegetation over time. The reason NDVI is related to vegetation is that healthy vegetation reflects very well in the near infrared part of the spectrum.

Fractional vegetation cover (f_c)

Fractional vegetation cover is the ratio of vegetation occupying a unit area. It is an important parameter used for separation of non-vegetated, partially vegetated and densely vegetated land surfaces. In this study this parameter is used to derive LAI. The formula by Choudhury et al. (1994) was applied to determine the f_c as:

$$f_c = \left(\frac{NDVI_{\max} - NDVI}{NDVI_{\max} - NDVI_{\min}} \right)^p \quad \textbf{(5.23)}$$

Where, p represents the ratio of the leaf angle distribution, and is taken to be 0.625, $NDVI_{max}$ is the NDVI value of full vegetation, $NDVI_{min}$ is the NDVI value of the bare soil, $NDVI$ is the NDVI value of the current pixel (NDVI map).

Leaf Area Index (LAI)

Leaf Area Index is the ratio of total upper leaf surface of vegetation divided by the surface area of the land on which the vegetation grows. It is an important surface biophysical parameter as a measure of vegetation cover and vegetation productivity.

The exponential relationship formulated by Choudhury (1987) cited in French et al. (2003) is used to determine the LAI as:

$$LAI = \frac{\log(1 - f_c)}{-\Lambda} \quad \textbf{(5.24)}$$

where f_c is the fractional vegetation cover and Λ is the leaf angle distribution taken to be 0.5.

In this study the LAI ranges from 0 for bare soil (open sand) to 10 for Douglas fir forest and is used as input for the SWAP model for the calculation of potential soil evaporation.

Canopy height (h)

Canopy height is one of the important physical parameter in calculating evapotranspiration using the Penman-Monteith equation. In the current study, vegetation height was determined with LIDAR derived AHN (Average Height of the Netherlands) data. One AHN image was prepared using the image mosaic function of ERDAS software from the sixteen AHN maps which were obtained in grid format. The AHN map of the study area was created after importing the image to ILWIS (Figure 3.2).

The XYZ points which represent vegetation (canopy) heights above New Amsterdam Level, NAP, were converted to an ILWIS raster map for each map sheet with Dutch RD coordinate system and with the same resolution to the AHN maps, and 16 vegetation height raster maps were produced. These maps contain vegetation heights and zeros for the agricultural and build-up areas. The zero pixels cannot be used in the comparison with the AHN map. Thus pixels with zero values were assigned to have undefined values. There also seem to be some zones with zeros probably as a result of poor flight coverage. This part of the image was removed for the sake of calculation. Finally one vegetation height map is produced from the 16 raster map sheets (Figure 5.6).

To obtain the vegetation (canopy) height from soil surface the standard AHN map was subtracted from the vegetation height above NAP map. Finally the average height for each forest type is calculated by using the cross operation in ILWIS from the vegetation height map and land cover map (Figure 5.7). Accordingly, the canopy height of Deciduous, Light coniferous, Dark coniferous and Mixed forest is found to be 17, 18, 19 and 21 meters respectively. Bosveld (1999) reported a value of 18 m for the height of matured Douglas fir (dark coniferous) in the study area. It is difficult to compare the AHN derived data with the results obtained by more traditional methods. Laser data are taking random samples with centimetres accuracy which are aggregated into 5x5 m pixels. Laser data are therefore not measuring maximum canopy heights. The pixel values should be interpreted as average vegetation height in the pixel.

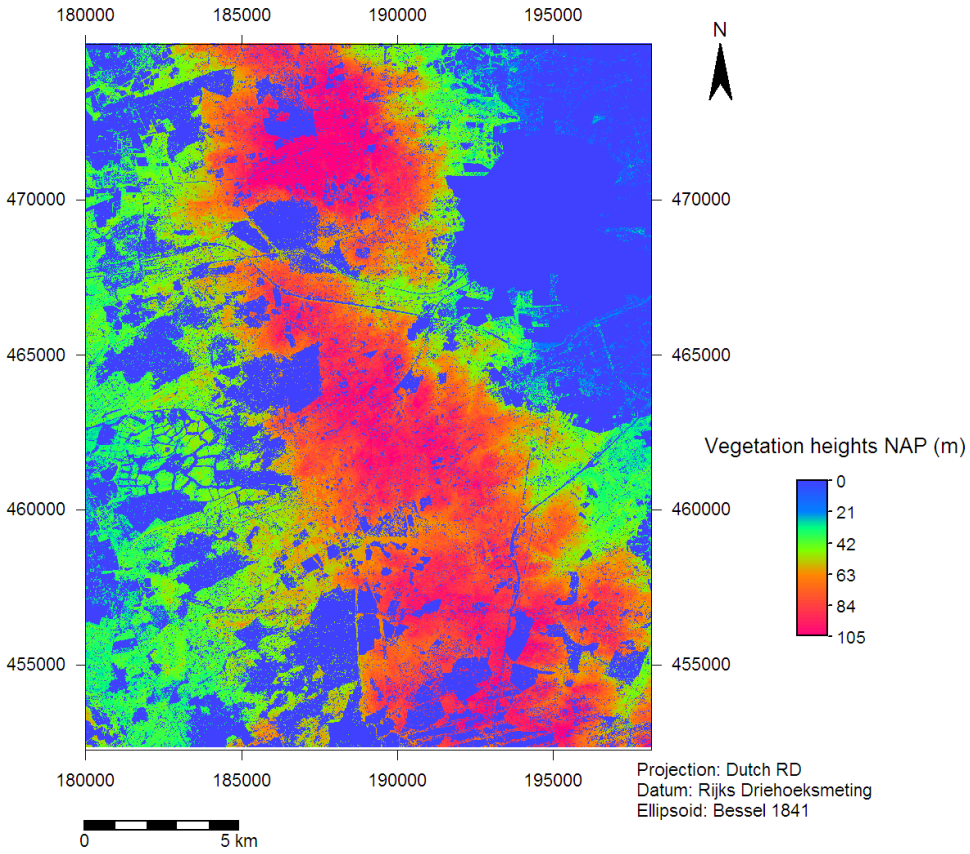

Figure 5.6 Vegetation heights above NAP

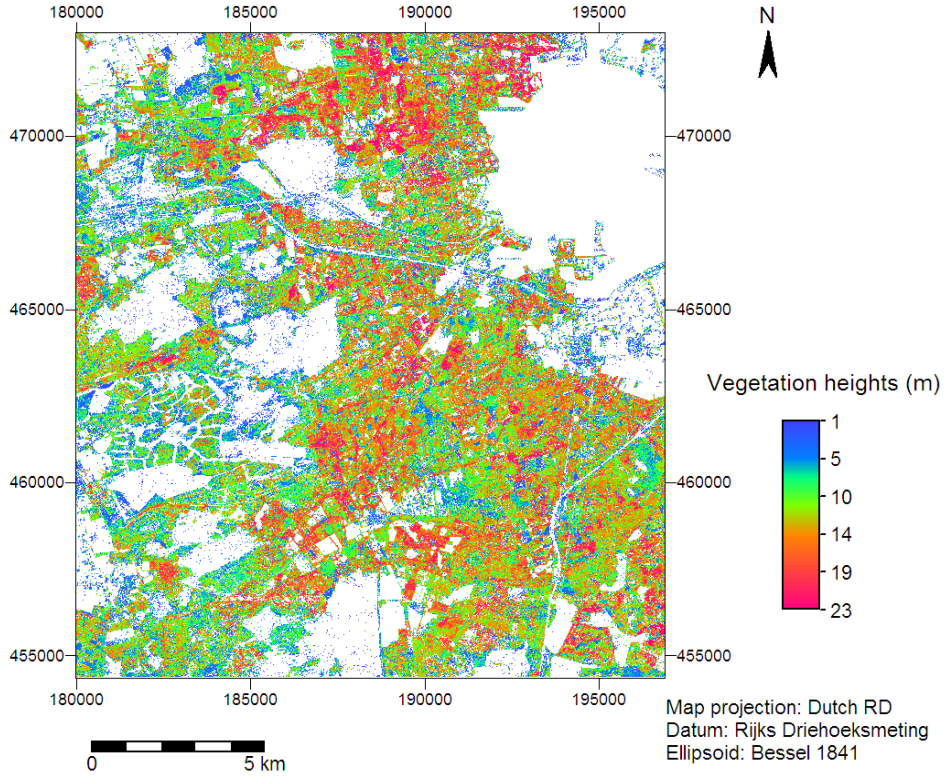

Figure 5.7 Vegetation heights from surface

Displacement height (d) and surface roughness for momentum transfer (z_{om})

Displacement height and surface roughness for momentum transport are also important parameters in calculating evapotranspiration and both are estimated using the empirical relationship with canopy height(Allen et al., 1998) as:

$$d = 0.67h \quad \textbf{(5.25)}$$

$$z_{om} = 0.123h \quad \textbf{(5.26)}$$

Where d is displacement height [m], h is canopy height [m] and z_{om} surface roughness for momentum transport [m].

Aerodynamic (r_a) and canopy resistances (r_s)

The aerodynamic resistance r_a for each vegetation type was calculated following Thom (1975). Under neutral atmospheric conditions r_a is given by:

$$r_a = \frac{1}{k^2 u_z}\left[\ln\left(\frac{z-d}{z_o}\right)\right]^2 \quad \textbf{(5.27)}$$

where z is measurement height above surface [m], u_z is wind speed at height z [m s^{-1}], d is zero plane displacement height [m], z_o is roughness length governing momentum transfer [m] and k is von Karman's constant. Accordingly the aerodynamic resistance for the dark and light coniferous forest was found to be 5.7, for deciduous forest 6.6, for mixed forest 6.8 and for grass and heath 33 and 38 m s^{-1} respectively.

Accepted canopy resistances for some of the natural vegetations in the study area are not available. The canopy resistance for the vegetation types under consideration are taken from different previous studies. Gehrels 1999 reported a minimum canopy resistance value of 80 s m^{-1} for the Molinia grass on the sandy soils at Radio Kootwijk site. The same canopy resistance value is assumed for Heath. Bosveld (1999) reported a canopy resistance value of 100 s m^{-1} for Douglas fir in the Kootwijk site. In this study, the same value is assumed for Scots pine. Resistance values of 61 and 119 s m^{-1} were used for mixed and deciduous forests respectively (Wullschleger et al., 2000).

5.2.3. Model parameterization

The EARTH model requires different parameters for the different (reservoirs). The first reservoir has one parameter, MAXIL. The SOMOS reservoir consists of five parameters, namely: saturated moisture content θ_s, residual moisture content θ_r and soil water content at field capacity θ_{fc}, saturated hydraulic conductivity K_s and the effective root depth D. The percolation zone is characterized by the number of reservoirs n and time constant (reservoir coefficient) f. Finally, the SATFLOW reservoir has saturated recession constant RC, storage coefficient STO, initial groundwater and local base level H_{base} as its parameters. In the present study, different approaches were used to estimate the unknown parameters. Some of them are determined from literature values and others are determined through optimization.

The soil water parameters θ_s, θ_{fc}, and θ_r represent the soil water content at saturation, field capacity and residual respectively over a depth interval in which soil is available to roots (effective root depth). The effective root depth is also the depth interval with high soil water content fluctuations. For the study area, Gehrels (1999) reported that the highest soil water contents and largest seasonal variations are present down to about 0.5 m and seasonal variations are still considerable between 0.5 and approximately 1.2 m.

For forest, Tiktak and Bouten (1990) defined the root zone as the layer in which 80% of the water uptake by the roots takes place, and in their study at two Douglas fir stands in the Veluwe

(Speulderbos and Kootwijk), they encounter a root depth of 80 cm at both locations. Based on these explanations the root depth for forest was fixed at 80 cm. For Molinia grass at Kootwijk Gehrels (1999) reported a root zone depth of 60 cm. The same value, 60 cm, was assumed for Molinia grass and Heath.

The average residual and maximum soil water content was obtained by multiplying the measured volumetric water content by the effective root zone depth. The measured volumetric saturated and residual water content and saturated hydraulic conductivity were taken from Gehrels (1999).

The storage coefficient STO is highly sensitive to estimate recharge from groundwater flow modelling and it is unsound to determine its value using an optimization program. From tabulated specific yield values the average value for coarse sand is about 0.27 with a minimum of 0.2 and a maximum of 0.35 (Fetter and Lee, 1994). The specific yield for the fluvio-glacial coarse-grained sandy soils of the study area is about 0.3 (Gehrels, 1999). For the present study a value of 0.25 is assumed with slight changes during calibration for some sites.

The specific drainage resistance was calculated using equation 5.13. Due to the elliptical shape of the regional topography, the groundwater flow pattern of the Veluwe area is somewhere between radial and parallel flow pattern. Thus a value of 3 is assigned for the shape factor beta and the value of the aquifer transmissivity is 6000 $m^2 d^{-1}$ (Gehrels, 1999). The flow path length to the drainage base is taken to be about 20 km. Finally the drainage resistance was found to be 22222 days.

The saturated recession coefficient RC is determined from the empirical equation 5.11. The value of drainage resistance was taken as calculated above and since the position of the sites is near the water divide, the value for the proportionality constant β is approximated to be 1. For the storage coefficient a value of 0.25 is assumed. Based on these assumptions the average recession coefficient is found to be 5500 days. However, the value is slightly modified during calibration for some sites.

The local base level or drainage base is an additional important parameter in the model calibration. The study area is characterized by relatively deep groundwater table with thick sandy unsaturated zones increasing from nearly 4 m along the edges to about 50 m in the centre. The drainage base is partly formed by a number of streams at an average elevation of 10 m above NAP and partly by the Veluwe Lake at 0 m above NAP. An average elevation of 5 m above NAP was assumed for drainage base in the present study.

5.3. SWAP modelling

5.3.1. Short overview of SWAP model

Many model codes exist that describe soil water flow in the unsaturated zone based on numerical solution of Richards equation of which the **S**oil-**W**ater-**A**tmosphere-**P**lant System (SWAP) is one of the most thoroughly documented and most powerful**.** SWAP is a one-dimensional soil physical finite-difference numerical model describing water flow in the unsaturated or partly saturated soils based on Richards equation (Van Dam, 2000). Most of the unsaturated soil water flow models are mainly focused on shallow water table conditions. However SWAP has previously been applied and validated for the simulation of deep water table conditions in the Veluwe (Gehrels, 1999).

The upper boundary of the model is defined by the soil surface with or without crop and the atmospheric conditions. The lateral boundary simulates the interaction with surface water while the lower boundary can be located in the unsaturated zone or on the top of the groundwater system.

The SWAP soil column is divided into homogenous compartments for which the transport and balance equations of water are solved. The model solves the Richards equation numerically if subjected to specific initial and boundary conditions with known relations between the soil water content (θ), pressure head (h) and unsaturated hydraulic conductivity (K).The accuracy of modelling groundwater recharge depends to a great extent on the exact knowledge of these soil hydraulic function.There are two options to obtain soil hydraulic function: one can be obtained directly from field measurement in tubular forms and the other is analytical function. In this study, tabular data from Gehrels (1999) was used.

During the process of water movement in the unsaturated zone the effect of roots is crucial, thus this factor is added to the Richards equation as a sink term R_w, expressing the rate of water uptake by plant roots per unit volume of soil (equation 2.5).

SWAP simulates vertical transport of water in the unsaturated zone, and subtracts the losses due to interception evaporation and transpiration from the input, rainfall, and determines change in storage and recharge. Daily model outputs include simulated actual soil evaporation Ea, actual transpiration Ta, and flow across the bottom of soil profile and moisture distribution in the soil profile.The model computes the potential transpiration rate T_p which is governed by atmospheric conditions. The potential root water extraction rate at certain depth, $S_p(z)$ may be determined by the root length density. However, in many applications of SWAP a uniform root length density is assumed (Feddes et al., 1978):

$$S_p = \frac{T_p}{D_{root}} \qquad \textbf{(5.28)}$$

Where D_{root} is the root layer thickness.

SWAP takes into account the water and salinity stresses and this is described by the function proposed by Feddes et al. (1978):

$$S_a(z) = \alpha_{rw}\alpha_{rs}S_p(z) \qquad \textbf{(5.29)}$$

Where $S_a(z)$ is actual root water extraction rate, and α_{rw} and α_{rs} are dimensionless reduction factors due to water and salinity stress, respectively.

The actual transpiration rate *Ta* (cm/day) then can be obtained by integrating *Sa(z)* over the root layer.

SWAP can separate potential soil evaporation and transpiration for partly covered soils using Leaf Area Index (LAI) or Soil Cover Fraction (SCF). The potential evaporation of soil under a standing crop can be derived from the potential evapotranspiration according to the equations proposed by Goudriaan (1977) and Belmans (1983) cited in Van Dam (2000):

$$E_p = ET_p e^{-k_{gr} LAI} \quad \textbf{(5.30)}$$

where E_p is potential soil evaporation rate [cm d^{-1}], ET_p is potential evapotranspiration rate [cm d^{-1}], k_{gr} is extinction coefficient for global solar radiation [-] and LAI is Leaf area index.

In case the leaf area index is unknown the soil cover fraction (SC) might be used to determine E_p:

$$E_p = (1 - SC) ET_p \quad \textbf{(5.31)}$$

In the present study, SWAP uses leaf area index to estimate potential soil evaporation. SWAP will determine actual soil evapotranspiration (E_a) using different approaches. In the present study, SWAP determines E_a by taking the minimum value of E_p.

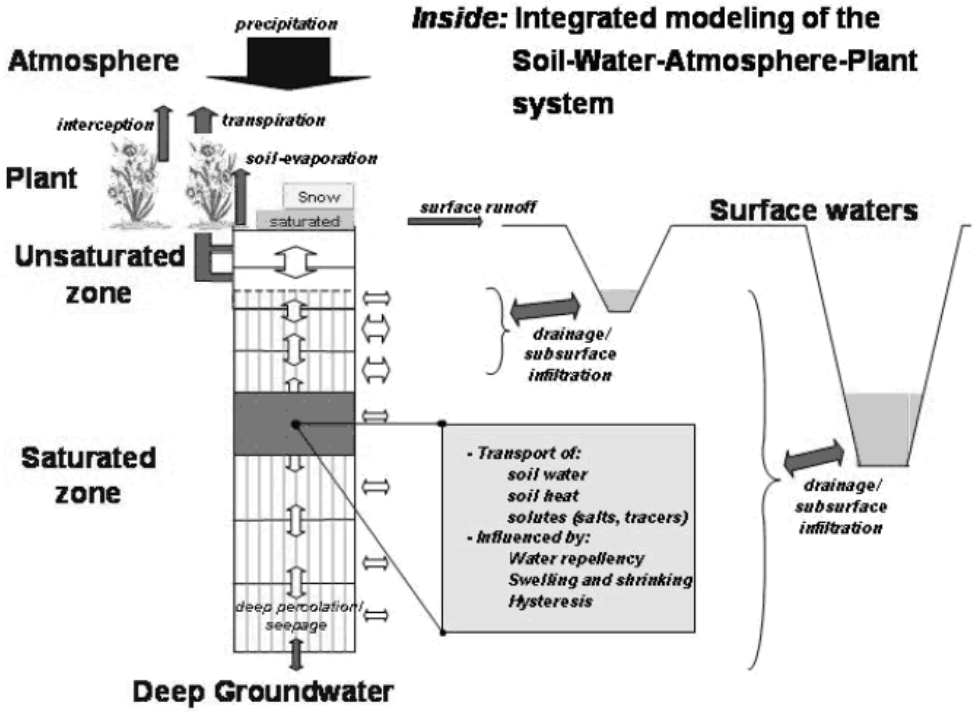

Figure 5.8 Schematized overview of the modelled system (From User's Guide of SWAP model version 3.0.3)

5.3.2. SWAP model adaptation

To be able to compare the SWAP and EARTH results more clearly, it is important to assign the same upper and bottom boundary conditions for both models. As mentioned before the bottom boundary of the EARTH model is a simple one-dimensional saturated groundwater follow model (SATFLOW). However, currently the SATFLOW is not included in the predefined bottom boundaries of SWAP model (Van Dam 2007, private communication). Hence in the present study it was attempted to run the SWAP model in combination with the one-dimensional saturated groundwater flow model (SATFLOW) in order to have the same bottom boundary as the EARTH model (Figure 5.9).

This process consists of two steps. First the SWAP model was used to simulate the soil water flow in the unsaturated zone (5 m thick) by assigning free drainage as its bottom boundary. Then the output of the SWAP i.e. the bottom flux was used as input to the saturated zone groundwater flow model (SAFLOW).

For deep groundwater tables such as the central Veluwe, it is also proved to be useful to add module LINRES (percolation zone) between the SWAP bottom flux and the linear groundwater reservoir (SATFLOW). Thus the redistribution of the SWAP bottom flux in time is dealt with the linear reservoir (LINRES). This allows to keep SWAP modelled thickness constant. This gives a better result as compared to the simulation results of SWAP and SATFLOW models without LINRES module (Gehrels, 1999).

The model adaptation has another advantage in the sense that in the absence of soil moisture data groundwater level data can be used for model calibration. The same approach was used in the present study.

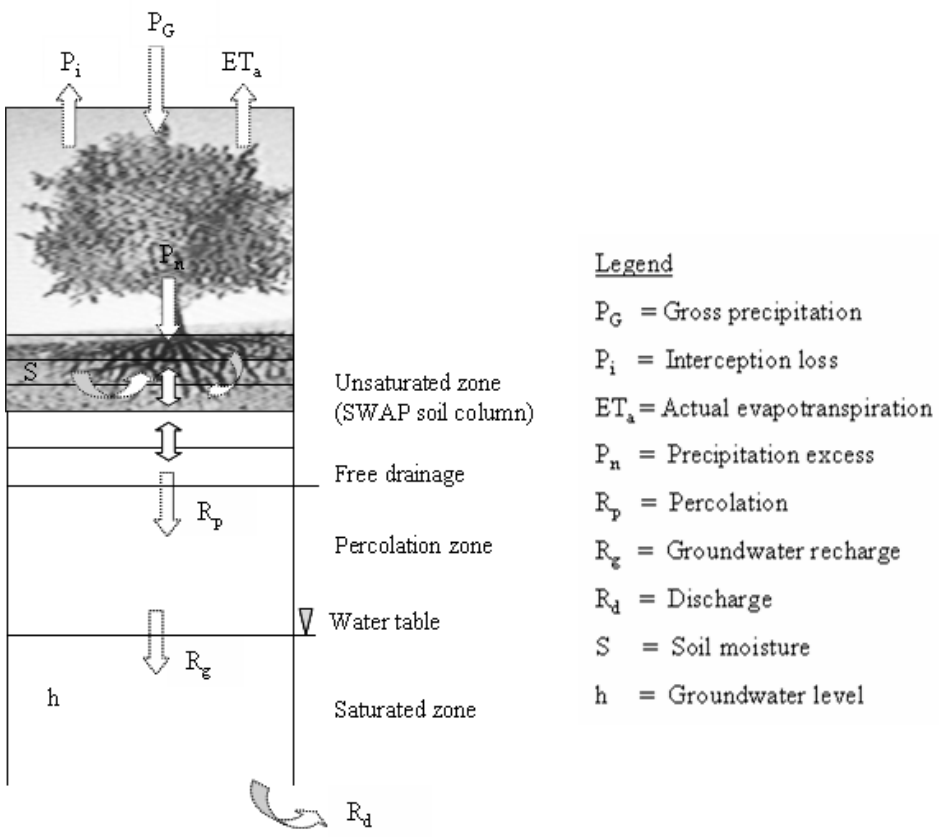

Figure 5.9 Schematization of the Adapted SWAP model

5.3.3. Model input

Simulation of water dynamics in the unsaturated zone requires input data concerning boundary conditions, geometry of the system and its physical parameters, initial conditions, and crop related data (parameters defining the relation between root water uptake and soil water status).

5.3.3.1. Boundary and initial conditions

The upper boundary condition is important for accurate simulation of changing soil water fluxes near the soil surface. In the present study, the upper boundary of the SWAP model was formulated by daily

net precipitation and potential evapotranspiration at the soil surface, the same as in the case of the EARTH model.

The methods employed to calculate the net precipitation and potential evapotranspiration are similar to the EARTH model. The only two differences are: 1) For the Penman-Monteith approach SWAP uses the built-in Penman-Monteith equation for the calculation of potential evapotranspiration using climatic data (minimum and maximum air temperatures at 2 m height (^{0}C), global solar radiation (kJ m^{-2} d^{-1}), wind speed at 2 m height (m s^{-1}), air humidity as vapour pressure at 2 m height (kPa)), minimum canopy resistance (s m^{-1}) and geographic location (geographical latitude (degrees), altitude above mean sea level (m), altitude of wind speed measurement above mean soil surface (m)) of the meteorological station from which the climatic data are obtained. 2) SWAP can separate soil evaporation and plant transpiration.

The lateral boundary is not important in this study because the study area is characterized by high elevation and porous media (coarse-grained sandy soils) as a result the interaction with surface water is rare. The precipitation excess usually infiltrates completely. Thus zero surface ponding and surface runoff were simulated.

Concerning the bottom boundary, Gehrels (1999) has conducted soil moisture measurements using capacitance probe on six sites in the study area at different depths to a maximum depth of 6 m with the purpose of obtaining information on the depth to which fluctuations of soil water content are manifest. He reported that the soil water content variations can still be observed to a depth of 3 m, but below 3 m the soil water content fluctuations are extremely small. Thus zero gradient of soil moisture pressure head is assumed at the bottom boundary of the current SWAP soil profile, 5 m and free drainage is simulated at the bottom of the SWAP soil profile in the unsaturated zone. The lower boundary of the model below the percolation zone is defined by a one-dimensional reservoir function similar to the bottom boundary of the EARTH model.

The drainage flux in the saturated part of the soil column refers to the groundwater flux to/from the local drainage system. The average groundwater level of the area is above the drainage base, thus the groundwater flux is to wards the drainage system and is simulated similar as in the EARTH model.

Initial soil moisture condition must be defined when transient soil water flow is modelled. In this study, the soil pressure head data as function of depth is not available hence the pressure head of each compartment is assumed to be in hydrostatic equilibrium with the initial groundwater levels.

5.3.3.2. System geometry and parameters

The SWAP soil profile has a total length of 500 cm for five sites and 300 cm for one site (B33A0067-Scots pine), because the thickness of the unsaturated zone for this site is only 300 cm. The soil profile was divided into sixty numerical compartments and grouped into five soil layers with different hydraulic properties. For accurate calculation of top boundary fluxes, the first compartments near the surface were set to a thickness of one centimetre. Similar soil geometry and soil water retention parameters were used for all the six sites under consideration. Hysteresis and preferential flow were not considered in this study.

The soil hydraulic properties i.e. the description of the soil layers to a depth of 5 m and soil water retention parameters (Van Genuchten-Mualem parameters): saturated moisture content θ_s, residual moisture content θ_r, saturated hydraulic conductivity K_s, and shape parameters n, α and λ were obtained from Gehrels (1999) (Table 5.6).

Table 5.6 Soil parameters input for SWAP model

Layer no.	Soil depth cm	θr $cm^3.cm^{-3}$	θs $cm^3.cm^{-3}$	Ks $cm.d^{-1}$	α cm^{-1}	n -	λ -	Soil type
1	25	0.025	0.44	133	0.021	1.62	0.5	A top soil cover sand
2	50	0.021	0.43	378	0.019	2.34	0.5	Bhs top soil cover sand
3	100	0.019	0.38	690	0.030	2.81	0.5	C sub soil fluvioglacial
4	300	0.015	0.36	695	0.030	2.85	0.5	C sub soil fluvioglacial
5	500	0.010	0.29	1579	0.059	3.22	0.5	C sub soil fluvioglacial

In this study, a simple crop development model available in SWAP was used which only requires data about the leaf area index, crop height, and rooting depth. Crop factors, crop heights and leaf area index are specified as in section 5.2.2.3.

Root depth is one of the factors that determine the amount of soil water available for transpiration. The root depth for each vegetation type is taken the same as in the EARTH model. The same rooting depth was assumed throughout the modelling period. Root water uptake reduction at either too dry or too wet conditions was described according to Feddes et al (1978) (equation 5.29).

6. Model calibration

The objective of model calibration is to minimize the deviation and obtain the best fit between measured and simulated variables. Calibration of a model helps to evaluate the performance of the model and to establish whether the model is acceptable as an image of reality or not. In unsaturated zone soil water flow modelling, model performance can be evaluated by comparison of observed and model simulated state variables such as soil water content, soil pressure head, groundwater level and actual evapotranspiration. In the present study, observed groundwater levels (OGWL) were used to calibrate both models. The description of the selected boreholes in terms of elevation, average groundwater level above NAP and average groundwater level from surface is summarized in (Table 6.1).

Both models were calibrated by trial and error procedures of adjusting model parameters manually. Comparison of groundwater levels was made over the modelling time span for both models. According to Anderson and Woessner (1992), three calibration procedures were carried out during the calibration process: first change the parameter value that cause the largest deviation, change just one parameter in each run; determine if the change of the parameter cause negative or positive effect on other part.

Table 6.1 Elevation and groundwater levels of the selected boreholes

Borehole name	Elevation above NAP (m)	Average GWL from surface (m)	Average GWL above NAP (m)
B33A0065-Molinia grass	46	18	28
B33A0103-Heath	41	21	20
B33A0067-Scots pine	26	3	23
B33D0217-Douglas fir	60	25	35
B33A0113-Deciduous	78	50	28
B33D0002-Mixed forest	65	23	42

6.1. EARTH model calibration

The principal model parameters used for calibration are the soil water content at field capacity θ_{fc}, maximum soil moisture content θ_s, number of reservoirs n, and the unsaturated recession coefficient f. The other parameters were not calibrated, but a priori set at fixed value. However, the values for the saturated recession coefficient and specific storage were only slightly adjusted for some of the sites to match the in situ measures of groundwater levels with the simulated values (Table 6.2).

Simulations were executed using Makkink and Penman-Monteith derived daily potential evapotranspiration and net precipitation as input. For the first 15 years of the simulation period, the simulated groundwater levels (SGWL) follow the observed values quite well. However, systematic deviations occurred in the last 5 years of the simulations probably as a result of increased groundwater abstraction. The model calibration result shows that there is no significant difference between the

simulation results using Makkink and Penman-Monteith derived evapotranspiration (Figure 6.1 and Figure 6.2).

Table 6.2 EARTH parameter sets for simulation of well level fluctuations in the six sites

Parameters	**B33A0065 (Molinia)**	**B33A0103 (Heath)**	**B33A0067 (Scots pine)**	**B33D0217 (Douglas fir)**	**B33A0113 (Deciduous)**	**B33D0002 (Mixed)**
Maximum soil moisture (mm)	248	280	390	420	420	420
Residual soil moisture (mm)	13.2	13.2	22	22	22	22
Initial soil moisture (mm)	248	280	360	320	420	420
Moisture content at field capacity (mm)	244	270	380	383	344	284
Maximum surface storage (mm)	0	0	0	0	0	0
Interception loss (mm)	0	0	0	0	0	0
Saturated hydraulic conductivity (mm d^{-1})	2000	2000	2000	2000	2000	2000
Unsaturated reservoir coefficient (day)	85	85	30	80	65	100
Number of reservoirs (number)	2	2	1	2	3	2
Saturated recession coefficient (day)	5500	5500	5500	7000	5500	7000
storage coefficient (-)	0.25	0.25	0.265	0.2	0.23	0.2
Initial water level (m)	22.62	14.35	17.16	29.98	22.47	36.97
Local base level (m)	5	5	5	5	5	5

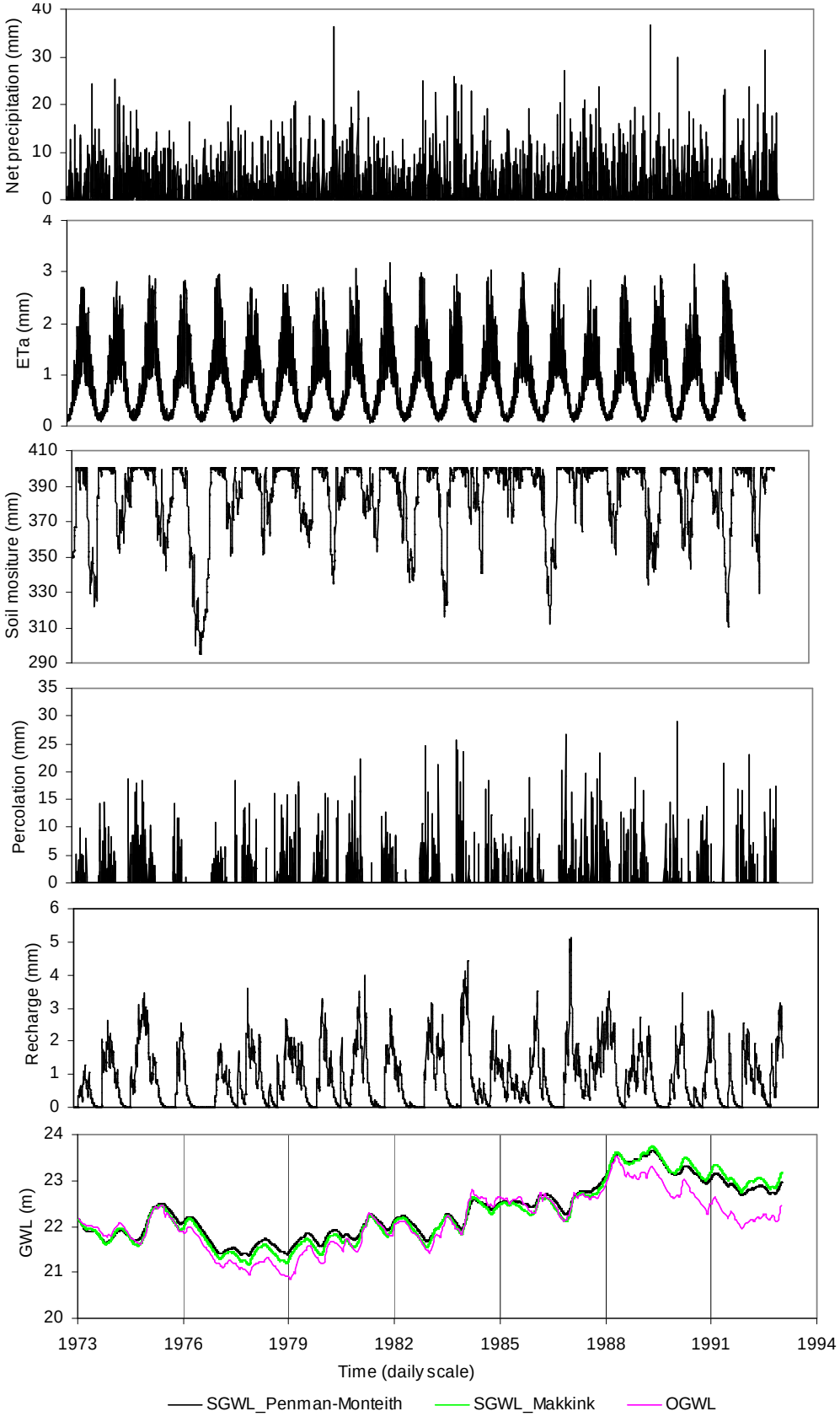

Figure 6.1 Example output of EARTH model at B33A0067 (Scots pine)

The top diagram shows precipitation excess (net precipitation). The second diagram represents loss from the root zone due to evapotranspiration (ETa). The precipitation shows uniform distribution throughout the year while the evapotranspiration shows seasonal variations. The diagram indicates high evapotranspiration in summer and low evapotranspiration in winter. The third diagram shows the seasonal soil moisture variation in which the soil shows low soil moisture in winter months and high soil moisture in the rainy season. Diagram four presents the net downward percolation from the root zone. The fifth diagram illustrates the downward flow of soil moisture from the percolation zone on its way to the water table as recharge. The last diagram shows the resulting groundwater level (GWL) fluctuations.

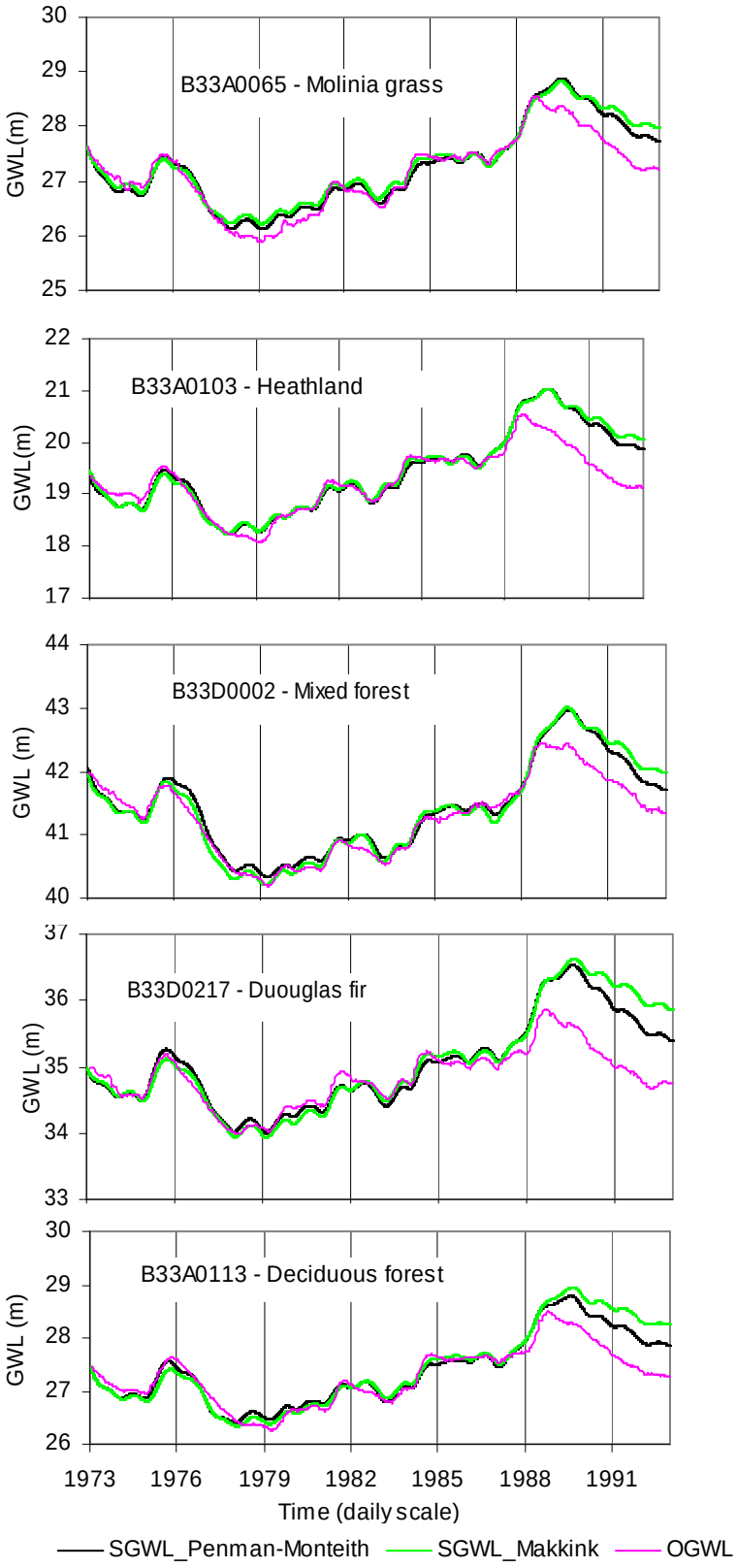

Figure 6.2 Observed and simulated groundwater levels at five sites using Makkink and Penman-Monteith derived evapotranspiration

6.2. SWAP model calibration

SWAP calibration was done by modifying the values of some of the soil retention parameters in the unsaturated zone in combination with the saturated zone parameters within a possible range of parameter values. From the unsaturated zone the shape parameters n, α and λ are found to be relatively sensitive to the calculated recharge and are slightly adjusted to match the observed and simulated groundwater levels (Table 6.3 and Table 6.4). In the saturated zone the parameters selected for model calibration are the unsaturated reservoir coefficient, saturated recession coefficient, number of reservoirs and storage coefficient (Table 6.5).

The initial groundwater levels were assumed to be in hydrostatic equilibrium with pressure head of each compartment for the initial soil moisture conditions as the data for the pressure head as function of depth is not available. It was observed that during the first periods, the conditions were dry; the soil layers took some time, approximately two years, to reach at field capacity, which limits the bottom flux movement at the bottom boundary. To improve the simulation of the initial conditions, first the model was run by assuming the soil pressure heads are in hydrostatic equilibrium with the initial groundwater levels for the initial soil moisture, then the final pressure heads obtained were used as initial pressure heads for the initial soil moisture and the simulation was repeated. By this approach the simulation of the initial conditions was improved.

Simulation using Makkink derived evapotranspiration resulted in a good fit between the simulated and observed groundwater levels at all the six sites, an almost identical result as the EARTH model (figure 6.3).

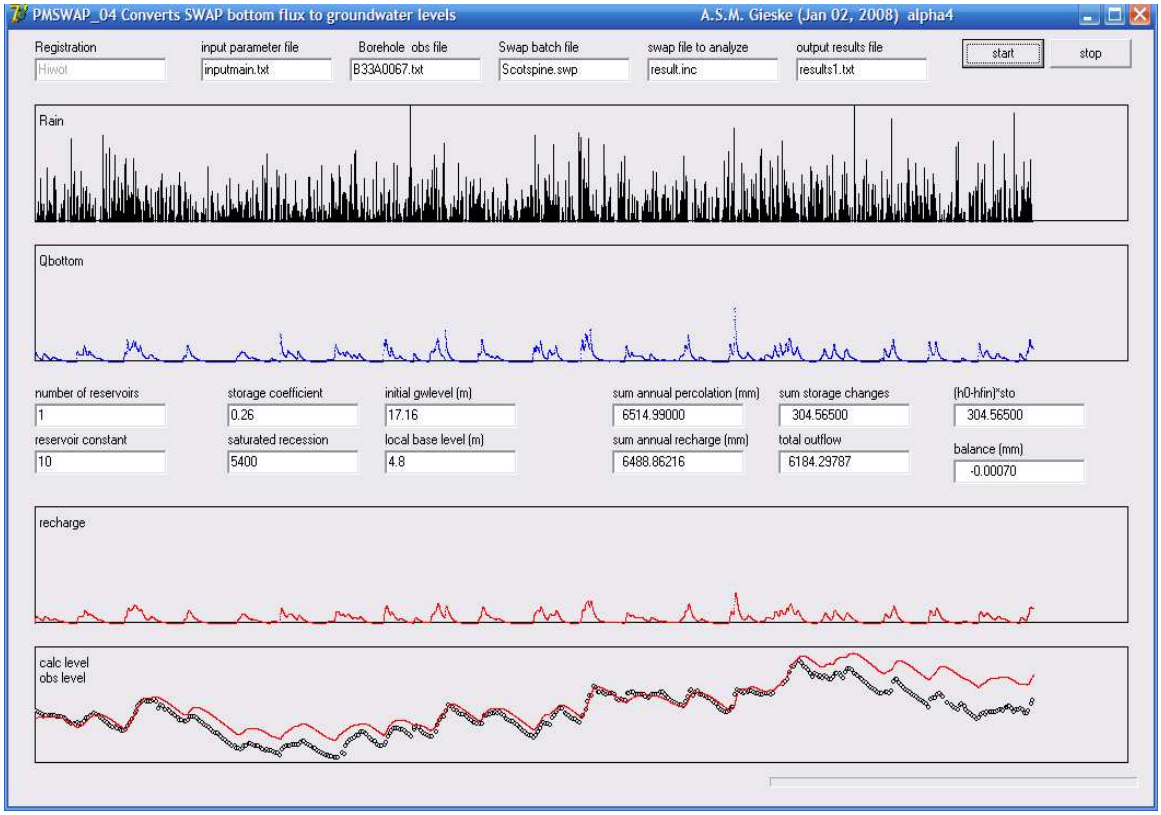

Figure 6.3 Example output of SWAP model at B33A0067 (Scots pine) using Makkink evapotranspiration

Table 6.3 Swap parameter sets for simulation of well level fluctuations (B33A0065-Molinia grass)

Layer no.	θr $cm^3.cm^{-3}$	θs $cm^3.cm^{-3}$	Ks $cm.d^{-1}$	α cm^{-1}	n -	λ -
1	0.025	0.44	133.0	0.021	1.62	0.5
2	0.021	0.43	378.7	0.019	2.87	0.5
3	0.019	0.38	690.0	0.03	2.81	0.5
4	0.013	0.36	695.0	0.03	2.93	0.5
5	0.01	0.29	1000.0	0.049	3.33	0.5

Table 6.4 Swap parameter sets for simulation of well level fluctuations (B33A0067-Scots pine)

Layer no.	θr $cm^3.cm^{-3}$	θs $cm^3.cm^{-3}$	Ks $cm.d^{-1}$	α cm^{-1}	n -	λ -
1	0.025	0.44	133.0	0.021	1.62	0.53
2	0.021	0.43	378.7	0.019	2.87	0.53
3	0.019	0.38	690.0	0.03	2.81	0.53
4	0.013	0.36	695.5	0.03	2.93	0.53

Table 6.5 Saturated zone parameter sets for simulation of well level fluctuations (extended SWAP model)

Parameters	B33A0065 (Molinia)	B33A0067 (Scots pine)	B33A0113 (Deciduous)	B33A0103 (Heath)	B33D0002 (Mixed)	B330217 (Douglas fir)
Number of reservoirs (number)	2	1	2	2	2	2
Reservoir coefficient (-)	70	10	60	60	90	90
Storage coefficient (-)	0.25	0.26	0.25	0.3	0.22	0.18
Saturated recession (day)	5450	5400	5700	4200	8900	9500
Initial groundwater level (m)	22.62	17.16	22.47	14.35	36.97	29.98
Local base level (m)	5	5	5.1	5.1	5.1	5

Model calibration for the simulations based on Penman-Monteith, available in SWAP, derived evapotranspiration also resulted in a good fit as in comparison to the simulations with Makkink derived evapotranspiration for some of the sites (Figure 6.4). However, for some of the sites the fit is not as good as the simulation based on Makkink derived evapotranspiration as indicated in Figure 6.5. This will be discussed later.

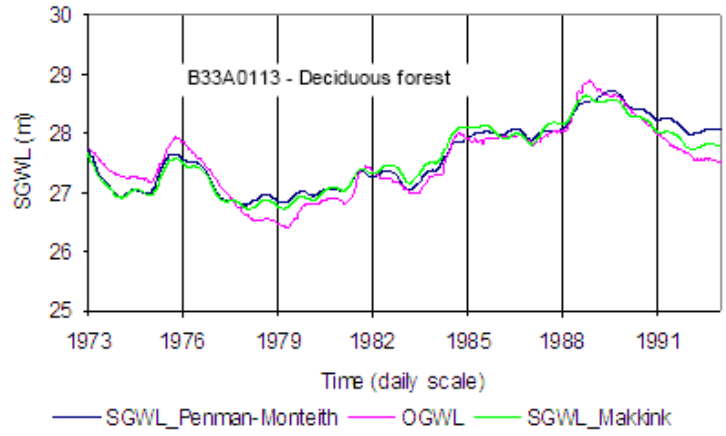

Figure 6.4 Observed and simulated groundwater levels using Penman-Monteith, calculated by SWAP, and Makkink derived evapotranspiration at B33A0113 (Deciduous forest)

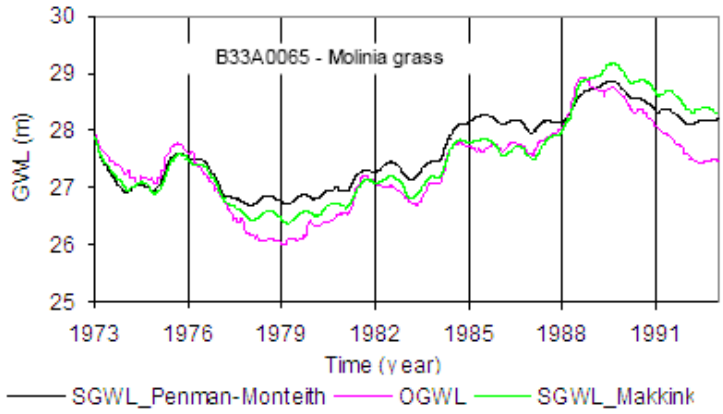

Figure 6.5 Observed and simulated groundwater levels using Penman-Monteith, calculated by SWAP, and Makkink derived evapotranspiration at B33A0065 (Molinia grass)

6.3. Calibration result evaluation

The model performance evaluation was carried out only for the first 15 years of the simulation period because the last 5 years showed fluctuations (man-induced) which could not be modelled by EARTH and SWAP models due to the design of the model structure. Groundwater abstractions are not considered with the EARTH and SWAP versions used in this study.

The model calibration resulted in minimizing the differences between the simulated and observed groundwater levels. The calibrated result was evaluated by qualitative and quantitative comparison of the simulated and observed groundwater levels. The qualitative comparisons are based on visual comparison of the simulated and observed groundwater level contour maps.

The quantitative model calibration was performed based on two approaches: 1) Using the correlation coefficient (R^2) in which the simulated groundwater levels are plotted versus the observed groundwater levels on a linear plot. All the sites show similar results, and as an example only the linear plot of observed and simulated groundwater levels for B33A0067 (Scots pine) is presented in Figure 6.6.

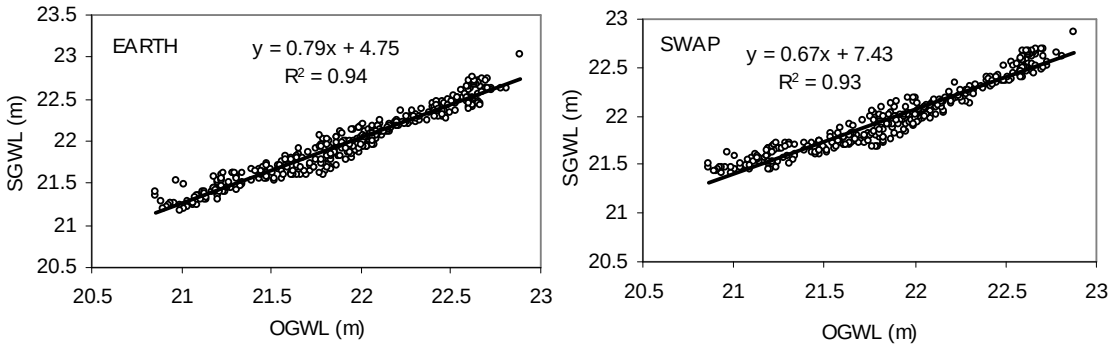

Figure 6.6 Correlation between observed and simulated groundwater levels at B33A0067 (Scots pine)

2) By calculating the average measure of the residuals using RMSE. The RMSE is the standard deviation of the residual error over a selected calibration period. It is the average of squared differences between observed and calculated variables.

$$RMSE = \left[\frac{1}{n} \sum_i^n (h_{obs} - h_{sim})_i^2 \right]^{0.5} \quad \textbf{(6.1)}$$

where h_{obs} and h_{sim} are observed and simulated groundwater levels respectively .

The results of the quantitative model performance evaluation methods are summarized in the table below.

Table 6.6 Error summary of the calibrated models

Site Name	EARTH		SWAP	
	RMSE	R2	RMSE	R2
B33A0065-Grassland	0.13	0.96	0.18	0.95
B33A0103-Heathland	0.13	0.95	0.21	0.89
B33A0067-Light coniferous	0.16	0.95	0.21	0.94
B33A0113-Deciduous	0.14	0.92	0.19	0.84
B33D002-Mixed forest	0.11	0.96	0.20	0.90
B33D0217-Dark coniferous	0.15	0.93	0.21	0.88

6.4. Sensitivity analysis

A sensitivity analysis was performed on the already calibrated EARTH and SWAP models for two sites (B33A0065-Molinia grass and B33A0067-Scots pine). The purpose of sensitivity analysis is to observe the model response to variations in the input data and evaluate the performance of the model. The simulated recharge rate is determined by crop factors, interception percentages and root zone parameters. Crop factor was selected for the current sensitivity analysis and this section analyses how the variations in crop factor affects the recharge estimates.

The sensitivity of the recharge estimation to the variation in crop factor values was evaluated by simulating recharge over the modelling period time span on a daily basis and afterwards averaged to annual values. The values for this parameter were varied in steps while keeping the other parameters fixed at their calibrated values. The sensitivity of recharge to different crop factor values for Molinia grass and Scots pine is shown in (Figure 6.7).

The crop factor has a strong effect on the simulated recharge. As the crop factor increases the simulated recharge decreases rapidly. This is because as the crop factor increases the water use rate of

plants increase. This causes actual evapotranspiration to increase and recharge to decrease. The sensitivity analysis shows that the groundwater recharge calculated with both models show high sensitivity to crop factor.

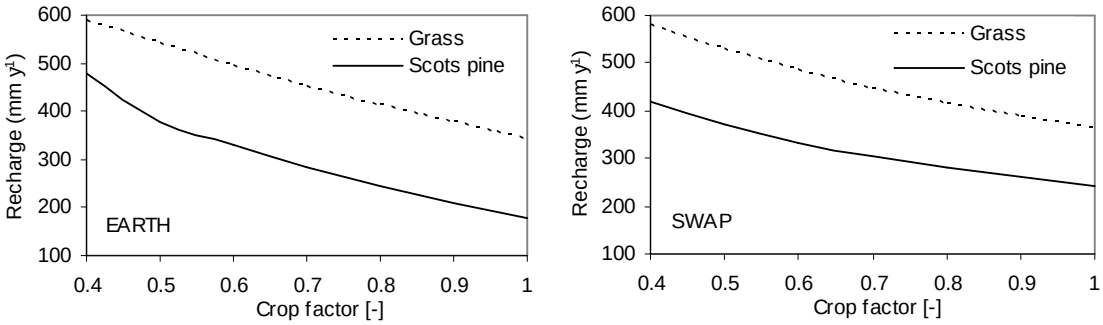

Figure 6.7 Sensitivity of annual groundwater recharge rate to crop factor

6.5. Conclusion

Model calibration was achieved by optimizing parameters by manual trial and error procedure. The performance of the model was evaluated based on visual interpretation of calibration results and an objective calibration criterion. From the visual interpretation it can be concluded that both models simulate the groundwater level fluctuation of the area quite well except for the last 5 years.

The sensitivity analysis also reveals that both models are sensitive to the selected parameter in a logical manner. The RMSE and correlation coefficient (R^2) for both models also indicate a very good model performance. In general, the qualitative and quantitative model performance evaluation and the sensitivity analysis indicate that the simulated groundwater levels agree very well with the measured values at all the six sites during the first 15 years of the simulation period and the performance the models is very good.

7. Results and discussion

The modelling results of the EARTH and SWAP models using the potential evapotranspiration calculated by Makkink and Penman-Monteith methods do not show significant difference for most of the sites. Thus the simulation results obtained by using Makkink evapotranspiration as input will be used for the analysis throughout the next sections.

7.1. Long-term simulation of groundwater level fluctuations

The groundwater regime of the study area is characterized by a deep groundwater table with low frequency and large amplitude fluctuations. To study the long-term rain-recharge relations and the fluctuation of water levels around their equilibrium soil moisture, actual evapotranspiration, percolation, recharge and groundwater level fluctuations were simulated for a period of twenty years (1973-1992) with EARTH and SWAP models. For calibration of the models, the simulations were compared with observed phreatic groundwater levels at six boreholes (Figure 7.1).

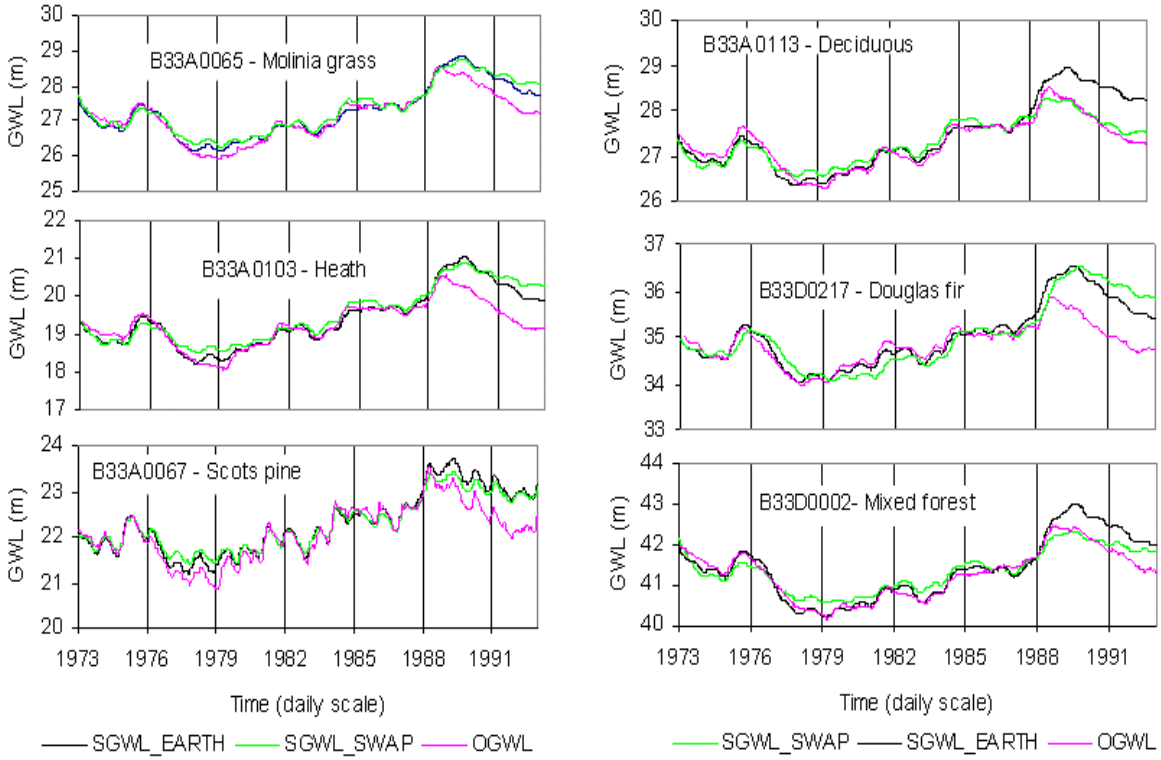

Figure 7.1 Observed and simulated groundwater levels at six sites with both SWAP and EARTH models

The model predictions follow the pattern of the observed groundwater level fluctuations. Both models appear to simulate the slow groundwater level fluctuations of the area with high accuracy in the first 15 years of the simulation period. However, systematic deviations occurred in the last 5 years of the simulations probably as a result of increased groundwater abstractions from existing and newly implemented groundwater schemes.

Figure 7.2 gives an overview of the distribution of residual errors over time (observed minus simulated groundwater levels) for two sites. The residual errors for the other sites also show the same

pattern. The long-term distribution of the residual errors shows a pattern i.e. they are not randomly distributed over time. This shows that the models may have some systematic deficiencies. These patterns in the distribution of the residuals could indicate that the encountered systematic deviations in the models could be caused by fluctuating groundwater abstraction increasing in the late 1980s. The short-term distribution of the residuals also shows some pattern. This could possibly be explained by a time lag between the simulated and observed groundwater levels.

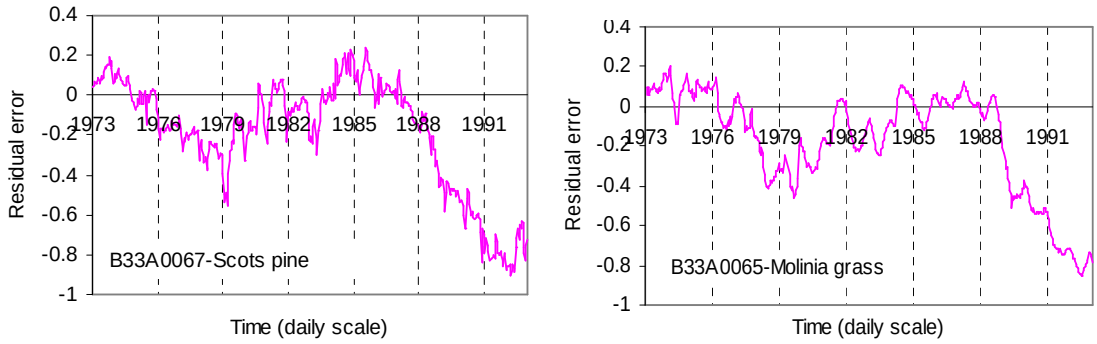

Figure 7.2 Distribution of residual errors for two sites

7.2. Groundwater abstraction

In the Veluwe, groundwater has been used for drinking water and industrial purposes since the 1930s. The extensive aquifer forms a major water supply for the region. At numerous places groundwater is extracted up to an annual volume exceeding $150x10^6$ m^3 in the region (Gehrels, 1999).

There are a total 203 abstraction wells in the study area with three categories of groundwater abstraction, i.e. drinking water supply, industrial usage and de-watering of excavations for engineering purpose. Based on the amount of annual abstraction and availability of data covering the modelling period, three abstraction wells with high annual abstraction rate were selected for the present analysis (Figure 7.3). Well GO 33010032 VITENS GELDERLAND and GO 33010111 GEMEENTE APELDOORN are used for drinking water supply while well GO 33010171 VHP SECURITY PAPERMILL is used for industrial purpose.

Figure 7.4 shows the annual abstraction rate from the three wells (1973-1992). An increase in groundwater abstraction was observed approximately between the year 1977-1980 with the highest peak 1978-1979, and 1988-1992 with the highest peak 1991-1992. The magnitude of the increment in abstraction is much higher for the period 1988-1992 than 1977-1980. So the effect of increased abstraction in 1977-1980 on the simulated groundwater level could be minor. The small deviation between the observed and simulated groundwater levels occurred around 1978-1981 at the sites with relatively shallow groundwater table sites (B33A0065-Molinia grass and B33A0067-Scots pine) could be caused due to this increased groundwater abstraction.

The systematic deviation between the simulated and observed groundwater levels encountered at all the six sites in the last 5 years (1988-1992) of the present modelling period could be caused due to the high groundwater abstraction observed in the years 1988-1992.

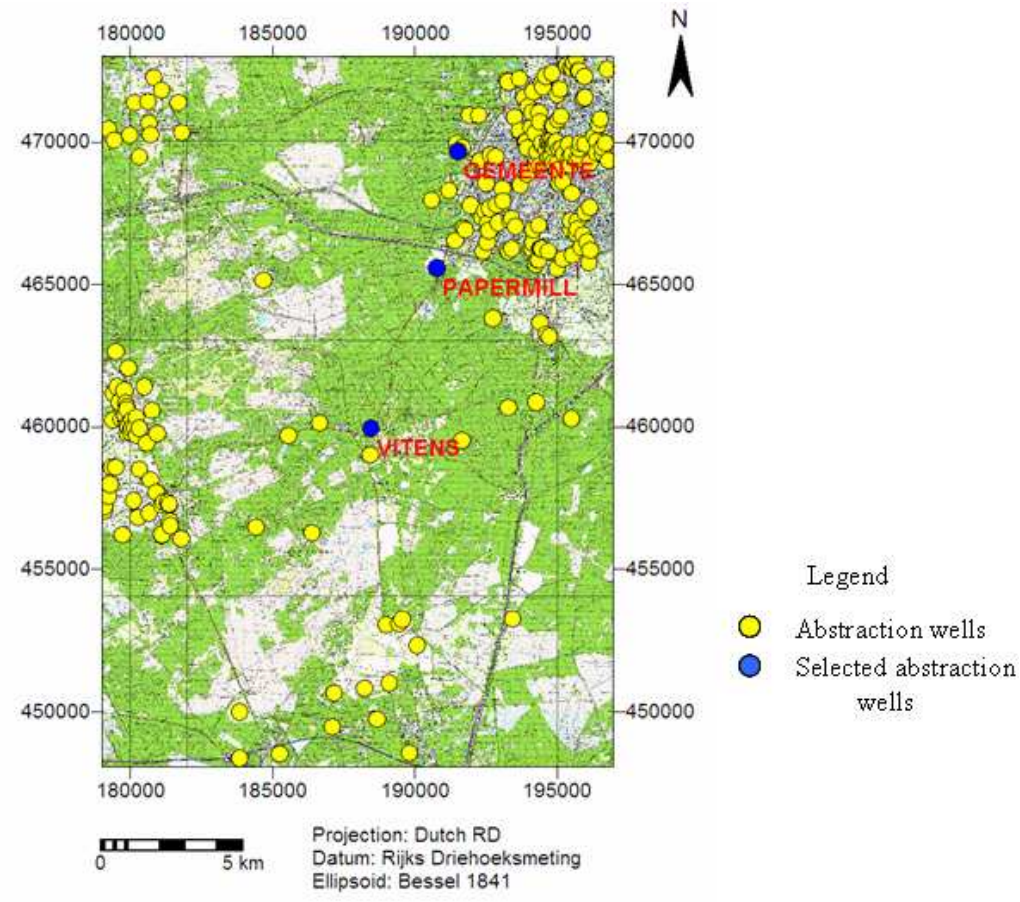

Figure 7.3 Location of abstraction wells

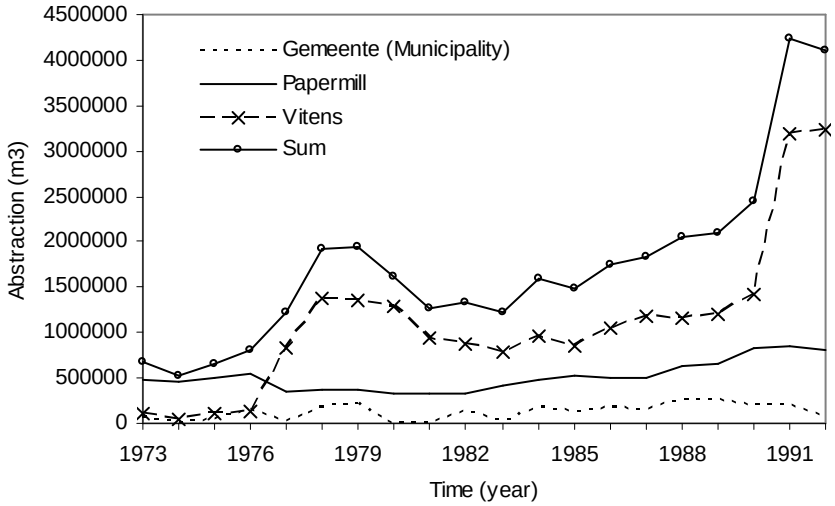

Figure 7.4 Annual groundwater abstraction over 1973-1992 for three abstraction wells

Berendrecht (2004) reported that at Kootwijk which is the central part of the present study area, two aquifers (aquifer 3 & 4) were influenced by groundwater abstraction. The drawdown for aquifer 4 shows a high increase starting in the year 1988 while the increase in drawdown at aquifer 3 starts earlier (around 1975) (Figure 7.5). The years with high drawdown coincides with the years that show

high groundwater abstraction. Thus the deviations between the simulated and observed groundwater levels in 1988-1992 could be caused due to aquifer 4 and that of 1978-1980 for the two sites could be due to aquifer three.

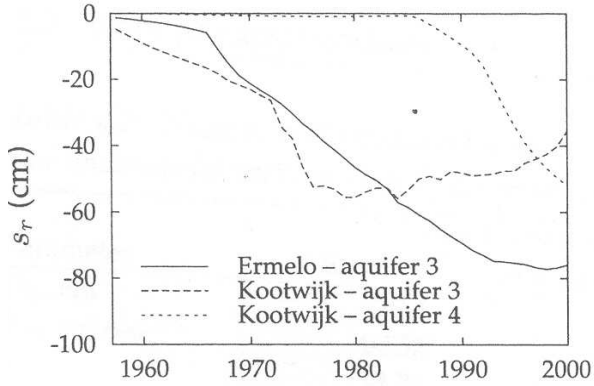

Figure 7.5 Representative drawdown for Kootwijk and Ermelo (Berendrecht, (2004)

Figure 7.6 gives an overview of the yearly total abstraction between 1951 and 1993 for the province of Gelderland. The total abstraction of groundwater was 82x106 m^3 y^{-1} in 1950 and it has steadily increased to 208x106 m^3 y^{-1} in 1971, followed by a sudden rise of 35x106 m^3 y^{-1} to 243x106 m^3 in 1972, after which the total has remained more or less constant. A steady increase up to 290x106 m^3 y^{-1} follows in the year 1988.

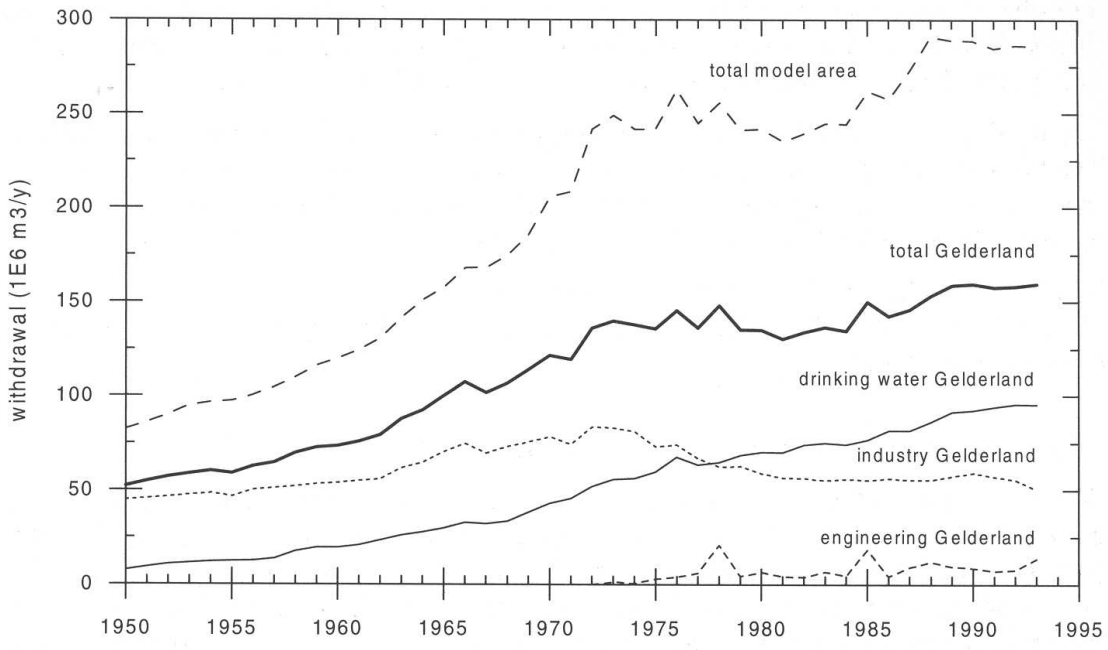

Figure 7.6 Annual sums of groundwater abstraction over 1951-1993 for the province of Gelderland (Gehrels, 1999)

Gehrels (1999) also had evaluated the impact of groundwater abstraction in the Veluwe area by considering the average impact of all groundwater abstractions together in the entire model area averaged over 1988-1993. He reported that the impact of groundwater abstractions on hydraulic head is especially noticeable in the phreatic infiltration areas of the Veluwe. The drawdown of groundwater

level in the unconfined areas in the Veluwe as a result of all groundwater abstraction averaged over (1988-1993) increases from 10 cm along the edges of the unconfined infiltration areas to more than 200 cm in the southern part of the Veluwe (Figure 7.7). The map also demonstrates that there is 100-200 cm decline of groundwater level in the present study area. Groundwater abstraction at pumping station Schalterberg which is located near the study area commenced in 1982 with 2.2 million, increased to 3.0 million in 1983. The effect of this increased abstraction can propagate to the present study area with time.

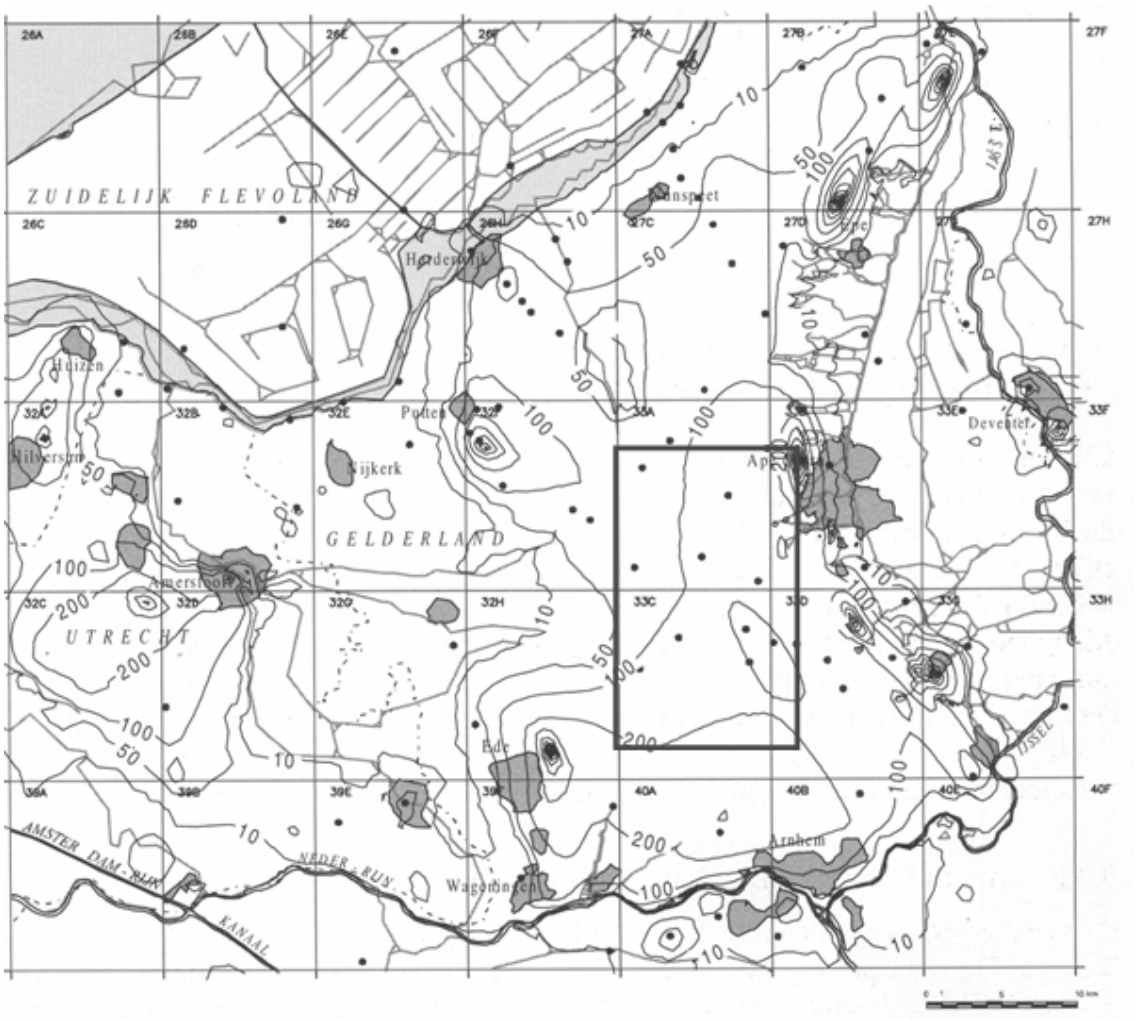

Figure 7.7 Groundwater level lowering (cm) as a result of all groundwater abstractions averaged over the period 1988-1993 (Gehrels, 1999)

In general the periods with increased groundwater abstraction and high drawdown coincides with periods that show systematic deviations between the simulated and observed groundwater levels in the present study. Thus from the overall discussion it could be concluded that the systematic deviations occurred in the present study are due to increased abstraction of groundwater in the area.

7.3. Soil water balance and recharge estimation

The main factors influencing water movement in the unsaturated zone are the rooting density and depth of vegetation, and the types of soil. The study area is characterized by porous sandy soils. So when it rains much of it evaporates from the vegetation cover and bare soil and from the root zone as transpiration. Thus only that remains infiltrates through the sandy soils to the deeper parts of unsaturated zone.

Soil moisture content, actual evapotranspiration and groundwater recharge were simulated with the SWAP and EARTH models. The modelled long-term annual soil water balances for the period 1973 to 1992 for each site from SWAP and EARTH models were calculated as:

$$\Delta S = P_G - E_i - E_a - R_p \qquad \textbf{(7.1)}$$

where P_G is gross precipitation [mm], E_i is interception evaporation [mm], E_a actual evapotranspiration [mm] and R_p percolation recharge [mm]. P_n is net precipitation [mm], E_p is potential evapotranspiration [mm] and R_g groundwater recharge [mm].

Table 7.1 Water balance results for the six sites as calculated with EARTH (1973-1992)

Borehole name	P_G	P_n	E_i	E_p	E_a	R_p	R_g	ΔS
B33A0065 (Molinia grass)	880	827	53	495	433	394	380	-1
B33A0103 (Heath)	880	827	53	506	431	396	382	-1
B33A0067 (Scots pine)	880	651	229	362	329	321	320	1
B33A0217 (Douglas fir)	880	541	339	343	334	208	201	-2
B33A0113 (Deciduous)	880	631	248	312	270	364	351	-2
B33A0002 (Mixed)	880	642	237	512	312	336	323	-6

Table 7.2 Water balance results for the six sites as calculated with SWAP (1973-1992)

Borehole name	P_G	P_n	E_i	E_p	E_a	R_p	R_g	ΔS
B33A0065 (Molinia grass)	880	827	53	537	432	395	381	0
B33A0103 (Heath)	880	827	53	509	416	410	400	1
B33A0067 (Scots pine)	880	651	229	362	325	326	325	0
B33A0217 (Douglas fir)	880	541	339	362	326	214	208	1
B33A0113 (Deciduous)	880	631	248	318	276	364	358	-8
B33A0002 (Mixed)	880	642	237	560	303	338	325	2

The EARTH and SWAP water balance estimates are nearly identical with about 5% variation (Table 7.1 and Table 7.2). Thus the analysis in this section is based on EARTH model outputs. The calculated groundwater recharge below the different vegetation types varies from 201 to 382 mm y^{-1}, whereas the actual evapotranspiration varies from 270 to 433 mm y^{-1}. The annual actual evapotranspiration for Molinia grass and Heath amounts to 433 and 431 mm respectively. Previous researchers have obtained similar values for the same site. For example, Gehrels (1999) found the annual actual evapotranspiration for Molinia grassland at the same site (Radio Kootwijk) for the year 1994 to be 434 mm using the 'Bowen ratio energy balance' method.

For dark coniferous (Douglas fir) forest, the calculated actual evapotranspiration, 334 mm y^{-1}, is slightly higher than the other forests. Bosveld (1999) found an almost the same value, 330 mm y^{-1},

using Peman-Monteith method for the same area. Tiktak and Bouten (1994) reported an actual evapotranspiration of 363 mm y^{-1} for Douglas fir stand on sandy soils in the Netherlands. Thus it can be concluded that the current value is in accordance with previous studies. The calculated groundwater recharge below the Douglas fir forest is the lowest of all vegetation types, 201 mm y^{-1}, in the study area.

The actual evapotranspiration for deciduous forest is found to be lower than the other forest types in the area, 270 mm y^{-1}. This value matches reasonably with the value of 284 mm y^{-1} from Dolman and Moors (1994). The calculated groundwater recharge rate below deciduous forest, 351 mm y^{-1}, is higher than that of the other forests, especially dark coniferous, but slightly lower than Grass and Heath. This shows that the amount of water use by deciduous forest is lower than the other vegetation types.

For light coniferous forest (Scots pine) an actual evapotranspiration of 329 mm y^{-1} was obtained. This figure is slightly higher than the actual evapotranspiration obtained by Elbers et al., (1996), 285 mm y^{-1}, but reasonably matches with 321 mm y^{-1} of Gehrels (1999). The groundwater recharge below this forest is lower than for deciduous forest but is higher than the dark coniferous forest. The actual evapotranspiration and recharge for mixed forests are almost similar to that of light coniferous.

In general the actual evapotranspiration for forest is lower than for grass and heath. On the contrary, recharge values below forest is lower than grass and heath lands. This shows that in forested areas, evaporation of intercepted rainfall contributes significantly to the total loss of water due to evapotranspiration causing recharge to be small.

The annual recharge and actual evapotranspiration of the study area is calculated from the annual recharge and evapotranspiration of each land cover. The annual actual evapotranspiration is found to be remarkably constant through time, with an average value of 350 mm y^{-1}. In contrast, the annual recharge shows a high temporal variability in accordance with the temporal variability of precipitation (Figure 1.1).

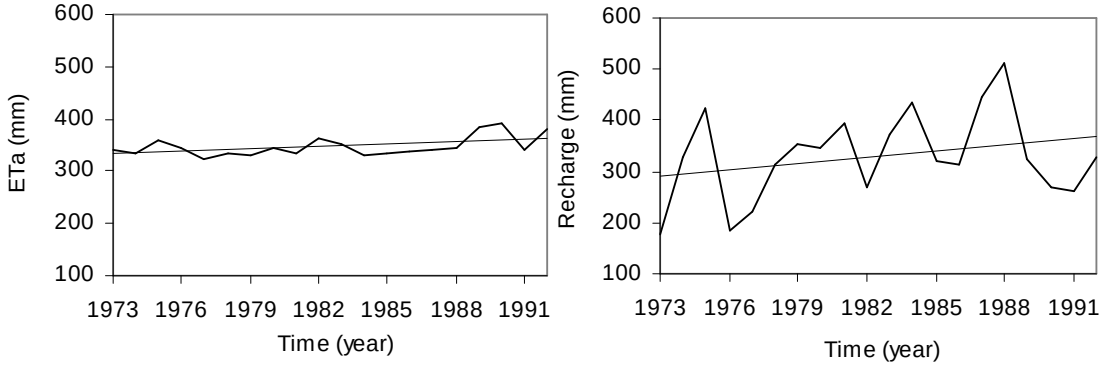

Figure 7.8 Annual actual evapotranspiration (left) and groundwater recharge (right)

The contribution of each land cover to the total mean annual evapotranspiration and recharge is calculated based on the area coverage of each land cover unit which was obtained from the ILWIS software histogram of the Land cover map. The highest recharge fluxes are from the area covered by mixed forest, light coniferous, Heath and Molinia grass (Table 7.3).

Table 7.3 Contribution of each land cover classes to mean annual recharge and evapotranspiration

Land cover type	Area coverage (%)	Recharge (mm y^{-1})	Evapotranspiration (mm y^{-1})
Molinia grass	11	39	50
Heath	11	42	52
Light coniferous	20	62	106
Dark coniferous	2	4	15
Deciduous	3	12	17
Mixed	38	124	210
Arable land	10	46	43
Build-up area	4.6	13	21
Sand	0.4	3	0.9
Mean annual		**345**	**515**

Finally the long-term average total evapotranspiration that also includes evaporation from tree interception for the Central Veluwe is found to be 515 mm y^{-1}. This value matches reasonably with the average annual evapotranspiration figure, 520 mm, for the whole Veluwe region reported by (Gehrels, 1999). The average groundwater recharge is found to be 345 mm y^{-1} which is slightly lower than the recharge obtained by Gehrels (1999), 360 mm y^{-1}, for the whole Veluwe region.

7.4. Comparing SWAP and EARTH models

SWAP is physically based numerical model based on Richards equation while EARTH is a conceptual reservoir-type model based on a simplified water balance equation. In terms of the required model input parameters and the approach of simulating soil water flow, the SWAP model is more complex than EARTH. It demands accurate estimates of a large number of site and vegetation type specific input parameters and variables that are not always available.

In the present study the same top and bottom boundary conditions were assigned to both models to be able to compare the results more clearly. Their difference is restricted only to the subsoil part in which SWAP simulates the soil water flow in the root zone based on Richards equation combined with a sink term while EARTH employs a simple water balance equation. Both approaches are capable of simulating the slow groundwater level fluctuation of the Central Veluwe. Regarding the goodness of fit with recorded groundwater levels, it can be stated that both models perform equally good. Also there is no significant difference between the water balance components of the two models. Thus the conceptual difference in the root zone did not result in a significant difference in the water balance components obtained from the two models.

The close agreement between the simulated results of the two models also indicates that the simple EARTH model is equally suitable as the more complex SWAP model at least for the condition of the Central Veluwe.

7.5. Comparing Makkink and Penman-Monteith based on the results of this research

The Makkink equation is based on radiation and is mostly applicable in the Netherlands while the Penman-Monteith method is based on radiation and aerodynamic concept and is applicable in all

climatic conditions (Kroes and Van Dam, 2003). The Makkink method is simple and needs small data while the Penman-Monteith method requires a lot of data that are not always available.
In the present study, both methods were used to calculate the potential evapotranspiration. No significant difference was observed between the simulation results of the two methods for the EARTH model. However, for the SWAP model, for some sites the simulation with Makkink derived evapotranspiration was found to yield better results than those obtained with Penman-Monteith method. The calculation of the potential evapotranspiration using the Penman-Monteith equation available is SWAP depends on atmospheric conditions and aerodynamic terms which include the aerodynamic and minimum canopy resistance. However, accepted minimum canopy resistances for the vegetation types under consideration are not available. Hence the average canopy resistances obtained from different literatures were used for the current study. Thus the slightly lower performance of the SWAP model when the SWAP mode of calculating evapotranspiration is used could be due to the uncertainties in the canopy resistances and other parameters.

7.6. Limitations

In the present study, field measured initial soil moisture data was not available. Hence during SWAP modelling the soil pressure heads of the soil compartments were assumed to be in hydrostatic equilibrium with the initial groundwater levels. Hence initial groundwater levels were assigned as initial pressure heads. It was observed that the soil compartments took some time to reach at equilibrium with the groundwater level. Due to this, the conditions were dry in the first periods and the soil layers took some time, approximately two years to reach at field capacity, which limits the bottom flux movement at the boundary and causes problem in the simulation of initial conditions.
The water stress in SWAP is described by the function proposed by Feddes et al. (1978).The reduction coefficient for root water uptake α_w is described as a function of soil water pressure head and potential transpiration rate. Thus calculation of actual evapotranspiration is highly interconnected with soil pressure heads, rate of potential evapotranspiration and soil hydraulic functions. Thus accurate estimation of these parameters and variables are crucial for accurate calculation of actual evapotranspiration in SWAP. However, the critical pressure head and potential transpiration values for each vegetation type in the study area are not available thus values of grass obtained from the SWAP manual were used for all the vegetation types. Accurate assessment of the root depth is also difficult since root depth may be variable. In this study from previous works the same root depth 0.8 m is assumed for the forests and 0.6 m for grass and heath.
Such simplifications and assumptions could reduce the performance of the models. As discussed before although the RMSE for both models is satisfactory, still the model prediction is not one to one as shown in (Figure 6.6). At some instants the models over estimate the groundwater level at other instants they underestimate. This could be due to the uncertainties arising from the large number of parameters involved, model input data and model concept.
In the present study, the effect of the groundwater abstraction could not be quantified further due to limitation in the model design. Abstraction is not considered with both the EARTH and SWAP versions used in this study.

8. Conclusions and Recommendations

8.1. Conclusions

The objective of this study was to assess the effect of meteorological forcing on groundwater recharge and water table fluctuations in Central Veluwe through unsaturated zone soil water flow modelling. Soil moisture, actual evapotranspiration, percolation, recharge and groundwater level fluctuations were simulated for a period of twenty years (1973-1992) using EARTH and SWAP models. The simulated groundwater levels were compared with the observed levels. Both models appear to simulate the slow groundwater level fluctuations of the study area with high accuracy in the first 15 years of the simulation period. However, systematic deviations occurred in the last 5 years of the simulations probably due to increased groundwater abstractions in the area. This indicates that natural groundwater level fluctuations for the groundwater system in the study area can be explained from the simulation of the vertical water flux through the unsaturated zone. However, the man-induced groundwater level fluctuations could not be explained using the unsaturated zone models because such artificial influences are not included in the design of the model structures. Thus in this research the effects of the abstractions on the groundwater level fluctuations cannot be quantified further.

Nearly identical actual evapotranspiration and groundwater recharge values were obtained from the simulation results of both models. The goodness of fit between the observed and simulated groundwater levels is also equally good for both models. It is recalled that both models share the same boundary conditions. Hence it can be concluded that the water balance calculation is depending more on the top boundary conditions than on the complex soil water flow in the unsaturated zone.

The calculated actual evapotranspiration for forest is found to be lower than for grass and heath. In contrast, high recharge values are estimated in areas that are mainly dominated by grass and heath while low values in areas covered by forest. This shows that loss of water due to interception from forest contributes significantly to the total loss of water due to evaporation. Thus for forests interception and transpiration should be considered separately.

The actual evapotranspiration from deciduous forest is found to be lower than the other vegetation types in the area. The seasonal shedding of leaves causes the water consumption and interception of the deciduous forest to be lower than the other vegetations. As a result the groundwater recharge below the deciduous forest is found to be higher than the other forests but slightly lower than grass and heath. The lowest groundwater recharge was obtained below Douglas fir forest which is caused from its high interception capacity. This study also reveals that the highest recharge fluxes are from the area covered by Mixed Forest, Light Coniferous, Heath and Molinia grass. This shows that these vegetation types have a dominant effect on the groundwater recharge of the study area.

The annual actual evapotranspiration is found to be constant through time. In contrast, the recharge rate shows a high temporal variability and follows a pattern similar to annual precipitation. It thus could be concluded that the encountered large variability in recharge is largely attributed to the variability in precipitation.

The long-term mean annual evapotranspiration that also includes evaporation from tree interception is found to be 515 mm y^{-1} while the groundwater recharge amounts to 345 mm y^{-1}. Groundwater recharge is only 39% of the mean annual precipitation and implies that 61% of precipitation is lost by evapotranspiration.

The overall conclusion of this study is that groundwater level fluctuations in the Central Veluwe are affected by natural climatic variations and anthropogenic influences.

8.2. Recommendations

Models should work hand in hand with field measurements for better estimation of hydrologic variables. For example, in SWAP modelling the problem with simulating the initial conditions can be improved by using field measured soil moisture data.

The performance of the models can be further improved by further refining the model input data (top boundary condition). In this study, due to limitation of data the canopy interception is estimated as a percentage of daily precipitation. However the forest canopy interception can be calculated using Gash interception model which is appropriate for forest interception.

The area is characterized by complex subsurface geology with different thickness aquifers. Thus a transient groundwater flow model should be developed to study the effect of groundwater abstraction on the water table fluctuations in detail.

References

Allen, R.G., Pereira, L.S., Raes, D. and Smith, M., 1998. Crop evapotranspiration: guidelines for computing crop water requirements. FAO irrigation and drainage paper; 56. FAO, Rome, 300 pp.

Anderson, M.P. and Woessner, W.W., 1992. Applied groundwater modelling: simulation of flow and advective transport. Academic Press, San Diego etc., 381 pp.

Berendrecht, W., 2004. State space modelling of groundwater fluctuations. PhD Thesis, Delft University, 149 pp.

Bosveld, F.C., 1999. Exchange processes between a coniferous forest and the atmosphere, Wageningen University, Wageningen, 181 pp.

Buckingham, E., 1907. Studies on the movement of soil moisture. USDA Bur.soils Bull, 38:61 pp.

Chen, T.S. and Ohring, G., 1984. On the relationship between clear-sky planetary and surface albedos. In: Journal of the Atmospheric Sciences, 41(1984)1, pp.156-158.

Choudhury, B.J., Ahmed, N.U., Idso, S.B., Reginato, R.J. and Daughtry, C.S.T., 1994. Relations between evaporation coefficients and vegetation indices studied by model simulations. Remote Sensing of Environment, 50(1): 1-17.

Cooper, T.A. and Lockwood, J.G., 1987. The influence of rainfall distribution in numerical simulation of evapotranspiration from multilayer model Pine canopy. Water resource Research, 23: 1645-1656.

De Vries, J.J., 1974. Groundwater flow systems and stream nets in the Netherlands. Ph.D Thesis, Vrije Universiteit, Amsterdam, 226 pp.

Dingman, S.L., 2002. Physical hydrology. Prentice Hall, Upper Saddle River, 646 pp.

Dolman, A.J. and Moors, E.J., 1994. Hydrologie en waterhuishouding van bosgebieden in Nederland; fase 1: toetsing instrumentarium. Rapport 333. DLO-Staring Centrum, Wageningen, pp. 73.

Dolman, H., Moors, E., Elbers, J., Snyders, W. and Hamaker, P., 2000. The role of forests in the hydrology of The Netherlands. Alterra Report.

Dufour, F.C., 2000. Groundwater in the Netherlands. Netherlands Institute of Applied Geosciences TNO, Delft/Utrecht, 96 pp.

Elbers, J.A., Dolman, A.J., Moors, E.J. and Snijders, W., 1996. Hydrologie en waterhuishouding van bosgebieden in Nederland; fase 2: meetopzet en eerste resultaten. Rapport 334. DLO-Staring Centrum, Wageningen, pp. 65.

Feddes, R.A., Kabat, P., Van Bakel, P.J.T., Bronswijk, J.J.B. and Halbertsma, J., 1988. Modelling soil water dynamics in the unsaturated zone -- State of the art. Journal of Hydrology, 100(1-3): 69-111.

Feddes, R.A., Kowalik, P.J. and Zaradny, H., 1978. Simulation of field water use and crop yield. Simulation Monographs, Pudoc, Wageningen, 189 pp.

Fetter, C.W. and Lee, K., 1994. Applied hydrogeology and hydrogeology laboratory manual. Prentice Hall, Englewood Cliffs, 691 pp.

Freeze, R.A. and Cherry, J.A., 1979. Groundwater. Prentice-Hall, Englewood Cliffs, 604 pp.

French, A.N., Schmugge, T.J., Kustas, W.P., Brubaker, K.L. and Prueger, J., 2003. Surface energy fluxes over El Reno, Oklahoma, using high-resolution remotely sensed data. Water Resources Research, 39(6): 1164-1175.

Gehrels, J.C., 1999. Groundwater level fluctuations. PhD Thesis, Faculty of Earth Sciences of the Vrije University, Amsterdam, 269 pp.

Jyrkama, M.I. and Sykes, J.F., 2007. The impact of climate change on spatially varying groundwater recharge in the grand river watershed (Ontario). Journal of Hydrology, 338(3-4): 237-250.

Kroes, J.G. and Van Dam, J.C., 2003. Reference Manual SWAP version 3.0.3. Wageningen, Alterra, Green World Research, pp. 211.

Lerner, D.N., Issar, A.S. and Simmers, I., 1990. Groundwater recharge : a guide to understanding and estimating natural recharge: International Association of Hydrogeologists. International Contributions to Hydrogeology: IAH International Association of Hydrogeologists; 8. Heise, Hannover, 345 pp.

Liang, S. et al., 2003. Narrowband to broadband conversions of land surface albedo: II. Validation. Remote Sensing of Environment, 84(1): 25-41.

Markham, B.L. and Barker, J.L., 1987. Radiometric properties of U.S. processed landsat MSS data. Remote Sensing of Environment, 22(1): 39-71.

Monteith, J.L., 1965. Evaporation and the environment. Symp. Soc. Experimental Biology, No.19, 206-234 pp.

Mualem, 1976. A New Model for Predicting the Hydraulic Conductivity of Unsaturated Porous Media. Journal of Hydrology, 12(3).

Richards, L.A., 1931. Capilary conduction of liquids through porous mediums. Physics,1:318-333.

Romano, N., Brunone, B. and Santini, A., 1998. Numerical analysis of one-dimensional unsaturated flow in layered soils. Advances in Water Resources, 21(4): 315-324.

Rutter, A.J., Kershaw, K.A., Robins, P.C. and Morton, A.J., 1971. A predictive model of rainfall interception in forests, 1. Derivation of the model from observations in a plantation of Corsican pine. Agricultural Meteorology, 9: 367-384.

Simmers, I.H., J.M.H. Kruseman .P.G. and Rushton K.R., 1997. Recharge of Phreatic Aquifers in (Semi-) Arid Areas. Faculty of Earth Sciences, Free University, Amsterdam, 277 pp.

Thom, A.S., 1975. Momentum, mass and heat exchange of plant communities. In: J.L. Monteith, (ed), Vegetation and the atmosphere, 1. Principles, Academic press, London, 57-109 pp.

Tiktak, A. and Bouten, W., 1990. Soil hydrological system characterization of the two ACIFORN stands using monitoring data and the soil hydrological model "SWIF" Universiteit van Amsterdam/ Dutch priority programme on acidification, No.102.2.01, Amsterdam, 62 pp.

Tiktak, A. and Bouten, W., 1994. Soil water dynamics and long-term water balances of a Douglas fir stand in the Netherlands. Journal of Hydrology, 156(1-4): 265-283.

Van Dam, J.C., 2000. Field - scale water flow and solute transport: SWAP model concepts, parameter estimation and case studies. Wageningen Agricultural University, Wageningen, 167 pp.

Van den Berg, E.H., 1995. Analysis of long-term annual water balances based on the simulation of soil moisture content and groundwater level fluctuations at the Veluwe, The Netherlands. M.Sc. Thesis, Vrije Universiteit, Amsterdam, 81 pp.

Van der Lee, J. and Gehrels, J.C., 1990. Modelling Aquifer Recharge: Introduction to the Lumped Parameter Model EARTH, Free University of Amsterdam.

Van der Lee, J. and Gehrels, J.C., 1997. Modelling of groundwater recharge of a fractured dolomite aquifer under semi-arid conditions. In: I. Simmers (ed), Recharge of phreatic aquifers in (semi-) arid areas. UNESCO / IAH Int. Contr. to Hydrogeology, Balkema, Rotterdam, pp. 129-144.

Van Genuchten, M.T., 1980. A Closed-form Equation for Predicting the Hydraulic Conductivity of Unsaturated Soils. Journal of Hydrology, 44: 892-898.

Wullschleger, S.D., Wilson, K.B. and Hanson, P.J., 2000. Environmental control of whole-plant transpiration, canopy conductance and estimates of the decoupling coefficient for large red maple trees. Agricultural and Forest Meteorology, 104(2): 157-168.

Appendices

Appendix 1 Meta data files for the Landsat Images data

August 26, 2000

GROUP=L1_METADATA_FILE
GROUP=METADATA_FILE_INFO
REQUEST_ID="080050915006100002"
PRODUCT_CREATION_TIME=2005-09-16T00:01:14Z
STATION_ID="EDC"
LANDSAT7_XBAND="1"
GROUND_STATION="EDC"
LPS_PROCESSOR_NUMBER=1
DATEHOUR_CONTACT_PERIOD="0222816"
SUBINTERVAL_NUMBER="01"
GROUP=PRODUCT_METADATA
PRODUCT_TYPE="L1G"
PROCESSING_SOFTWARE="NLAPS_4.8.0E17"
EPHEMERIS_TYPE="DEFINITIVE"
SPACECRAFT_ID="Landsat7"
SENSOR_ID = "ETM+"
ACQUISITION_DATE =2002-08-16
WRS_PATH =197
STARTING_ROW =024
ENDING_ROW =024
BAND_COMBINATION ="123456678"
PRODUCT_UL_CORNER_LAT =52.6840210
PRODUCT_UL_CORNER_LON =5.4756126
PRODUCT_UR_CORNER_LAT =52.2789955
PRODUCT_UR_CORNER_LON =8.2487679
PRODUCT_LL_CORNER_LAT =51.1036911
PRODUCT_LL_CORNER_LON =4.9252906
PRODUCT_LR_CORNER_LAT =50.7112503
PRODUCT_LR_CORNER_LON =7.6080341
PRODUCT_UL_CORNER_MAPX =261793.683
PRODUCT_UL_CORNER_MAPY =5842951.220
PRODUCT_UR_CORNER_MAPX =448749.066
PRODUCT_UR_CORNER_MAPY =5792335.494
PRODUCT_LL_CORNER_MAPX =14767.828
PRODUCT_LL_CORNER_MAPY =5669255.475
PRODUCT_LR_CORNER_MAPX =401723.214
PRODUCT_LR_CORNER_MAPY =5618639.749
PRODUCT_UL_CORNER_LAT_PAN =52.6840973
PRODUCT_UL_CORNER_LON_PAN =5.4755321
PRODUCT_UR_CORNER_LAT_PAN =52.2790413
PRODUCT_UR_CORNER_LON_PAN =8.2488947
PRODUCT_LL_CORNER_LAT_PAN =51.1036415
PRODUCT_LL_CORNER_LON_PAN =4.9251699
PRODUCT_LR_CORNER_LAT_PAN =50.7111740
PRODUCT_LR_CORNER_LON_PAN =7.6081071
PRODUCT_UL_CORNER_MAPX_PAN = 261788.668
PRODUCT_UL_CORNER_MAPY_PAN = 5842959.959
PRODUCT_UR_CORNER_MAPX_PAN = 448757.806
PRODUCT_UR_CORNER_MAPY_PAN = 5792340.509
PRODUCT_LL_CORNER_MAPX_PAN = 214759.089
PRODUCT_LL_CORNER_MAPY_PAN = 5669250.460
BAND4_SL_GAIN_CHANGE = 0
BAND5_SL_GAIN_CHANGE = 0
BAND6_SL_GAIN_CHANGE1 = 0
BAND6_SL_GAIN_CHANGE2 = 0
BAND7_SL_GAIN_CHANGE = 0
BAND8_SL_GAIN_CHANGE = 0
SUN_AZIMUTH = 148.8511919
SUN_ELEVATION = 48.7419355
PRODUCT_LR_CORNER_MAPX_PAN = 401728.229
PRODUCT_LR_CORNER_MAPY_PAN = 5618631.010
PRODUCT_UL_CORNER_LAT_THM =52.6838684
PRODUCT_UL_CORNER_LON_THM =5.4757733
PRODUCT_UR_CORNER_LAT_THM =52.2789688
PRODUCT_UR_CORNER_LON_THM =8.2481089
PRODUCT_LL_CORNER_LAT_THM = 51.1040382
PRODUCT_LL_CORNER_LON_THM = 4.9256163
PRODUCT_LR_CORNER_LAT_THM = 50.7117157
PRODUCT_LR_CORNER_LON_THM = 7.6075940
PRODUCT_UL_CORNER_MAPX_THM = 261803.714
QCALMAX_BAND61 = 255.0
QCALMIN_BAND61 = 1.0
QCALMAX_BAND62 = 255.0
QCALMIN_BAND62 = 1.0
QCALMAX_BAND7 = 255.0
QCALMIN_BAND7 = 1.0
QCALMAX_BAND8 = 255.0
QCALMIN_BAND8 = 1.0
GROUP = PRODUCT_PARAMETERS
CORRECTION_METHOD_GAIN_BAND1 = "CPF"
CORRECTION_METHOD_GAIN_BAND2 = "CPF"
CORRECTION_METHOD_GAIN_BAND3 = "CPF"
CORRECTION_METHOD_GAIN_BAND4 = "CPF"
CORRECTION_METHOD_GAIN_BAND5 = "CPF"
CORRECTION_METHOD_GAIN_BAND61 = "CPF"
CORRECTION_METHOD_GAIN_BAND62 = "CPF"
CORRECTION_METHOD_GAIN_BAND7 = "CPF"
CORRECTION_METHOD_GAIN_BAND8 = "CPF"
CORRECTION_METHOD_BIAS = "IC"
BAND1_GAIN = "H"
BAND2_GAIN = "H"
BAND3_GAIN = "H"
BAND4_GAIN = "L"
BAND5_GAIN = "H"
BAND6_GAIN1 = "L"
BAND6_GAIN2 = "H"
BAND7_GAIN = "H"
BAND8_GAIN = "L"
BAND1_GAIN_CHANGE = "0"
BAND2_GAIN_CHANGE = "0"
BAND3_GAIN_CHANGE = "0"
BAND4_GAIN_CHANGE = "0"
BAND5_GAIN_CHANGE = "0"
BAND6_GAIN_CHANGE1 = "0"
BAND6_GAIN_CHANGE2 = "0"
BAND7_GAIN_CHANGE = "0"
BAND8_GAIN_CHANGE = "0"
BAND1_SL_GAIN_CHANGE = 0
BAND2_SL_GAIN_CHANGE = 0
BAND3_SL_GAIN_CHANGE = 0
STRIPING_BAND8 = "BAND_AVERAGE"
BANDING = "Y"
COHERENT_NOISE = "Y"
MEMORY_EFFECT = "N"
SCAN_CORRELATED_SHIFT = "Y"
INOPERABLE_DETECTORS = "Y"
DROPPED_LINES = "Y"
GROUP = PROJECTION_PARAMETERS

GROUP = PRODUCT_PARAMETERS
CORRECTION_METHOD_GAIN_BAND1 = "CPF"
CORRECTION_METHOD_GAIN_BAND2 = "CPF"
CORRECTION_METHOD_GAIN_BAND3 = "CPF"
CORRECTION_METHOD_GAIN_BAND4 = "CPF"
CORRECTION_METHOD_GAIN_BAND5 = "CPF"
CORRECTION_METHOD_GAIN_BAND61 = "CPF"
CORRECTION_METHOD_GAIN_BAND62 = "CPF"
CORRECTION_METHOD_GAIN_BAND7 = "CPF"
CORRECTION_METHOD_GAIN_BAND8 = "CPF"
CORRECTION_METHOD_BIAS = "IC"
BAND1_GAIN = "H"
BAND2_GAIN = "H"
BAND3_GAIN = "H"
BAND4_GAIN = "L"
BAND5_GAIN = "H"
BAND6_GAIN1 = "L"
BAND6_GAIN2 = "H"
BAND7_GAIN = "H"
BAND8_GAIN = "L"
BAND1_GAIN_CHANGE = "0"
BAND2_GAIN_CHANGE = "0"
BAND3_GAIN_CHANGE = "0"
BAND4_GAIN_CHANGE = "0"
BAND5_GAIN_CHANGE = "0"
BAND6_GAIN_CHANGE1 = "0"
BAND6_GAIN_CHANGE2 = "0"
BAND7_GAIN_CHANGE = "0"
BAND8_GAIN_CHANGE = "0"
BAND1_SL_GAIN_CHANGE = "0"
BAND2_SL_GAIN_CHANGE = "0"
BAND3_SL_GAIN_CHANGE = "0"
BAND4_SL_GAIN_CHANGE = "0"
BAND5_SL_GAIN_CHANGE = "0"
BAND6_SL_GAIN_CHANGE1 = "0"
BAND6_SL_GAIN_CHANGE2 = "0"
BAND7_SL_GAIN_CHANGE = "0"
BAND8_SL_GAIN_CHANGE = "0"
END_GROUP = PRODUCT_PARAMETERS
GROUP = CORRECTIONS_APPLIED
STRIPING_BAND1 = "NONE"
STRIPING_BAND2 = "NONE"
STRIPING_BAND3 = "NONE"
STRIPING_BAND4 = "NONE"
STRIPING_BAND5 = "NONE"
STRIPING_BAND61 = "NONE"
STRIPING_BAND62 = "NONE"
STRIPING_BAND7 = "NONE"
STRIPING_BAND8 = "NONE"
BANDING = "N"
COHERENT_NOISE = "N"
MEMORY_EFFECT = "N"
SCAN_CORRELATED_SHIFT = "N"
INOPERABLE_DETECTORS = "N"
DROPPED_LINES = N
END_GROUP = CORRECTIONS_APPLIED
END_GROUP = L1G_PRODUCT_METADATA
END_GROUP = METADATA_FILE

May 25, 2001

GROUP = METADATA_FILE
PRODUCT_CREATION_TIME = 2004-02-12T17:23:45Z
PRODUCT_FILE_SIZE = 757.2
STATION_ID = "EDC"
GROUND_STATION = "EDC"
GROUP = ORTHO_PRODUCT_METADATA
SPACECRAFT_ID = "Landsat7"
SENSOR_ID = "ETM+"
ACQUISITION_DATE = 2001-05-25
WRS_PATH = 197
WRS_ROW = 024
SCENE_CENTER_LAT = +51.7067576
SCENE_CENTER_LON = +6.5594855
SCENE_UL_CORNER_LAT = +52.6896223
SCENE_UL_CORNER_LON = +5.5954995
SCENE_UR_CORNER_LAT = +52.3012719
SCENE_UR_CORNER_LON = +8.2397882
SCENE_LL_CORNER_LAT = +51.0894874
SCENE_LL_CORNER_LON = +4.9242146
SCENE_LR_CORNER_LAT = +50.7155044
SCENE_LR_CORNER_LON = +7.4817245
SCENE_UL_CORNER_MAPX = 269923.500
SCENE_UL_CORNER_MAPY = 5843184.000
SCENE_UR_CORNER_MAPX = 448162.500
SCENE_UR_CORNER_MAPY = 5794819.500
SCENE_LL_CORNER_MAPX = 214605.000
SCENE_LL_CORNER_MAPY = 5667681.000
SCENE_LR_CORNER_MAPX = 392815.500
GRID_CELL_ORIGIN = "Center"
UL_GRID_LINE_NUMBER = 1
UL_GRID_SAMPLE_NUMBER = 1
GRID_INCREMENT_UNIT = "Meters"
GRID_CELL_SIZE_PAN = 14.250
GRID_CELL_SIZE_PAN = 14.250
GRID_CELL_SIZE_THM = 57.000
GRID_CELL_SIZE_REF = 28.500
FALSE_NORTHING = 0
ORIENTATION = "NUP"
RESAMPLING_OPTION = "NN"
MAP_PROJECTION = "UTM"
END_GROUP = PROJECTION_PARAMETERS
GROUP = UTM_PARAMETERS
ZONE_NUMBER = +32
END_GROUP = UTM_PARAMETERS

GROUP = PRODUCT_PARAMETERS
CORRECTION_METHOD_GAIN_BAND1 = "CPF"
CORRECTION_METHOD_GAIN_BAND2 = "CPF"
CORRECTION_METHOD_GAIN_BAND3 = "CPF"
CORRECTION_METHOD_GAIN_BAND4 = "CPF"
CORRECTION_METHOD_GAIN_BAND5 = "CPF"
CORRECTION_METHOD_GAIN_BAND61 = "CPF"
CORRECTION_METHOD_GAIN_BAND62 = "CPF"
CORRECTION_METHOD_GAIN_BAND7 = "CPF"
CORRECTION_METHOD_GAIN_BAND8 = "CPF"
CORRECTION_METHOD_BIAS = "IC"
BAND1_GAIN = "H"
BAND2_GAIN = "H"
BAND3_GAIN = "H"
BAND4_GAIN = "L"
BAND5_GAIN = "H"
BAND6_GAIN1 = "L"
BAND6_GAIN2 = "H"
SUN_AZIMUTH = 148.2162594
SUN_ELEVATION = 56.1599006
QA_PERCENT_MISSING_DATA = 0
CLOUD_COVER = 0
PRODUCT_SAMPLES_PAN = 18248
PRODUCT_LINES_PAN = 16564
PRODUCT_SAMPLES_REF = 9124
PRODUCT_LINES_REF = 8282
PRODUCT_SAMPLES_THM = 4562
PRODUCT_LINES_THM = 4141
OUTPUT_FORMAT = "GEOTIFF"
END_GROUP = ORTHO_PRODUCT_METADATA
GROUP = L1G_PRODUCT_METADATA
BAND_COMBINATION = "123456678"
CPF_FILE_NAME = "L7CPF20010401_20010630_05"
GROUP = MIN_MAX_RADIANCE
LMAX_BAND1 = 191.600
LMIN_BAND1 = -6.200
LMAX_BAND2 = 196.500
LMIN_BAND2 = -6.400
LMAX_BAND3 = 152.900
LMIN_BAND3 = -5.000
LMAX_BAND4 = 241.100
LMIN_BAND4 = -5.100
LMAX_BAND5 = 31.060
LMIN_BAND5 = -1.000
LMAX_BAND61 = 17.040
LMIN_BAND61 = 0.000
QCALMAX_BAND2 = 255.0
QCALMIN_BAND2 = 1.0
QCALMAX_BAND3 = 255.0
QCALMIN_BAND3 = 1.0
QCALMAX_BAND4 = 255.0
QCALMAX_BAND4 = 255.0
QCALMIN_BAND4 = 1.0
QCALMAX_BAND5 = 255.0
QCALMIN_BAND5 = 1.0
QCALMAX_BAND61 = 255.0
QCALMIN_BAND61 = 1.0
QCALMAX_BAND62 = 255.0
QCALMIN_BAND62 = 1.0
QCALMAX_BAND7 = 255.0
QCALMIN_BAND7 = 1.0
QCALMAX_BAND8 = 255.0
QCALMIN_BAND8 = 1.0
BAND1_SL_GAIN_CHANGE = "0"
BAND2_SL_GAIN_CHANGE = "0"
BAND3_SL_GAIN_CHANGE = "0"
BAND4_SL_GAIN_CHANGE = "0"
BAND5_SL_GAIN_CHANGE = "0"
BAND6_SL_GAIN_CHANGE1 = "0"
BAND6_SL_GAIN_CHANGE2 = "0"
BAND7_SL_GAIN_CHANGE = "0"
BAND8_SL_GAIN_CHANGE = "0"
END_GROUP = PRODUCT_PARAMETERS
GROUP = CORRECTIONS_APPLIED
STRIPING_BAND1 = "NONE"
STRIPING_BAND2 = "NONE"
STRIPING_BAND3 = "NONE"
STRIPING_BAND4 = "NONE"
STRIPING_BAND5 = "NONE"
STRIPING_BAND61 = "NONE"
STRIPING_BAND62 = "NONE"

BAND7_GAIN = "H"
BAND8_GAIN = "L"
BAND1_GAIN_CHANGE = "0"
BAND2_GAIN_CHANGE = "0"
BAND3_GAIN_CHANGE = "0"
BAND4_GAIN_CHANGE = "0"
BAND5_GAIN_CHANGE = "0"
BAND6_GAIN_CHANGE1 = "0"
BAND6_GAIN_CHANGE2 = "0"
BAND7_GAIN_CHANGE = "0"
BAND8_GAIN_CHANGE = "0"
STRIPING_BAND7 = "NONE"
STRIPING_BAND8 = "NONE"
BANDING = "N"
COHERENT_NOISE = "N"
MEMORY_EFFECT = "N"
SCAN_CORRELATED_SHIFT = "N"
INOPERABLE_DETECTORS = "N"
DROPPED_LINES = N
END_GROUP = CORRECTIONS_APPLIED
END_GROUP = L1G_PRODUCT_METADATA
END_GROUP = METADATA_FILE

August 16, 2002

GROUP = L1_METADATA_FILE
REQUEST_ID = "080050915006100002"
PRODUCT_CREATION_TIME = 2005-09-16T00:01:14Z
STATION_ID = "EDC"
LANDSAT7_XBAND = "1"
GROUND_STATION = "EDC"
LPS_PROCESSOR_NUMBER = 1
DATEHOUR_CONTACT_PERIOD = "0222816"
SUBINTERVAL_NUMBER = "01"
GROUP = PRODUCT_METADATA
PRODUCT_TYPE = "L1G"
PROCESSING_SOFTWARE = "NLAPS_4.8.0E17"
EPHEMERIS_TYPE = "DEFINITIVE"
SPACECRAFT_ID = "Landsat7"
SENSOR_ID = "ETM+"
ACQUISITION_DATE = 2002-08-16
WRS_PATH = 197
STARTING_ROW = 024
ENDING_ROW = 024
BAND_COMBINATION = "123456678"
PRODUCT_UL_CORNER_LAT = 52.6840210
PRODUCT_UL_CORNER_LON = 5.4756126
PRODUCT_UR_CORNER_LAT = 52.2789955
PRODUCT_UR_CORNER_LON = 8.2487679
PRODUCT_LL_CORNER_LAT = 51.1036911
PRODUCT_LL_CORNER_LON = 4.9252906
PRODUCT_LR_CORNER_LAT = 50.7112503
PRODUCT_LR_CORNER_LON = 7.6080341
PRODUCT_UL_CORNER_MAPX = 261793.683
PRODUCT_UL_CORNER_MAPY = 5842951.220
PRODUCT_UR_CORNER_MAPX = 448749.066
PRODUCT_UR_CORNER_MAPY =5792335.494
PRODUCT_LL_CORNER_MAPX = 214767.828
PRODUCT_LL_CORNER_MAPY = 5669255.475
PRODUCT_LR_CORNER_MAPX = 401723.214
PRODUCT_LR_CORNER_MAPY=5618639.749
PRODUCT_UL_CORNER_LAT_PAN=52.6840973
PRODUCT_UL_CORNER_LON_PAN = 5.4755321
PRODUCT_UR_CORNER_LAT_PAN = 52.2790413
PRODUCT_UR_CORNER_LON_PAN = 8.2488947
PRODUCT_LL_CORNER_LAT_PAN = 51.1036415
PRODUCT_LL_CORNER_LON_PAN = 4.9251699
PRODUCT_LR_CORNER_LAT_PAN = 50.7111740
PRODUCT_LR_CORNER_LON_PAN = 7.6081071
PRODUCT_UL_CORNER_MAPX_PAN = 261788.668
PRODUCT_UL_CORNER_MAPY_PAN = 5842959.959
PRODUCT_UR_CORNER_MAPX_PAN = 448757.806
PRODUCT_UR_CORNER_MAPY_PAN = 5792340.509
PRODUCT_LL_CORNER_MAPX_PAN = 214759.089
PRODUCT_LL_CORNER_MAPY_PAN = 5669250.460
PRODUCT_UR_CORNER_LON_THM = 8.2481089
PRODUCT_LL_CORNER_LAT_THM = 51.1040382
PRODUCT_LL_CORNER_LON_THM = 4.9256163
GROUP = MIN_MAX_PIXEL_VALUE
QCALMAX_BAND1 = 255.0
QCALMIN_BAND1 = 1.0
QCALMAX_BAND2 = 255.0
QCALMIN_BAND2 = 1.0
QCALMAX_BAND3 = 255.0
QCALMIN_BAND3 = 1.0
QCALMAX_BAND4 = 255.0
QCALMIN_BAND4 = 1.0
QCALMAX_BAND5 = 255.0
QCALMIN_BAND5 = 1.0
CORRECTION_METHOD_GAIN_BAND7 = "CPF"
CORRECTION_METHOD_GAIN_BAND8 = "CPF"
CORRECTION_METHOD_BIAS = "IC"
PRODUCT_LR_CORNER_LAT_THM = 50.7117157
PRODUCT_LR_CORNER_MAPX_PAN = 401728.229
PRODUCT_LR_CORNER_MAPY_PAN = 5618631.010
PRODUCT_UL_CORNER_LAT_THM = 52.6838684
PRODUCT_UL_CORNER_LON_THM = 5.4757733
PRODUCT_UR_CORNER_LAT_THM = 52.2789688
PRODUCT_LR_CORNER_LON_THM
=7.6075940PRODUCT_UL_CORNER_MAPX_THM=261803.714
PRODUCT_UL_CORNER_MAPY_THM = 5842933.741
PRODUCT_UR_CORNER_MAPX_THM = 448704.078
PRODUCT_UR_CORNER_MAPY_THM = 5792332.911
PRODUCT_LL_CORNER_MAPX_THM = 214792.755
PRODUCT_LL_CORNER_MAPY_THM = 5669293.016
PRODUCT_LR_CORNER_MAPX_THM = 401693.121
PRODUCT_LR_CORNER_MAPY_THM = 5618692.185
PRODUCT_SAMPLES_PAN = 13594
PRODUCT_LINES_PAN = 12630
PRODUCT_SAMPLES_REF = 6797
PRODUCT_LINES_REF = 6315
PRODUCT_SAMPLES_THM = 3398
PRODUCT_LINES_THM = 3157
BAND1_FILE_NAME = "L71197024_02420020816_B10.FST"
BAND2_FILE_NAME = "L71197024_02420020816_B20.FST"
BAND3_FILE_NAME = "L71197024_02420020816_B30.FST"
BAND4_FILE_NAME = "L71197024_02420020816_B40.FST"
BAND5_FILE_NAME = "L71197024_02420020816_B50.FST"
BAND61_FILE_NAME = "L71197024_02420020816_B61.FST"
BAND62_FILE_NAME="L72197024_02420020816_B62.FST"
BAND7_FILE_NAME = "L72197024_02420020816_B70.FST"
BAND8_FILE_NAME = "L72197024_02420020816_B80.FST"
METADATA_L1_FILE_NAME =
"L71197024_02420020816_MTL.FST"
CPF_FILE_NAME = "L7CPF20020701_20020930.04"
END_GROUP = PRODUCT_METADATA
GROUP = MIN_MAX_RADIANCE
LMAX_BAND1 = 191.600
LMIN_BAND1 = -6.200
LMAX_BAND2 = 196.500
LMIN_BAND2 = -6.400
LMAX_BAND3 = 152.900
LMIN_BAND3 = -5.000
LMAX_BAND4 = 241.100
LMIN_BAND4 = -5.100
LMAX_BAND5 = 31.060
LMIN_BAND5 = -1.000
LMAX_BAND61 = 17.040
LMIN_BAND61 = 0.000
LMAX_BAND62 = 12.650
LMIN_BAND62 = 3.200
LMAX_BAND7 = 10.800
LMIN_BAND7 = -0.350
LMAX_BAND8 = 243.100
LMIN_BAND8 = -4.700
BAND6_GAIN_CHANGE2 = "0"
BAND7_GAIN_CHANGE = "0"
BAND8_GAIN_CHANGE = "0"
BAND1_SL_GAIN_CHANGE = 0
BAND2_SL_GAIN_CHANGE = 0
BAND3_SL_GAIN_CHANGE = 0
BAND4_SL_GAIN_CHANGE = 0
BAND5_SL_GAIN_CHANGE = 0
BAND6_SL_GAIN_CHANGE1 = 0
BAND6_SL_GAIN_CHANGE2 = 0
BAND7_SL_GAIN_CHANGE = 0
BAND8_SL_GAIN_CHANGE = 0
SUN_AZIMUTH =148.8511919
SUN_ELEVATION =48.7419355

QCALMAX_BAND61 = 255.0
QCALMIN_BAND61 = 1.0
QCALMAX_BAND62 = 255.0
QCALMIN_BAND62 = 1.0
QCALMAX_BAND7 = 255.0
QCALMIN_BAND7 = 1.0
QCALMAX_BAND8 = 255.0
QCALMIN_BAND8 = 1.0
END_GROUP = MIN_MAX_PIXEL_VALUE
GROUP = PRODUCT_PARAMETERS
CORRECTION_METHOD_GAIN_BAND1 = "CPF"
CORRECTION_METHOD_GAIN_BAND2 = "CPF"
CORRECTION_METHOD_GAIN_BAND3 = "CPF"
CORRECTION_METHOD_GAIN_BAND4 = "CPF"
CORRECTION_METHOD_GAIN_BAND5 = "CPF"
BAND3_GAIN = "H"
BAND4_GAIN = "L"
CORRECTION_METHOD_GAIN_BAND61 = "CPF"
CORRECTION_METHOD_GAIN_BAND62 = "CPF"
BAND1_GAIN = "H"
BAND2_GAIN = "H"
BAND5_GAIN = "H"
BAND6_GAIN1 = "L"
BAND6_GAIN2 = "H"
BAND7_GAIN = "H"
BAND8_GAIN = "L"
BAND1_GAIN_CHANGE = "0"
BAND2_GAIN_CHANGE = "0"
BAND3_GAIN_CHANGE = "0"
BAND4_GAIN_CHANGE = "0"
BAND5_GAIN_CHANGE = "0"
BAND6_GAIN_CHANGE1 = "0"
OUTPUT_FORMAT = "FASTL7A"
END_GROUP = PRODUCT_PARAMETERS
GROUP = CORRECTIONS_APPLIED
STRIPING_BAND1 = "BAND_AVERAGE"
STRIPING_BAND2 = "BAND_AVERAGE"
STRIPING_BAND3 = "BAND_AVERAGE"
STRIPING_BAND4 = "BAND_AVERAGE"
STRIPING_BAND5 = "BAND_AVERAGE"
STRIPING_BAND61 = "BAND_AVERAGE"
STRIPING_BAND62 = "BAND_AVERAGE"
STRIPING_BAND7 = "BAND_AVERAGE"
STRIPING_BAND8 = "BAND_AVERAGE"
BANDING = "Y"
COHERENT_NOISE = "Y"
MEMORY_EFFECT = "N"
SCAN_CORRELATED_SHIFT = "Y"
INOPERABLE_DETECTORS = "Y"
DROPPED_LINES = "Y"
END_GROUP = CORRECTIONS_APPLIED
GROUP = PROJECTION_PARAMETERS
REFERENCE_DATUM = "WGS84"
REFERENCE_ELLIPSOID = "WGS84"
GRID_CELL_SIZE_PAN = 14.250
GRID_CELL_SIZE_THM = 57.000
GRID_CELL_SIZE_REF = 28.500
ORIENTATION = "NOM"
RESAMPLING_OPTION = "NN"
MAP_PROJECTION = "UTM"
END_GROUP = PROJECTION_PARAMETERS
GROUP = UTM_PARAMETERS
ZONE_NUMBER = 032

Appendix 2 ILWIS script for Plant biophysical parameters calculation

Latig{dom=VALUE.dom;vr=-
=0.0000:90.0000:0.0001}:=iff(subsetimage_1>0,crdy(transform(mapcrd(subsetimage_1),latlon)),0)
Lon{dom=VALUE.dom;vr=-
180.0000:180.0000:0.0001}:=iff(subsetimage_1>0,crdx(transform(mapcrd(subsetimage_1),latlon)),0)
Dayangle_map:=lati-lati+dayangle(228)
Solardecination:=lati-lati+solardeclination(228)
Et_map:=lati-lati+et(228)*229.18
Localsolartime:=10+15/60+50/360+4*Lon/60+Et_map/60
Hourangle:=15*(Localsolartime-12)*pi/180
Lati_rad:=pi*Lati/180
Costheta:=sin(lati_rad)*sin(Solardecination)+cos(lati_rad)*cos(Solardecination)*cos(Hourangle)
E0_map:=lati-lati+E0(228)
//RADIANCES//
radiance_band1.mpr{dom=value.dom,vr=0:300:0.001}:=(191.6+6.2)/254*(subsetimage_1-1)-6.2
radiance_band2.mpr{dom=value.dom,vr=0:300:0.001}:=(196.5+6.4)/254*(subsetimage_2-1)-6.4
radiance_band3.mpr{dom=value.dom,vr=0:300:0.001}:=(152.9+5)/254*(subsetimage_3-1)-5
radiance_band4.mpr{dom=value.dom,vr=0:300:0.001}:=(241.1+5)/254*(subsetimage_4-1)-5
radiance_band5.mpr{dom=value.dom,vr=0:300:0.001}:=(31.06+1)/254*(subsetimage_5-1)-1
radiance_band7.mpr{dom=value.dom,vr=0:300:0.001}:=(10.8+0.35)/254*(subsetimage_6-1)-0.35
//REFLECTANCES//
reflectance_band1{dom=value.dom;vr=0:1:0.0001}:=(radiance_band1*pi)/(E0_map*costheta*1969)
reflectance_band2{dom=value.dom;vr=0:1:0.0001}:=(radiance_band2*pi)/(E0_map*Costheta*1840)
reflectance_band3{dom=value.dom;vr=0:1:0.0001}:=(radiance_band3*pi)/(E0_map*costheta*1551)
reflectance_band4{dom=value.dom;vr=0:1:0.0001}:=(radiance_band4*pi)/(E0_map*costheta*1044)
reflectance_band5{dom=value.dom;vr=0:1:0.0001}:=(radiance_band5*pi)/(E0_map*costheta*225.7)
reflectance_band7{dom=value.dom;vr=0:1:0.0001}:=(radiance_band7*pi)/(E0_map*costheta*82.07)
//PLANETARY BROADBAND ALBEDO//
Planatary_Albedo=0.356*reflectance_band1+0.130*reflectance_band3+0.373*reflectance_band4+0.0
85*reflectance_band5+0.072*reflectance_band7-0.001
// BROADBAND SURFACE ALBEDO//
Surface_albedo=(Planatary_Albedo-0.0536)/0.5625
//Normalized Difference Vegetation Index, Fractional vegetation cover, Leaf Area Index//
NDVI=(reflectance_band4-reflectance_band3)/(reflectance_band4+reflectance_band3)
fc=1-((NDVImax-NDVI)/(NDVImax-NDVImin))^0.625
LAI=log(1-fc)/-0.5

Appendix 3 De Bilt weather station daily meteorological data (1973)

Date	U (m/s)	Tmean (C)	Tmin (C)	Tmax (C)	n (hr)	n/N (fra)	P (Kpa)	RH (%)
1-Jan-1973	1.5	-2.7	-8.1	1.1	6.1	0.78	102.72	88
2-Jan-1973	1.5	1.8	-1	3.8	0	0	102.88	93
3-Jan-1973	2.1	3.5	2.5	4.6	0	0	103	95
4-Jan-1973	2.1	2.3	-0.9	4.5	0	0	103.52	98
5-Jan-1973	1.5	0.3	-0.5	1.4	1.5	0.19	104	99
6-Jan-1973	2.6	2.9	1.1	4.1	0	0	103.99	99
7-Jan-1973	1.5	2.3	0.3	3.8	0	0	103.87	99
8-Jan-1973	1	4	3.2	5.2	0	0	103.66	92
9-Jan-1973	1	3.6	2.7	4.9	0	0	103.36	97
10-Jan-1973	1	2.9	1.3	5	0	0	103.13	95
11-Jan-1973	1	3.2	2.3	4.3	0	0	103.16	82
12-Jan-1973	2.1	1.9	-1.4	3	0	0	103	84
13-Jan-1973	2.6	-1.3	-4	1.6	5.6	0.69	102.39	91
14-Jan-1973	3.6	3.2	-0.2	5.8	0	0	101.49	90
15-Jan-1973	5.1	5.7	3.7	8.9	2.7	0.33	100.18	85
16-Jan-1973	2.6	2.3	-2.8	4.1	0	0	100.63	94
17-Jan-1973	3.1	0.6	-3.5	3.2	0	0	101.03	97
18-Jan-1973	4.1	1.7	0.8	2.9	0	0	101.72	93
19-Jan-1973	2.6	-0.2	-1.4	1.2	0	0	101.64	94
20-Jan-1973	3.6	1.1	-0.6	4.9	0	0	100.47	94
21-Jan-1973	3.6	3.2	0.6	5.3	0	0	100.55	94
22-Jan-1973	3.6	2.3	-0.5	6.2	0.2	0.02	101.99	94
23-Jan-1973	3.1	2.4	0.2	3.6	0	0	102.92	97
24-Jan-1973	3.1	3.9	2.8	5.4	0	0	103.2	92
25-Jan-1973	3.6	2.7	0.3	4.4	0	0	102.79	89
26-Jan-1973	5.1	5.4	4	6.7	0	0	101.66	95
27-Jan-1973	5.7	6	3.9	7.4	0.3	0.03	100.53	90
28-Jan-1973	3.1	4.7	1.6	7	2.7	0.31	101.69	85
29-Jan-1973	3.6	7.6	4.7	9	0.2	0.02	101.71	94
30-Jan-1973	3.6	7.3	6.1	8.4	0	0	101.43	94
31-Jan-1973	2.6	3.8	0.1	7.3	5.1	0.57	101.44	90
1-Feb-1973	1.5	1.5	-2.6	5.4	0.6	0.07	101.91	96
2-Feb-1973	2.1	1.7	-1	5.2	1.6	0.18	102.92	98
3-Feb-1973	2.6	0.8	-0.4	1.6	0	0	103.51	100
4-Feb-1973	2.6	-1.8	-2.9	-0.3	0	0	103.46	98
5-Feb-1973	4.1	0.9	-3.1	4.9	0	0	102.82	97
6-Feb-1973	5.1	6.5	4.6	8	0	0	102.07	92
7-Feb-1973	6.2	7.8	7	9	0	0	101.38	90
8-Feb-1973	7.2	6.9	6.1	7.5	0	0	100.77	92
9-Feb-1973	6.2	5.3	1.3	7.8	2	0.21	100.12	87
10-Feb-1973	4.6	3.1	1.2	5.4	1.1	0.11	100.42	89
11-Feb-1973	3.6	3.4	0.1	6.3	2.2	0.23	101.57	90
12-Feb-1973	8.2	5.4	2.5	7.5	0	0	99.39	89
13-Feb-1973	7.2	1.5	0.1	4.1	3	0.31	98.18	87
14-Feb-1973	6.2	1.4	-0.8	3.7	2.7	0.27	98.42	84
15-Feb-1973	3.6	2.5	0.4	5.4	0.2	0.02	99.34	79
16-Feb-1973	3.1	0.2	-2.4	4.2	5.2	0.52	100.94	87
17-Feb-1973	2.6	0.9	-2.4	2.5	0	0	101.57	94
18-Feb-1973	3.1	2.5	0.5	3.8	0	0	101.59	93
19-Feb-1973	1	4.8	0.6	6.7	0	0	102.15	95
20-Feb-1973	2.6	7	5.2	8.6	0	0	102.6	95
21-Feb-1973	4.6	7	4.9	8.5	0	0	101.95	89
22-Feb-1973	5.7	4.7	3.4	6.3	0.3	0.03	101.23	83
23-Feb-1973	6.7	2.6	-0.5	5.3	1.5	0.14	100.32	83
24-Feb-1973	3.6	0.9	-3.6	4.8	5.8	0.55	100.06	88
25-Feb-1973	2.1	0.7	-3.4	5	6.8	0.64	100.8	87
26-Feb-1973	2.1	0.2	-5	6.2	5.2	0.49	101.46	87
27-Feb-1973	1.5	0.5	-4.3	6	8.8	0.82	102.7	77
28-Feb-1973	4.1	2	-2.6	4.2	-0.1	0	103.09	85

Appendix 3 Contd.

1-Mar-1973	5.1	4.7	2.3	7.4	0.6	0.06	102.6	71
2-Mar-1973	4.1	4.3	1.3	8.5	4.2	0.38	102.56	88
3-Mar-1973	4.6	6.1	1.2	8.4	0	0	102.62	91
4-Mar-1973	4.1	7.1	5.1	8.8	0	0	102.61	90
5-Mar-1973	3.1	6.8	4	10.4	1.4	0.13	102.25	89
6-Mar-1973	4.1	4.9	2.1	8.2	5	0.45	101.93	87
7-Mar-1973	3.6	3.8	-0.9	7.9	6.9	0.61	103.09	83
8-Mar-1973	2.6	5.9	-0.5	10.6	7.7	0.68	103.48	87
9-Mar-1973	2.6	4.9	0.1	8.4	1.6	0.14	103.39	85
10-Mar-1973	1.5	2.7	-3.7	9.1	9.1	0.8	103.25	75
11-Mar-1973	2.6	4.6	1.2	9.3	3.6	0.31	102.64	84
12-Mar-1973	4.1	4	2.1	6.9	6.7	0.58	102.34	72
13-Mar-1973	3.1	2.4	-0.8	6	7.4	0.64	102.55	73
14-Mar-1973	3.6	3	-1.9	7.6	9.5	0.81	102.66	77
15-Mar-1973	3.6	4.7	0.3	10.7	7.3	0.62	102.99	74
16-Mar-1973	2.1	2.9	-3.6	8.9	8.2	0.69	103.03	81
17-Mar-1973	3.1	5.2	0.4	8.1	0	0	102.47	91
18-Mar-1973	5.1	6.4	2.1	9.7	0.9	0.08	101.89	79
19-Mar-1973	3.6	4.7	1.5	7.9	0.7	0.06	102.57	78
20-Mar-1973	2.1	6.6	3.6	10.6	-0.1	0	103.02	78
21-Mar-1973	2.6	6	0.6	9.9	0	0	102.89	84
22-Mar-1973	2.6	5.5	-0.8	13.4	9.1	0.74	102.5	76
23-Mar-1973	2.1	6.3	-2.5	15.4	10.3	0.84	101.91	72
24-Mar-1973	3.1	8.7	1.2	18.7	9.7	0.78	101.02	67
25-Mar-1973	2.6	7.1	0.2	12.1	1.1	0.09	101.24	86
26-Mar-1973	2.6	5.4	-0.5	11.5	3.2	0.26	102.14	87
27-Mar-1973	2.1	4.6	-0.5	8.9	1.1	0.09	102.08	92
28-Mar-1973	2.1	6.7	3.5	11.7	4.1	0.32	101.95	86
29-Mar-1973	3.6	6.9	3.1	10.7	5.1	0.4	102.69	83
30-Mar-1973	3.1	6	-1.9	12.3	8.8	0.69	101.98	79
31-Mar-1973	3.6	5.5	0.1	10.8	7.9	0.61	102.08	68
1-Apr-1973	6.7	6.9	3.5	9.8	0	0	101.26	81
2-Apr-1973	10.8	5.3	3.3	9.5	0.1	0.01	99.34	87
3-Apr-1973	6.2	3.7	-1.7	7.7	8.4	0.64	101.91	67
4-Apr-1973	6.7	3.3	-3.1	7.6	0.2	0.02	102.62	82
5-Apr-1973	5.1	8.2	6.2	10.1	-0.1	0	101.72	89
6-Apr-1973	6.2	6.6	4.6	9.3	1.5	0.11	101.15	75
7-Apr-1973	5.1	5	0.6	9.9	5.7	0.43	101.1	78
8-Apr-1973	3.6	3.7	-0.5	8.4	7.4	0.55	101.3	74
9-Apr-1973	4.6	3.1	-1.3	7	5.9	0.44	101.31	64
10-Apr-1973	4.6	4	-1.7	8.7	10.5	0.78	101.14	68
11-Apr-1973	5.7	5	2.3	8	4.8	0.35	100.83	78
12-Apr-1973	4.6	3.1	-0.5	7.1	3.7	0.27	101.32	84
13-Apr-1973	2.6	3.1	-1	8	4	0.29	102.1	86
14-Apr-1973	2.1	4.3	-2.8	9	4.3	0.31	102.64	82
15-Apr-1973	3.6	7.3	5.4	9.8	0	0	102.48	88
16-Apr-1973	3.6	8.7	6.9	12.9	1.6	0.11	102.69	89
17-Apr-1973	5.7	7.4	4.6	10.8	3.7	0.26	102.59	77
18-Apr-1973	5.1	6.3	3.8	9.2	1	0.07	101.74	84
19-Apr-1973	5.7	5.3	1.4	10	8.1	0.57	101.14	78
20-Apr-1973	3.1	4.9	1	10.1	8.1	0.57	100.97	76
21-Apr-1973	2.6	3.8	0.1	7.5	0.1	0.01	100.93	91
22-Apr-1973	3.6	6.7	1.2	12.3	8.8	0.61	101.16	70
23-Apr-1973	3.1	6.8	2	11.5	5.5	0.38	101.23	77
24-Apr-1973	5.7	9.2	6	14.4	10.5	0.73	101.35	68
25-Apr-1973	4.1	8.3	2.5	14	12.8	0.88	101.87	64
26-Apr-1973	1.5	7.3	3.2	12.6	4.9	0.34	101.83	78
27-Apr-1973	3.1	8.7	2.9	14.6	12.4	0.85	101.13	70
28-Apr-1973	2.1	8.7	2.3	12.1	0	0	100.33	67
29-Apr-1973	2.6	8.2	0.3	13.6	2.1	0.14	100.46	81
30-Apr-1973	4.1	9.2	-1.8	15.6	0.7	0.05	100.77	87

Appendix 4: Daily rainfall data (mm) from ElSpeet, Harskamp, Kootwijk and Beekbergen Stations (1973)

Date	Elspeet	Harskamp	Kootwijk	Beekbergen
01-Jan-73	0	0	0	0
02-Jan-73	0	0	0	0
03-Jan-73	0	0	0.1	0
04-Jan-73	0	0	0.1	0.2
05-Jan-73	0	0	0	0.1
06-Jan-73	0.5	0.1	0.6	0.6
07-Jan-73	0.4	0.1	0.3	0.5
08-Jan-73	0.1	0.2	0.1	0.1
09-Jan-73	0.1	0.2	0.2	0.3
10-Jan-73	0.9	0.4	0.7	1
11-Jan-73	0	0	0	0
12-Jan-73	0	0	0	0
13-Jan-73	0	0	0	0
14-Jan-73	0	0	0	0
15-Jan-73	1.4	1.1	0.9	0.8
16-Jan-73	0	0	0	0.1
17-Jan-73	0	0	0.3	0
18-Jan-73	0	0	0	0.1
19-Jan-73	0	0	0.1	0
20-Jan-73	0	0	0	0
21-Jan-73	4	4.1	4	3.7
22-Jan-73	1	0.3	0.5	0.4
23-Jan-73	1	0.4	1	1
24-Jan-73	0.4	0.3	0.1	0.5
25-Jan-73	0	0	0	0
26-Jan-73	0.5	0	0.8	0.2
27-Jan-73	8.2	6.9	8.5	8.9
28-Jan-73	2.1	0.9	2	4.1
29-Jan-73	2.2	0.8	1.9	1.6
30-Jan-73	0	0.5	0.3	0.3
31-Jan-73	2.9	4.8	5.4	4.6
01-Feb-73	0.1	0.2	0	0.2
02-Feb-73	2.3	0.6	1.6	3.9
03-Feb-73	0.1	0	0	0.1
04-Feb-73	0	0	0	0
05-Feb-73	0	0	0.2	0
06-Feb-73	0.1	1.4	0.2	0.2
07-Feb-73	0.1	0.4	0.2	0.1
08-Feb-73	2.3	2.7	2.5	2.9
09-Feb-73	12.3	6.7	12.1	12.1
10-Feb-73	4.8	4.5	4.4	4.9

Appendix 4 Contn'd

11-Feb-73	6.6	8.6	6.8	9
12-Feb-73	4	1.3	1.9	2.2
13-Feb-73	19.6	14.7	16.4	18.4
14-Feb-73	2.5	1.6	1.9	1.8
15-Feb-73	0	0.2	0	0
16-Feb-73	0	0	0	0
17-Feb-73	0	0	0.1	0.2
18-Feb-73	2.9	3.8	4	4.5
19-Feb-73	6.9	9.2	8.1	5.6
20-Feb-73	0.3	0.4	1	0.9
21-Feb-73	0.1	0.6	0.5	0.6
22-Feb-73	1.1	2.2	2.3	2.4
23-Feb-73	3.1	1.2	2.2	2.8
24-Feb-73	1.5	3.4	3.5	2.6
25-Feb-73	3.8	1.3	2.5	1.8
26-Feb-73	0.1	0	0.1	0.2
27-Feb-73	0.1	0.5	0.2	1.2
28-Feb-73	0	0	0	0
01-Mar-73	0.1	0.2	0.4	0.2
02-Mar-73	4	3.1	5.3	5.4
03-Mar-73	0.6	1.2	0.9	0.9
04-Mar-73	2.4	1.3	3	3.1
05-Mar-73	0.1	0	0	0.1
06-Mar-73	0.3	0.4	0.5	0.7
07-Mar-73	8.9	7.1	7.8	7.3
08-Mar-73	0.1	0	0.1	0.2
09-Mar-73	0	0	0	0
10-Mar-73	0	0	0.1	0
11-Mar-73	0	0.2	0	0.1
12-Mar-73	0.2	0.2	0.1	0
13-Mar-73	0	0	0	0
14-Mar-73	0	0	0	0
15-Mar-73	0.1	0	0	0
16-Mar-73	0	0	0	0
17-Mar-73	0.9	0.6	0.6	0.6
18-Mar-73	0.2	0.3	0.4	0.4
19-Mar-73	0.4	1.3	0	0.6
20-Mar-73	0	0	0	0
21-Mar-73	0	0	0	0
22-Mar-73	0	0	0	0
23-Mar-73	0	0	0	0
24-Mar-73	0	0	0	0
25-Mar-73	0	0	0	0
26-Mar-73	3	1.2	2.8	2.4
27-Mar-73	0.1	0	0	0.1
28-Mar-73	2.4	3.3	2	3.1
29-Mar-73	2	3.7	1.5	1.2
30-Mar-73	0	0.1	0.2	0.1
31-Mar-73	0.7	0.3	0.3	0

Appendix 4 Contn'd

01-Apr-73	0	0	0	0
02-Apr-73	14.3	10.1	12	10.6
03-Apr-73	24.5	17.2	20.9	22.9
04-Apr-73	0.6	0.4	1.1	1.5
05-Apr-73	9.1	5.8	7.7	7.5
06-Apr-73	3.8	4.1	4.2	5
07-Apr-73	3.1	1.6	1.2	2.7
08-Apr-73	4.8	3.2	3.1	3.6
09-Apr-73	2.4	0.8	4.5	2.7
10-Apr-73	1.1	0.2	0.3	1
11-Apr-73	3.4	1.8	2.9	3.3
12-Apr-73	2.9	1.5	2.8	2.1
13-Apr-73	1.1	4.1	4	1.4
14-Apr-73	0	0.3	0.2	0.1
15-Apr-73	1.7	1.7	2.1	1.6
16-Apr-73	0.5	0.6	0.5	0.4
17-Apr-73	0.6	0.4	0.5	0.3
18-Apr-73	9.5	4.7	12.6	8.1
19-Apr-73	6.5	9.6	8.6	8.2
20-Apr-73	1.3	1.7	1.5	5
21-Apr-73	7	12.1	7.1	5.4
22-Apr-73	1.8	6.7	2.8	1.6
23-Apr-73	0	0	0	0.2
24-Apr-73	0	0.3	0.2	0
25-Apr-73	0	0	0	0
26-Apr-73	0	0	0	0
27-Apr-73	0	0	0	0
28-Apr-73	0	0	0	0.2
29-Apr-73	2.5	6.9	9.1	7.2
30-Apr-73	0.6	0.5	0.8	0.7

Appendix 5 Piezometric levels and groundwater abstraction data

Description of the boreholes that are used for modelling

Location	code	X-coordinate	Y-coordinate	Elevation (cm NAP)	Average GWL (cm NAP)	Start measuring	End measuring
B33A0065	33AP0065	185440	464660	4623	2769	01/10/1927	05/10/2007
B33A0067	33AP0067	181030	463970	2568	2270	20/09/1927	05/10/2007
B33A0103	33AP0103	183390	472340	4135	1953	03/09/1970	05/10/2007
B33A0113	33AP0113	189780	471810	7842	2803	03/07/1972	06/02/2007
B33D0002	33DP0002	191650	458900	6480	4177	21/09/1959	14/04/1996
B33D0217	33DP0026	193505	460835	5979	3528	14/02/1973	26/04/2006

Location and annual abstraction rate of six Pumping wells in the study area

Name	X - coordinate	Y- coordinate	Wetrealtieomschrijving
GO 31020281 Kamp A en F v d mts	189450	453065	Vergunning
GO 33010171 VHP SECURITY PAPERMILL	190775	465525	Vergunning
GO 33010481 HET LIERDERHOLT VAKANTIEOORD	193280	460650	Registratieplicht
GO 36010321 RIJKSWATERSTAAT	183860	448320	Registratieplicht
GO 33010111 GEMEENTE APELDOORN	191505	469630	Vergunning
GO 33010032 VITENS GELDERLAND	188450	459900	Vergunning

Abstraction rate from the pumping wells

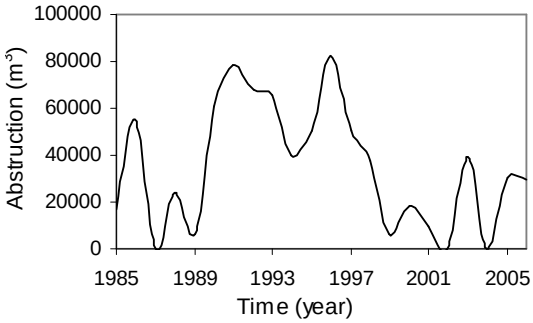

GO 31020281 Kamp A en F v d mts

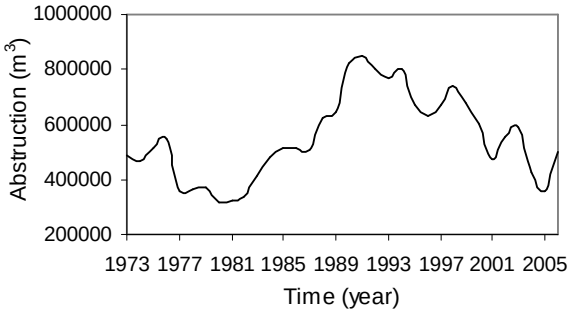

GO 33010171 VHP SECURITY PAPERMILL

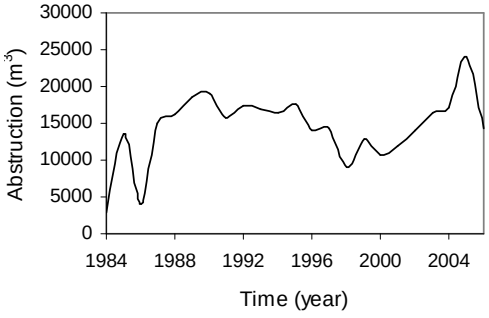

GO 33010481 HET LIERDERHOLT

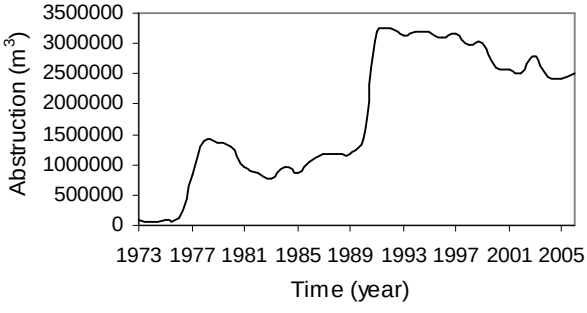

GO 33010032 VITENS GELDERLAND

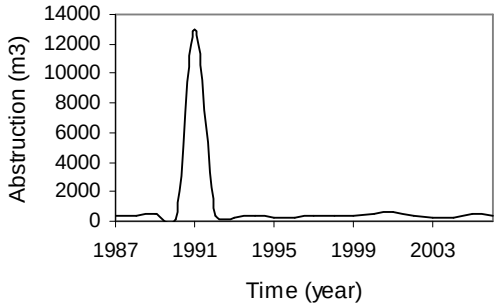

GO 36010321 RIJKSWATERSTAAT

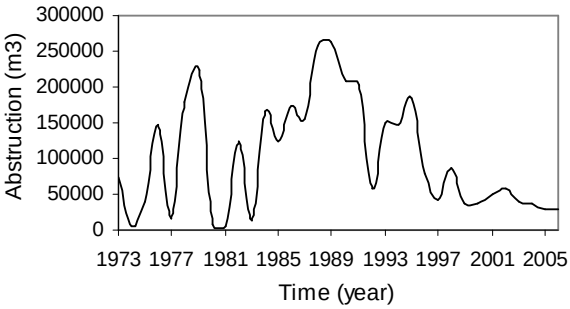

GO 33010111 GEMEENTE APELDOORN

Appendix 6 Example of SWAP main iput data at B33A0065 (Molinia grass)

```
*******************************************************************************
* Filename: veluGrass.swp
* Contents: SWAP 2.10 - Main input data
*******************************************************************************
* Case: Veluwe - grasland
*******************************************************************************
*   The main input file .swp contains the following sections:
*         - General section
*         - Meteorology section
*         - Crop section
*         - Soil water section
*         - Lateral drainage section
*         - Bottom boundary section
*         - Heat flow section
*         - Solute transport section

*** GENERAL SECTION ***
*******************************************************************************
* Part 1: Environment
 PROJECT   = 'Grass'           ! Project description, [A80]
 PATHWORK  = ''                ! Path to work directory, [A80]
 PATHATM   = 'Data\Weather\'   ! Path to directory with weather files, [A80]
 PATHCROP  = 'Data\Crops\'     ! Path to directory with crop files, [A80]
 PATHDRAIN = 'Data\Drainage\'  ! Path to directory with drainage files, [A80]
 SWSCRE    = 1         ! Switch, display progression of simulation run:
                       !   SWSCRE = 0:  no display to screen
                       !   SWSCRE = 1:  display waterbalance to screen
                       !   SWSCRE = 2:  display daynumber to screen
 SWERROR   = 1      ! Switch for printing errors to screen [Y=1, N=0]
*******************************************************************************
* Part 2: Simulation period
 TSTART  = 01-jan-1973 ! Start date of simulation run, give day-month-year, [date]
 TEND    = 31-dec-1992 ! End   date of simulation run, give day-month-year, [date]
*******************************************************************************
* Part 3: Output dates
* Output times for balances
 SWYRVAR = 0         ! Switch, output at fixed or variable dates:
                     ! SWYRVAR = 0: each year output of balance at the same date
                     ! SWYRVAR = 1: output of balance at different dates

* If SWYRVAR = 0 specify fixed date:
 DATEFIX = 31 12     ! Specify day and month for output of yearly balances, [ddmm]
```

Appendix 6 contd.

```
* If SWYRVAR = 1 specify all output dates [dd-mmm-yyyy], maximum MAOUT dates:
  OUTDAT =
  * End of table
* Intermediate output dates
  SWMONTH = 0        ! Switch, output each month, [Y=1, N=0]
  PERIOD = 1         ! Fixed output interval, ignore = 0, [0..366, I]
  SWRES  = 0         ! Switch, reset output interval counter each year, [Y=1, N=0]
  SWODAT = 0         ! Switch, extra output dates are given in table, [Y=1, N=0]
* If SWODAT = 1, specify all intermediate output dates [dd-mmm-yyyy],
* maximum MAOUT dates:
  OUTDATINT =
*End of table
* Part 4: Output files
  OUTFIL   = 'Result'   ! Generic file name of output files, [A16]
  SWHEADER = 0       ! Print header for each balance period, [Y=1, N=0]
* Optional output files for water quality models or specific use
  SWAFO  = 0       ! Switch, output file with formatted hydrological data
                   ! SWAFO = 0: no output
                   ! SWAFO = 1: output to a file named *.AFO
                   ! SWAFO = 2: output to a file named *.BFO
  SWAUN  = 0       ! Switch, output file with unformatted hydrological data, [Y=1, N=0]
                   ! SWAUN = 0: no output
                   ! SWAUN = 1: output to a file named *.AUN
                   ! SWAUN = 2: output to a file named *.BUN
* if SWAFO = 1 or 2,   or if SWAUN = 1 or 2 then specify SWDISCRVERT and  CritDevMasBalAbs
  SWDISCRVERT = 0   ! Switch to convert vertical discretization   [Y=1, N=0]
                    !   only when SWAUN=1 or SWAFO=1 the generated output
                    !   files (*.afo,*.bfo,*.aun,*.bun) are influenced
                    ! SWDISCRVERT = 0: no conversion
                    ! SWDISCRVERT = 1: convert vertical discretization,
                    !  numnodNew and dzNew are required
* Critical Absolute Deviation in water balance
* (when exceeded: simulation continues, but file with errors is created (file-extension *.DWB))
  CritDevMasBalAbs = 0.1  ! Critical Absolute Deviation in water balance [1.0d-30..1.0 cm, R]
* Only If SWDISCRVERT = 1 then numnodNew and dzNew are required
  NUMNODNEW = 17    ! New number of nodes [1...macp,I,-]
! thickness of compartments [1.0d-6...5.0d2, cm, R]
  DZNEW = 10.0 10.0 10.0 10.0 10.0   10.0 10.0 10.0 10.0 10.0
      10.0 20.0 20.0 20.0 40.0   40.0 40.0
  SWVAP  = 1       ! Switch, output profiles of moisture, solute and temperature, [Y=1, N=0]
  SWATE  = 0       ! Switch, output file with soil temperature profiles, [Y=1, N=0]
  SWBLC  = 1       ! Switch, output file with detailed yearly water balance [Y=1, N=0]
```

Appendix 6 contd.

```
* Required only when SWMACRO= 1 or 2 (see lateral section): input of SWDRF and SWSWB
  SWBMA  = 0        ! Switch, output file with detailed yearly water balance Macropores [Y=1, N=0]
* Required only when SWDRA=2 (see lateral section): input of SWDRF and SWSWB
  SWDRF  = 0        ! Switch, output drainage fluxes, only for extended drainage [Y=1, N=0]
  SWSWB  = 0        ! Switch, output surface water reservoir, only for ext. dr. [Y=1, N=0]
**********************************************************************
*** METEOROLOGY SECTION ***
* General data
  METFIL = 'Debilt'      ! File name of meteorological data without extension, [A16]
  SWETR  =  1            ! Switch, use reference ET values of meteo file [Y=1, N=0]
* If SWETR = 0, then LAT,ALT and ALTW must have realistic values
  LAT    =   52.0        ! Latitude of meteo station, [-60..60 degrees, R, North = +]
  ALT    =   10.0        ! Altitude of meteo station, [-400..3000 m, R]
  ALTW   =   2.0         ! Altitude of wind speed measurement (10 m is default) [0..99 m, R]
  SWRAIN =  0            ! Switch for use of actual rainfall intensity:
                         ! SWRAIN = 0: Use daily rainfall amounts
                         ! SWRAIN = 1: Use daily rainfall amounts + mean intensity
                         ! SWRAIN = 2: Use daily rainfall amounts + duration
* as function of time TIME [0..366 d, R], maximum 30 records
   TIME    RAINFLUX
* End of table
**********************************************************************
*** CROP SECTION ***
* Part 1: Crop rotation scheme during simulation period
* Specify information for each crop (maximum MACROP):
* CROPSTART = date of crop emergence, [dd-mmm-yyyy]
* CROPEND = date of crop harvest, [dd-mmm-yyyy]
* CROPNAME = crop name, [A16]
* CROPFIL = name of file with crop input parameters, no extension, [A16]
* CROPTYPE = type of crop model: simple = 1, detailed general = 2, detailed grass = 3
  CROPSTART      CROPEND       CROPNAME   CROPFIL     CROPTYPE
  01-jan-1973    31-dec-1992     'Grass'    'Grass'        1
* End of table
**********************************************************************
* Part 2: Fixed irrigation applications
  SWIRFIX = 0    ! Switch for fixed irrigation applications
                 ! SWIRFIX = 0: no irrigation applications are prescribed
                 ! SWIRFIX = 1: irrigation applications are prescribed
* If SWIRFIX = 1:
  SWIRGFIL  = 0  ! Switch for file with fixed irrigation applications:
                 ! SWIRGFIL = 0: data are specified in the .swp file
                 ! SWIRGFIL = 1: data are specified in a separate file
```

Appendix 6 contd.

```
* If SWIRGFIL  = 0 specify information for each fixed irrigation event (max. MAIRG):
* IRDATE   = date of irrigation, [dd-mmm-yyyy]
* IRDEPTH  = amount of water, [0.0..100.0 cm, R]
* IRCONC   = concentration of irrigation water, [0.0..1000.0 mg/cm3, R]
* IRTYPE   = type of irrigation: sprinkling = 0, surface = 1
    IRDATE   IRDEPTH     IRCONC   IRTYPE
    * --- end of table
* If SWIRGFIL  = 1 specify name of file with data of fixed irrigation applications:
                    ! File name without extension .irg [A16]
*******************************************************************************
*** SOIL WATER SECTION ***
* Part 1: Initial moisture condition
 SWINCO = 2 ! Switch, type of initial moisture condition:
                ! 1 = pressure head as function of depth is input
                ! 2 = pressure head of each compartment is in hydrostatic equilibrium
                !    with initial groundwater level
* If SWINCO = 1, specify initial pressure head  H [-1.d10..1.d4 cm, R] as function of
* soil depth ZI [-10000..0 cm, R], maximum MACP data pairs:
    ZI        H
* End of table
   * If SWINCO = 2, specify:
  GWLI   = -2762.0  ! Initial groundwater level, [-10000..100 cm, R]
*******************************************************************************
* Part 2: Ponding and Runoff
 PONDMX  = 0.0001  ! Maximum thickness of ponding water layer, [0..1000 cm, R]
 RSRO    =    0.999    ! drainage Resistance of Surface RunOff [0.001..1.0 d, R]
 RSROEXP = 1.0       ! exponent in relation of surface runoff [0.1....10.0, R]
*******************************************************************************
* Part 3: Soil evaporation
  SWCFBS = 1   ! Switch for use of coefficient CFBS for soil evaporation [Y=1, N=0]
                ! 0 = CFBS is not used
                ! 1 = CFBS used to calculate potential evaporation from potential
                !    evapotranspiration or reference evapotranspiration
* If SWCFBS = 1, specify coefficient CFBS:
  CFBS   = 1.1 ! Coefficient for potential soil evaporation, [0.5..1.5 -, R]
  SWREDU = 0   ! Switch, method for reduction of potential soil evaporation:
                ! 0 = reduction to maximum Darcy flux
                ! 1 = reduction to maximum Darcy flux and to maximum Black (1969)
                ! 2 = reduction to maximum Darcy flux and to maximum Bo/Str.
                !(1986)
 COFRED =      ! Soil evaporation coefficient of Black, [0..1 cm/d1/2, R],
               ! or Boesten/Stroosnijder, [0..1 cm1/2, R]
```

Appendix 6 contd.

RSIGNI = ! Minimum rainfall to reset models Black and Bo/Str., [0..1 cm/d, R]

****

* Part 4: Vertical discretization of soil profile
* Specify the following data (maximum MACP 'layers'):
* Specify the following data (maximum MACP 'compartments'):
* ISOILLAY = indicator (number) of soil layer, start with 1 at soil surface, [1..MAHO, I]
* ISUBLAY = number of sub layer, start with 1 at soil surface, [1..MACP, I]
* HSUBLAY = height of sub layer, [0.0..1000.0 cm, R]
* HCOMP = height of compartments in this layer, [0.0..1000.0 cm, R]
* NCOMP = number of compartments in this layer (= HSUBLAY/HCOMP), [1..MACP, I]

ISOILLAY	ISUBLAY	HSUBLAY	HCOMP	NCOMP
1	1	5.0	1.0	5
1	2	10.0	2.0	5
1	3	10.0	2.5	4
2	4	10.0	2.5	4
2	5	15.0	3.0	5
3	6	20.0	4.0	5
3	7	30.0	5.0	6
4	8	40.0	8.0	5
4	9	70.0	10.0	7
4	10	90.0	15.0	6
5	11	100.0	20.0	5
5	12	100.0	25.0	4

* --- end of table

****

* Part 5: Soil hydraulic functions
* Specify for each soil type (maximum MAHO):
* ORES = Residual water content, [0..0.4 cm3/cm3, R]
* OSAT = Saturated water content, [0..0.95 cm3/cm3, R]
* ALFA = Shape parameter alfa of main drying curve, [0.0001..1 /cm, R]
* NPAR = Shape parameter n, [1..4 -, R]
* KSAT = Saturated hydraulic conductivity, [1.d-5..1000 cm/d, R]
* LEXP = Exponent in hydraulic conductivity function, [-25..25 -, R]
* ALFAW = Alfa parameter of main wetting curve in case of hysteresis, [0.0001..1 /cm, R]

ISOILLAY1	ORES	OSAT	ALFA	NPAR	KSAT	LEXP	ALFAW
1	0.025	0.44	0.021	1.62	133.0	0.500	0.0227
2	0.021	0.43	0.019	2.87	378.7	0.500	0.0227
3	0.019	0.38	0.030	2.81	690.0	0.500	0.0227
4	0.013	0.36	0.030	2.93	695.0	0.500	0.0227
5	0.010	0.29	0.049	3.33	1000.0	0.500	0.0216

* --- end of table

Appendix 6 contd.

```
**************************************************************************
* Part 6: Hysteresis of soil water retention function

 SWHYST = 0   ! Switch for hysteresis:
              ! 0 = no hysteresis
              ! 1 = hysteresis, initial condition wetting
              ! 2 = hysteresis, initial condition drying
* If SWHYST = 1 or 2, specify:
 TAU      ! Minimum pressure head difference to change wetting-drying, [0…1 cm, R]
**************************************************************************
* Part 7: Maximum rooting depth
 RDS  = 500.0   ! Maximum rooting depth allowed by the soil profile, [1…5000 cm, R]
**************************************************************************
* Part 8: Similar media scaling of soil hydraulic functions
 SWSCAL = 0 ! Switch for similar media scaling [Y=1, N=0]; no hysteresis is
              allowed
             ! in case of similar media scaling
* If SWSCAL = 1, specify:
 NSCALE =  ! Number of simulation runs, [1..MASCALE, I]
* Supply the scaling factors for each simulation run and each soil type:
 RUN     SOIL1       SOIL2
  * End of table
**************************************************************************
* Part 9: Preferential flow due to soil volumes with immobile water
 SWMOBI = 0  ! Switch for preferential flow due to immobile water, [Y=1, N=0]; no
               hysteresis
               ! or scaling is allowed in case of preferential flow

* If SWMOBI = 1, specify mobile fraction as function of log -h for each soil type:
* PF1    first datapoint, log -h (cm), [0..5, R]
* FM1    first datapoint,  mobile fraction (1.0 = totally mobile), [0...1, R]
* PF2    second datapoint, log -h (cm), [0..5, R]
* FM2    second datapoint, mobile fraction (1.0 = totally mobile), [0..1, R]
* Also specify volumetric water content in immobile soil volume (THETIM), [0…0.3, R]
 ISOILLAY2    PF1    FM1    PF2    FM2   THETIM
* End of table
**************************************************************************
* Part 10: Preferential flow due to macro pores
 SWMACRO = 0  ! Switch for macro pores, [0..2, I]
**************************************************************************
* Part 11: Snow and frost
SWSNOW = 0   ! Switch, calculate snow accumulation and melt. [Y=1, N=0]
```

Appendix 6 contd.

```
* If SWSNOW = 1, then specify SWE and CX
 SNOWINCO =     ! the initial SWE (Snow Water Equivalent), [0.0...1000.0 cm, R]
 SNOWCOEF       ! calibration factor for snowmelt, [0.0...10.0 -, R]
 SWFROST = 0  ! Switch, in case of frost: stop soil water flow [Y=1, N=0]
*****************************************************************************
* Part 12 Numerical solution of Richards' equation; criteria to reach convergence
 DTMIN     = 1.0d-8  ! Minimum timestep, [1.d-8..0.1 d, R]
 DTMAX     =    0.2  ! Maximum timestep, [ 0.01..0.5 d, R]
 THETOL    =  0.001  ! Maximum dif. water content between iterations, [1.d-5..0.01 cm3/cm3, R]
 GWLCONV   =  100.0  ! Maximum dif. groundwater level between iterations, [1.d-5..1000 cm, R]
 CritDevMasBalDt = 0.001  ! Critical Deviation in water balance of timestep [1.0d-5..100.0 cm, R]
 MSTEPS    = 100000  ! Maximum number of iteration steps to solve Richards', [ 2..100000 -, I]
 SWBALANCE =     0   ! Switch to allow compensation of water balance, [Y=1, N=0]
*****************************************************************************************
*** LATERAL DRAINAGE SECTION ***
*********************************************************************
* Specify whether lateral drainage should be included
  SWDRA = 0  ! Switch, simulation of lateral drainage:
                  ! 0 = No simulation of drainage
                  ! 1 = Simulation with basic drainage routine
                 ! 2 = Simulation with extended drainage routine (includes surface
                       water man.)
* If SWDRA = 1 or SWDRA = 2 specify name of file with drainage input data:
  DRFIL =          ! File name with drainage input data, no extension [A16]
* Specify whether runon from external source (fiel) should be included
  SWRUNON = 0  ! Switch, input of runon:
                       ! 0 = No input of runon
                       ! 1 = runon input
* If SWRUNON = 1 specify name of file with runon input data
*                  (file may be an output-*.wba-file of other Swap-simulation):
  RUFIL =       ! File name (with extension) with input data, must have extension (e.g..WBA) [A16]
*********************************************************************
*** BOTTOM BOUNDARY SECTION ***
*********************************************************************
* Bottom boundary condition
  SWBBCFILE  = 0    ! Switch for file with bottom boundary conditions:
                      ! SWBBCFILE = 0: data are specified in the .swp file
                      ! SWBBCFILE = 1: data are specified in a separate file
* If SWBBCFILE = 1 specify name of file with bottom boundary conditions:
  BBCFIL = ' '       ! File name without extension .bbc [A16]
* If SWBBCFILE = 0 specify the following data in this file:
```

Appendix 6 contd.

```
* Choose one of the following options [1..8,-,I]:
        ! 1  Use groundwater level
        ! 2  Use regional bottom flux
        ! 3  Calculate bottom flux from hydraulic head of deep aquifer
        ! 4  Calculate bottom flux as function of groundwater level
        ! 5  Use soil water pressure head of bottom compartment
        ! 6  Bottom flux equals zero
        ! 7  Free drainage of soil profile
        ! 8  Free outflow at soil-air interface

 SWBOTB = 7  ! Switch for bottom boundary [1..8,-,I]
```

Appendix 7 Example of SWAP daily out put, water balance increments, at B33A0065 (Molinia grass)

Date	Day	Dcum	Rain	Irrig	Interc	Runon	Runoff	Tpot	Tact	Epot	Eact	Drainage	QBottom
01-Jan-73	1	1	0	0	0	0	0	0.027	0.027	0.009	0.009	0	-0.041
02-Jan-73	2	2	0	0	0	0	0	0.013	0.013	0.005	0.005	0	-0.04
03-Jan-73	3	3	0	0	0	0	0	0.013	0.013	0.005	0.005	0	-0.04
04-Jan-73	4	4	0.01	0	0	0	0	0.013	0.013	0.005	0.005	0	-0.039
05-Jan-73	5	5	0	0	0	0	0	0.013	0.013	0.005	0.005	0	-0.039
06-Jan-73	6	6	0.05	0	0	0	0	0.013	0.013	0.005	0.005	0	-0.039
07-Jan-73	7	7	0.03	0	0	0	0	0.013	0.013	0.005	0.005	0	-0.039
08-Jan-73	8	8	0.01	0	0	0	0	0.013	0.013	0.005	0.005	0	-0.038
09-Jan-73	9	9	0.02	0	0	0	0	0.013	0.013	0.005	0.005	0	-0.038
10-Jan-73	10	10	0.07	0	0	0	0	0.013	0.013	0.005	0.005	0	-0.038
11-Jan-73	11	11	0	0	0	0	0	0.013	0.013	0.005	0.005	0	-0.037
12-Jan-73	12	12	0	0	0	0	0	0.013	0.013	0.005	0.005	0	-0.037
13-Jan-73	13	13	0	0	0	0	0	0.027	0.027	0.009	0.009	0	-0.037
14-Jan-73	14	14	0	0	0	0	0	0.013	0.013	0.005	0.005	0	-0.036
15-Jan-73	15	15	0.09	0	0	0	0	0.027	0.027	0.009	0.009	0	-0.036
16-Jan-73	16	16	0	0	0	0	0	0.013	0.013	0.005	0.005	0	-0.036
17-Jan-73	17	17	0.01	0	0	0	0	0.013	0.013	0.005	0.005	0	-0.036
18-Jan-73	18	18	0	0	0	0	0	0.013	0.013	0.005	0.005	0	-0.036
19-Jan-73	19	19	0	0	0	0	0	0.013	0.013	0.005	0.005	0	-0.036
20-Jan-73	20	20	0	0	0	0	0	0.013	0.013	0.005	0.005	0	-0.036
21-Jan-73	21	21	0.37	0	0	0	0	0.013	0.013	0.005	0.005	0	-0.036
22-Jan-73	22	22	0.04	0	0	0	0	0.02	0.02	0.007	0.007	0	-0.036
23-Jan-73	23	23	0.08	0	0	0	0	0.013	0.013	0.005	0.005	0	-0.036
24-Jan-73	24	24	0.03	0	0	0	0	0.02	0.02	0.007	0.007	0	-0.036
25-Jan-73	25	25	0	0	0	0	0	0.02	0.02	0.007	0.007	0	-0.036
26-Jan-73	26	26	0.03	0	0	0	0	0.02	0.02	0.007	0.007	0	-0.036
27-Jan-73	27	27	0.79	0	0	0	0	0.02	0.02	0.007	0.007	0	-0.036
28-Jan-73	28	28	0.25	0	0	0	0	0.033	0.033	0.012	0.012	0	-0.036
29-Jan-73	29	29	0.15	0	0	0	0	0.02	0.02	0.007	0.007	0	-0.036
30-Jan-73	30	30	0.03	0	0	0	0	0.02	0.02	0.007	0.007	0	-0.036
31-Jan-73	31	31	0.46	0	0	0	0	0.04	0.04	0.014	0.014	0	-0.036